A HISTORY-DEPENDENT MODEL OF MUSCLE SPINDLE FUNCTION

A Dissertation
Presented to
The Academic Faculty

by

Kyle Phillip Blum

In Partial Fulfillment
of the Requirements for the Degree
Doctor of Philosophy in the
Wallace H. Coulter Department of Biomedical Engineering

Georgia Institute of Technology
Emory University
August 2018

A HISTORY-DEPENDENT MODEL OF MUSCLE SPINDLE FUNCTION

Approved by:

Dr. Lena H. Ting, Advisor
Biomedical Engineering
Emory University

Dr. T. Richard Nichols
Biological Sciences
Georgia Institute of Technology

Dr. Timothy C. Cope
Biological Sciences
Georgia Institute of Technology

Dr. Robert Butera
Electrical and Computer Engineering
Georgia Institute of Technology

Dr. Kenneth S. Campbell
Physiology
University of Kentucky

Date Approved: 04/11/2018

To Elizabeth

ACKNOWLEDGEMENTS

The work presented here would not be possible without the personal and scientific contributions of many people. I am grateful for the help of each of them.

Thanks to the current and former post docs and graduate students of the Laboratory for Neuroengineering and the Neuromechanics Lab I was fortunate to spend time with, Lucas McKay, Stacie Chvatal, Andrew Sawers, Jessica Allen, Yun Seong Song, Brian Horslen, Jeff Bingham, Hongchul Sohn, Kim Lang, Aiden Payne, and Luke Drnach, who have all put their time into helping this work directly or indirectly. The personal and scientific conversations I've been able to have with such a great group of people have helped me develop positively as a scientist and a human. I will always look back at the times spent solving problems on the white boards with you fondly.

I owe an enormous thanks to each one of my committee members. I can honestly say I had a uniquely involved committee made up of members that went out of their way to help me develop my technical abilities as well as teach me what it means to be an academic scientist. Early on, I was fortunate to travel to Wright State University where Tim Cope welcomed me into his lab to collect data which would lay the foundation for this thesis. Tim was extremely generous with his time and resources and I am so happy I got to know him professionally as well as personally. Without his dedication to my training, this work would not have been completed. In a similar fashion, Ken Campbell at University of Kentucky has spent much of his time helping me troubleshoot my models and discussing technical aspects of this project, as well as having me visit his lab to learn the basics of his work in muscle physiology. I got to know Richard Nichols early in my graduate career

through a research rotation project, and his continued support and conversations with me about this thesis provided invaluable perspectives from which to consider my ideas. I was also fortunate to have Rob Butera on my committee, who helped me with decisions about my models and discussed with me the merits of various science fiction.

Of course, I owe a huge amount of thanks to my thesis advisor, Lena Ting. Without her patience and steadfast desire to be involved in the training of her students, this work would not have been possible. It seems laughable to attempt to place all of Lena's contributions to my time at Georgia Tech and Emory into a single paragraph, because an appropriate amount of space to do so would likely double the length of this thesis. In brief, Lena's dedication to my scientific development was the best I could have hoped for as a graduate student. She was an advocate for my ideas, let me flounder when it was necessary (an important part of any PhD thesis!), and always pushed me for higher standards of work. It is this dedication that has led my desire to pursue academic science as a career, and hopefully become as good of a mentor as Lena has been for me.

Finally, I owe the biggest thanks to my fiancé, Elizabeth. She's been more understanding and patient with me than I deserve, forgiving me for long hours and keeping me grounded when I would otherwise be driven crazy. I hope she is aware and proud of her vital role in this work and in the career that I am embarking on.

TABLE OF CONTENTS

ACKNOWLEDGEMENTS iv

LIST OF TABLES ix

LIST OF FIGURES x

SUMMARY xii

CHAPTER 1. Introduction 1
1.1 A brief history of the understanding of muscle spindle structure 1
1.2 Responses of muscle spindle Ia afferents to stretch stimuli 3
1.3 Non-classical muscle spindle function in the control of movement 8
1.4 Current models of muscle spindle sensory function 10
1.5 Objective of this thesis 11

CHAPTER 2. Force encoding in muscle spindles during stretch of passive muscle 13
2.1 Attribution of efforts 13
2.2 Introduction 13
2.3 Methods 17
2.3.1 Ethics Statement 17
2.3.2 Data Collection 18
2.3.3 Sample Size 20
2.3.4 Data inclusion and exclusion 20
2.3.5 Initial burst correlations 21
2.3.6 Candidate models 22
2.3.7 Fascicle length-related variable estimates 23
2.3.8 Time lags and parameter search limits 23
2.3.9 Cross validation 24
2.3.10 Model selection 25
2.4 Results 26
2.4.1 Response of muscle spindles Ia afferents to stretch 27
2.4.2 Relationship of muscle spindle Ia initial burst magnitude to force- and length-related transients 27
2.4.3 Relationship of muscle spindle Ia IFRs to musculotendon length- and force-related variables 30
2.4.4 Force-related but not length-related variables reproduce rate relaxation in fast stretches 30
2.4.5 Rate change in force, dF/dt, reproduces the initial burst and dynamic response to stretch 31
2.4.6 Muscle fascicle length-related variables do not reproduce muscle spindle Ia IFRs 33
2.4.7 Force-related model parameters are consistent across stretch velocity in all recorded afferents 34

2.4.8 The most likely model of muscle spindle IFRs uses musculotendon force-related variables 38
2.5 Discussion 42

CHAPTER 3. Muscle spindle Ia afferent responses to stretch are robustly explained by differential sensitivity to force and yank 51
3.1 Attribution of Efforts 51
3.2 Introduction 51
3.3 Methods 54
3.3.1 Animal care 54
3.3.2 Terminal physiological experiments 54
3.3.3 Sample size 56
3.3.4 Data inclusion and exclusion 56
3.3.5 Muscle fiber force estimation 56
3.3.6 Pseudolinear models for predicting firing responses 58
3.3.7 Parameter estimation for force-related model 60
3.3.8 Axonal stimulation dataset 61
3.3.9 Oxaliplatin dataset 62
3.3.10 Applying estimated fiber force-related currents to model neuron 62
3.3.11 Conductance-based model neuron for reproducing spiking activity 63
3.4 Results 65
3.4.1 Responses of muscle spindle Ia afferents to stretch 65
3.4.2 Estimated intrafusal muscle force during stretch resembles history-dependent Ia afferent spiking 68
3.4.3 Pseudolinear combinations of estimated muscle fiber force and yank predicted Ia spiking waveforms across stretch conditions 69
3.4.4 Best fit force-related model performance consistent across trial characteristics, despite varied model parameters 74
3.4.5 Changes to muscle spindle encoding caused by axonal stimulation predicted by reducing yank and constant component of pseudolinear model 75
3.4.6 Changes to muscle spindle encoding caused by oxaliplatin chemotherapy predicted by reduced fiber force component of pseudolinear model 79
3.4.7 Range of afferent phenotypes predicted by estimated intrafusal force-related currents applied to a model neuron 81
3.5 Discussion 85

CHAPTER 4. A thixotropic model of muscle spindle function based on cross-bridge Dynamics 91
4.1 Introduction 91
4.2 Methods 94
4.2.1 Intrafusal muscle model 94
4.2.2 Model of muscle spindle responses to stretch of intrafusal muscle 103
4.2.3 Occlusion between dynamic and static components 104
4.2.4 Simulations 105
4.3 Results 107
4.3.1 Response of intrafusal muscle model to imposed stretch and shortening 107

4.3.2 Response of the muscle spindle rate model to ramp-hold-release stretch 109
4.3.3 Model dynamic response has fractional power relationship with stretch velocity 109
4.3.4 Reduction in dynamic response caused by prior movement scales inversely with inter-stretch time interval 111
4.3.5 Reduction in dynamic response caused by prior movement scales with amplitude of pre-movement stretch 114
4.3.6 Activation dependence of muscle spindle model response to stretch 116
4.4 Discussion 119

CHAPTER 5. Conclusions 124
5.1 Future experimental directions 126
5.2 Future computational directions 129

REFERENCES 132

LIST OF TABLES

Table 3-1 **Unit Ionic Conductances and Reversal Potentials used in model neuron** 64

Table 4-1 **Constant sarcomere model parameters** 99

LIST OF FIGURES

Figure 1-1	**Schematic diagram of a mammalian muscle spindle.**	4
Figure 2-1	**Similarity of muscle spindle IFRs and musculotendon force-related variables during stretch.**	28
Figure 2-2	**Linear regression of perturbation acceleration and muscle dF/dt to muscle spindle initial burst amplitude in 6 afferents.**	30
Figure 2-3	**Reconstruction of muscle spindle firing rates by two candidate models.**	32
Figure 2-4	**Estimated muscle fascicle length.**	35
Figure 2-5	**Single muscle spindle afferent statistics and model parameter estimates.**	37
Figure 2-6	**Comparison of candidate models' abilities to predict muscle spindle Ia afferent IFRs.**	41
Figure 3-1	**Muscle fiber force estimation from recorded data.**	59
Figure 3-2	**Responses of muscle spindle Ia afferents to stretch.**	68
Figure 3-3	**Measured and estimated history-dependent variables of the muscles and Ia afferents.**	71
Figure 3-4	**Comparison of the ability of force- and length-related models to predict Ia afferent firing responses to stretch.**	73
Figure 3-5	**Comparison of force- and length-related models to predict Ia afferent firing rates across all trials and afferents.**	76
Figure 3-6	**Variability in four model parameters across perturbation characteristics for each afferent.**	77
Figure 3-7	**Estimated muscle fiber force-related model predicts changes in muscle spindle encoding caused by axonal stimulation.**	79

Figure 3-8	**Estimated muscle fiber force-related model predicts changes in muscle spindle encoding caused by oxaliplatin-induced channelopathy.**	82
Figure 3-9	**Estimated fiber force-related model predicts range of muscle spindle afferent phenotypes when used as input to model neuron.**	84
Figure 3-10	**Estimated muscle fiber force model predicts inter-afferent variability of healthy afferent firing properties across perturbation velocity and acceleration.**	86
Figure 4-1	**Two-state dynamic system of myosin binding and unbinding.**	97
Figure 4-2	**Schematic of length variables accounted for in muscle model.**	99
Figure 4-3	**Rate equations for myosin dynamics.**	104
Figure 4-4	**Response of the intrafusal muscle model to different stretch sequences.**	110
Figure 4-5	**Different predicted muscle spindle afferent response phenotypes predicted by changing the relative weights of contribution from the static and dynamic fibers.**	112
Figure 4-6	**Responses of model to increasing stretch velocity.**	113
Figure 4-7	**Responses of model to increasing inter-stretch intervals.**	115
Figure 4-8	**Responses of model to increasing pre-stretch amplitude.**	117
Figure 4-9	**Changes in model responses to stretch with changes in activation state of the intrafusal muscle fiber models.**	119

SUMMARY

Proprioception, or the sense of one's own body, is an essential part of the neural control of movement, as evidenced by the profound deficits in movement abilities after loss of proprioceptive afferent information to the central nervous system. Muscle spindles are primary proprioceptive sense organs embedded within skeletal muscles that that are thought to be sensors of muscle length and velocity. However, the relationship of muscle spindle firing with muscle length and velocity is history-dependent and we do not have a mechanistic understanding of these phenomenon, which are implicated in a range of both healthy and impaired states. Thus, understanding the nature of mechanotransduction in muscle spindles is critical for understanding sensorimotor control. Here, we present the first-ever model capable of history-dependent muscle spindle encoding based on hypothesized muscle contractile mechanisms governing muscle spindle encoding for sensorimotor control. First, we predicted Ia afferent firing rates in response to passive stretch using only recorded force variables, in contrast to previous studies focusing on length-related variables. We showed that muscle force-related variables could parsimoniously explain muscle spindle primary, or Ia, afferent firing features even in history-dependent conditions, when length-related variables could not. Next, we found that changing single parameters in our simple descriptive model could account for not only variability in firing features across different Ia afferents, but also changes to Ia afferent firing in neural impairments. Finally, we built a mechanistic model based on history-dependent muscle cross bridge cycling that was capable of producing many classical yet unexplained features of muscle spindle sensory responses across different movement and

activation contexts. Our multi-scale muscle spindle function is the first-ever muscle spindle model capable of history-dependent sensory encoding observed in muscle spindles. Our model could advance sensorimotor control research by providing a model of history-dependent muscle spindle function across healthy and impaired conditions at multiple scales.

CHAPTER 1. INTRODUCTION

In the nearly two centuries since Charles Bell first described the "the nervous circle which connects the voluntary muscles to the brain" (Bell 1826), we have learned a great deal about the importance of the sense of movement provided by muscle, joint, and skin mechanoreceptors: it is now firmly established as essential to human and animal neural control of movement. Profound deficits in movement are observed after loss of proprioceptive information (Rothwell et al. 1982; Akay et al. 2014), and dysfunction of proprioceptive circuits may underlie many sensorimotor disorders, such as spasticity, which manifests in multiple neurological disorders (Sheean 2002).

Muscle spindles are a class of proprioceptors within the muscle that provide sensory information in response to muscle stretch and are generally considered to play a primary role in position and movement sense of limbs, along with contributions from Golgi tendon organ, skin, and joint receptors (Proske and Gandevia 2012; Proske and Gandevia 2009). Understanding the nature of sensory encoding in proprioceptors, particularly muscle spindles, is thus critical for understanding both healthy and impaired sensorimotor control.

1.1 A brief history of the understanding of muscle spindle structure

Just before the turn of the 20th century, Sherrington (Sherrington 1894) and Ruffini (Ruffini 1898) independently came to the conclusion that the function of the "neuromuscular spindle" was of a sensory nature, and not as a "muscle bud" or center of an inflammatory process within the muscle, as had been argued at the time (P. Matthews 1981). It was these works of Sherrington (Sherrington 1894) and Ruffini (Ruffini 1898)

that led to the general view of the muscle spindle that is still accepted today: they are sensory organs consisting of so-called "intrafusal" muscle fibers that are richly innervated by both afferent and efferent supplies (Hulliger 1984).

Ruffini can be credited as the first to document many anatomical and morphological features of the muscle spindle in great detail (Ruffini 1898). In his anatomical illustrations, he identified the encapsulated equatorial region of the bundle of intrafusal fibers, on which the larger sensory afferent fibers – now known to correspond to the large Ia afferent neurons – terminated. He observed a second neural fiber-type which terminated on the juxtaequatorial regions (adjacent to the equatorial regions), now known to be the endings of group II afferent neurons. Finally, Ruffini also correctly identified specialized motor neurons of the muscle spindle, called gamma motor neurons, which terminated in the polar regions of the intrafusal fibers made up of striated muscle.

The general anatomical descriptions originally set forth by Ruffini have not been corrected in any significant way to this day. Instead, in the following decades, these general features of the spindle were subdivided and expanded as the need arose. It was not until 1950s that a significant expansion to Ruffini's anatomical descriptions was made by Cöers and Durand , who demonstrated that the "flower spray" endings identified by Ruffini were probably motor in function (Coërs and Durand 1956). In 1962, Ian Boyd stressed the structural differences between some of the intrafusal fibers based on the spatial concentration of intracellular nuclei (Boyd 1962). Intrafusal fibers with large concentrations of nuclei within the sensory region of the fiber, arranged in a sort of "bag," were aptly named the "nuclear bag fibers." The fibers with a more diffuse concentration of nuclei in a "chain" arrangement were named the "nuclear chain fibers" (Boyd 1962).

In the 1960s, there was an additional expansion of Ruffini's anatomical descriptions, dividing the nuclear bag fibers into two groups: bag1 and bag2 fibers based on several morphological differences. First, there are significantly fewer elastic fibers in bag1 compared to bag2, which presumably differentiate the function of the two fibers (Gladden 1976; Cooper and Gladden 1974). Second, sarcomere-level differences between the nuclear bag1, bag2, and chain fibers were also identified, further implying a functional separation between the three fiber types (Banks, Harker, and Stacey 1977).

Today, we have a schematized understanding of the structure of mammalian muscle spindles that is based largely on Ruffini's original descriptions and the later expansions of them (Figure 1-1). The prevailing hypotheses of the structure-function relationship of muscle spindles is that, with some degree of overlap, the nuclear bag1 fibers are primarily responsible for the "dynamic" component of activity in the muscle spindle afferent response to stretch, whereas the nuclear bag2 and chain fibers are primarily responsible for the "static" component of activity (Banks et al. 1997).

Other important discoveries of morphological features of the muscle spindle have been made at multiple scales in more recent years, such as the discovery of synaptic-like vesicles within the sensory receptor (Bewick 2015) and identification of specific mechosensitive ion channels within the sensory endings (Carrasco, Vincent, and Cope 2017; Bewick and Banks 2015), though the details of these studies are not yet widely incorporated into a schematic of the muscle spindle.

1.2 Responses of muscle spindle Ia afferents to stretch stimuli

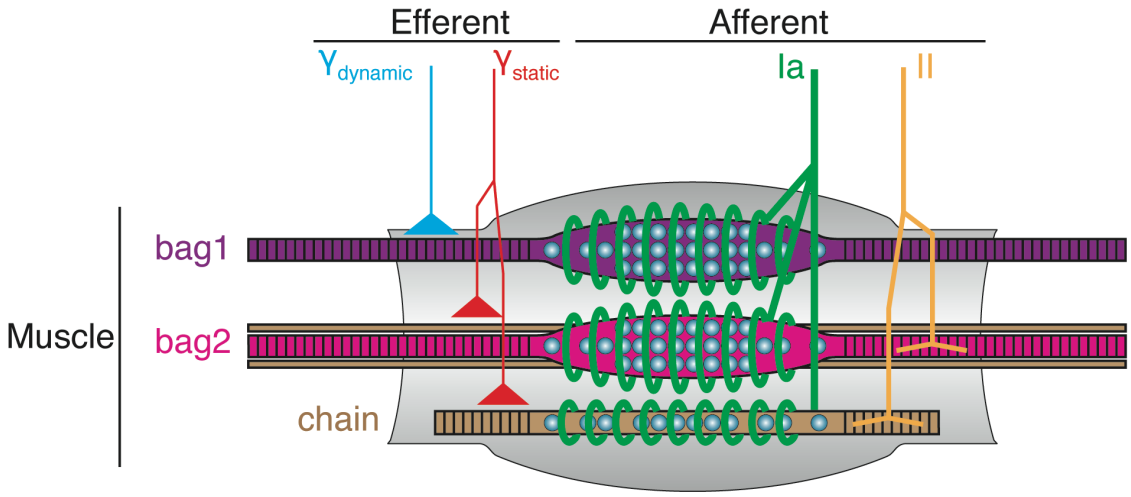

Figure 1-1 – Schematic diagram of a mammalian muscle spindle. The spindle consists of several encapsulated intrafusal muscle fibers richly innervated by both sensory afferents and motor efferents. The nuclear bag1, bag2, and chain fibers differ not only in structure, but also in sensory and motor innervation. The focus of this thesis is the coding properties of the Ia afferent, which terminates in the equatorial region of the bag1, bag2, and chain fibers.

A considerable about of research in the last century has gone into understanding functional responses of the muscle spindle sensory receptors to movement. Central to this research is the question: What are the stimuli encoded by the action potentials in muscle spindle sensory afferents?

Muscle spindles have long been considered as muscle length and velocity receptors (Houk, Rymer, and Crago 1981; P. Matthews 1981). In part, this is due to their in-parallel alignment with extrafusal muscle (Fulton and Pi-Suñer, 1927), because mechanical elements in this arrangement share a common length and velocity (B. H. C. Matthews 1933). More important to the classification of the muscle spindle as a muscle length and velocity sensor was the increase in the firing rate of action potentials by the spindle afferent fibers during applied eccentric movements. In 1927, Fulton and Pi-Suñer discovered that in a distally-detached muscle from a decerebrate cat, the muscle receptor responsible for

the myotatic stretch reflex must lie in parallel to the contractile tissues (Fulton and Pi-Suñer, 1927). They correctly postulated that "the end organs within the fleshy parts of the muscle are responsible for the [knee-jerk reflex]," and that these sensors are primarily concerned with sensing the elongation of the muscle.

B.H.C. Matthews was the first to record from single muscle spindle afferents in frog (B. H. C. Matthews 1931) and in cat (B. H. C. Matthews 1933), in which he was also the first to study the dynamic temporal behavior of the so called "A-1" endings (now known to be Ia afferents of the muscle spindle) to elongation of the muscle. He showed that, during ramp-hold stretches applied to the soleus muscle in cat, the A-1 ending would fire with increased sensitivity during the positive-velocity portion of the stretch, with a lower sensitivity during isometric hold: a finding that perpetuated the idea of muscle spindle primary endings as velocity and length sensors.

In the years that followed, a primary focus was placed on relating the frequency of discharges in muscle spindle afferents with characteristics of the applied stretch, such as length, velocity, or even acceleration. There are far too many studies to discuss explicitly here, but a few important findings are highlighted. P.B.C. Matthews, a bastion of this work, defined functional measurements of muscle spindle responses that are still used today. One of his most important contributions came in 1963, when he described the nonlinear change in so-called "dynamic response" with increasing stretch velocity (P. B. C. Matthews 1963). This measurement was related to the plateau response following the stretch and named "dynamic index" which is a commonly-used description of a muscle spindle's sensitivity to the velocity of stretch. The budding philosophy of the day became that muscle spindles might encode specific variables of the stimulus, such as length and velocity, independently

as a sum of components (P. B. C. Matthews 1981). However, the work of Houk, Rymer, and Crago raised concerns with this idea, and instead put forward strong evidence of a more complicated fractional power relationship between the firing of a muscle spindle and the velocity of stretch, multiplied by a length-dependent stiffness (Houk, Rymer, and Crago 1981).

As more studies were performed on the specific aspects of a stretch stimulus that were encoded by muscle spindles, more addendums were made to the rule of length and velocity encoding by the spindle afferents. As time went on, firing rates of muscle spindle primary afferents were shown to have nonlinear, non-unique, history-dependent relationships to musculotendon length and velocity that confounded the idea of these signals as idealized responses to length and velocity.

One aspect of the muscle spindle response to stretch that had largely been ignored was the high-frequency burst of action potentials upon stretch initiation. This burst at the onset of stretch is observed after the muscle has been at rest and is likely due the initial, history-dependent short-range stiffness of muscle fibers (Lennerstrand and Thoden 1968; P. Matthews and Stein 1969; Richmond and Abrahams 1979; Schäfer 1967; Schäfer and Kijewski 1974; Proske and Stuart 1985). Although the physiological relevance of initial bursts has been questioned (P. Matthews 1981), it is present in awake humans in both upper (Dimitriou 2014) and lower (Day et al. 2017) limb muscle spindle afferents. Because the initial burst temporally corresponds with the positive peak in acceleration at the beginning of a ramp stretch, it has been considered as an acceleration signal (Lennerstrand and Thoden 1968; Schäfer 1967; Schäfer and Kijewski 1974). However, the initial burst is not present when the muscle is repeatedly stretched and shortened and takes several seconds

to recover in amplitude after appearing at stretch onset (Haftel et al. 2004; Proske and Stuart 1985), which reduces its ability to act as a faithful acceleration signal.

The initial burst is one of several "history-dependent" properties of muscle spindle IFRs that resemble history-dependent forces when both active (Huyghues-Despointes, Cope, and Nichols 2003; Campbell and Lakie 1998; Campbell and Moss 2000; Campbell and Moss 2002) and passive extrafusal muscle fibers are stretched (Proske and Morgan 1999). These history-dependent phenomena have been at least partially attributed to the history-dependent kinetics of contractile mechanisms (i.e. actin-myosin cross bridge behavior) present in both extrafusal and intrafusal fibers (Nichols and Cope 2004; Proske, Tsay, and Allen 2014). History-dependence is specifically thought to arise from actin-myosin cross-bridge interactions in the intrafusal fibers, akin to the history-dependence manifested in the stretch reflex and extrafusal muscle fiber force (Haftel et al. 2004; Nichols and Cope 2004; Campbell and Lakie 1998; Campbell and Moss 2000; Campbell and Moss 2002).

Muscle spindle firing has been modestly implied previously to relate to musculotendon tension or joint torque, but the supporting evidence has been indirect and qualitative. In P.B.C. Matthews' early work, he showed passive tension traces from the muscle in response to stretch alongside muscle spindle IFRs, implying similarity between the two (P. B. C. Matthews 1963). Later, Hunt and Ottoson (Hunt and Ottoson 1975) showed similarities between tension in intrafusal fibers and the muscle spindle receptor potentials from a tail muscle in cat, accounting for so-called "receptor adaptation" during plateau of stretch, though varying amounts of muscle mass near the motor compared to that near the receptor created inconsistencies in the tension traces of the fiber. Lewis and Proske

(Lewis and Proske 1972a) also alluded to tension information in spindle firing rates. In humans, rate adaptation in muscle spindles when the wrist is held isometrically after ramp stretch resembles wrist torque profiles generated by cross-bridge mechanisms (Cordo et al. 2002).

1.3 Non-classical muscle spindle function in the control of movement

A common question when discussing nonlinear or history-dependent muscle spindle function is one related to its relevance in sensorimotor control. A few areas in which nonlinear or history-dependent muscle spindle function has affected the neural control of movement are described here.

First, Haftel and collegues showed that history-dependent sensory feedback from muscle spindle Ia afferents crosses the monosynaptic stretch reflex pathway in the spinal cord (Haftel et al. 2004). In the anesthetized rat, when repeated ramp-release sequences were applied to the musculotendon, history-dependent dynamic responses to stretch were observed in the Ia axons of the muscle spindle afferents such that prior movements significantly decreased the dynamic sensitivity of the Ia afferent to identical stretch stimuli. Simultaneously, they observed ventral root potentials that had analogously history-dependent dynamic responses to the muscle stretch, though it did not exhibit an initial burst at the onset of the first stimulus. Nevertheless, these findings showed direct evidence for the crossing of muscle spindle history-dependent sensory signals into the motor domain.

In the intact hindlimb of anesthetized cats, horizontal plane perturbations applied to the foot elicited highly sensitive, directionally-tuned bursts at perturbation onset resembling the initial bursts previously observed from sagittal plane perturbations applied

to the isolated muscle (Honeycutt et al. 2012). This study concluded that the rapid autogenic proprioceptive pathways, which are driven by muscle spindle sensory feedback, are largely responsible for driving the muscle responses which maintain balance. Although history dependence was not examined specifically in this context, the history-dependent nature of the initial burst and dynamic observed in isolated muscles response (Proske and Stuart 1985; Haftel et al. 2004) combined with the findings of this study implies that history-dependence plays a large role in the sensorimotor control of posture. Indeed, similar initial bursts of activity as seen in muscle spindle responses have even been observed in the sensorimotor responses for balance in humans and animal (Lockhart and Ting 2007; Welch and Ting 2009; Welch and Ting 2008; Safavynia and Ting 2013b; Safavynia and Ting 2013a) and are permanently absent after the selective loss of large proprioceptive afferents, including muscle spindle Ia afferents (Lockhart and Ting 2007).

History-dependent effects in muscle spindle encoding are also apparent in psychophysical proprioception research (Proske and Gandevia 2012). In this realm, the activation-history of the spindle-bearing muscle, and thus, the spindle's intrafusal fibers, is considered the most important factor in determining the sensitivity of the muscle spindle afferent response to movements. Proske and Gandevia claim that several features of conscious proprioception have a basis in muscle history-dependence, or thixotropy. For example, they claim the common report that proprioceptive senses are more accurate during active movements than during passive ones is probably based on thixotropic effects in muscle spindles. Further, direction and distribution of proprioceptive errors coincide with the expected changes in the position sensitivity of the muscle spindle due to thixotropic effects (Proske, Tsay, and Allen 2014). They also attribute proprioceptive

"drift" experienced by blindfolded subjects to muscle spindle history dependence (Tsay et al. 2014). More recent psychophysical research has even claimed that muscle spindle thixotropy affects perception of force (Luu et al. 2011; Monjo and Forestier 2018).

1.4 Current models of muscle spindle sensory function

Muscle spindle models have thus far been developed with a phenomenological approach, transforming musculotendon kinematic information into receptor potentials that match firing rate features observed *in vivo* from highly stereotyped and idealized stretch perturbations from isolated muscles (Hasan 1983; Lin and Crago 2002; Mileusnic et al. 2006). Considerable effort and detail has been put into reproducing firing features such as initial burst, dynamic response, and receptor adaptation in response to an idealized ramp-hold stretch paradigm. These models have been generalized for a small range of behaviors, including different levels of fusimotor activation.

Phenomenological models relating muscle spindle activity to easily-recorded variables have shown to be useful in a number of applications, such as for neural interfaces (Prochazka and Gorassini 1998a; Weber et al. 2006; Weber et al. 2007; Rigosa et al. 2011). However, these models only give an accurate representation during steady-state locomotion and are not generalizable to other behavioral states such as standing balance.

The phenomenological nature of these transformations of intrafusal fiber mechanics into spindle receptor potentials for a specific stretch-type has allowed for a reduction in computational power necessary for simulation, but also increased the likelihood that these models are over-fit to the data (Burnham and Anderson 2003; Blum,

Lamotte D'Incamps, Zytnicki, and Ting 2017b), and thus not extendable to arbitrary muscle stretches, such as a repetitive stimulus (Haftel et al. 2004).

Currently, there are no model of muscle spindle function that is capable of faithfully representing the sensory signals across behavioral states, because no current models incorporate movement- or activation-history dependence.

1.5 Objective of this thesis

Can we build a model capable of generally representing the history-dependent and nonlinear features of muscle spindle firing that we believe are important in sensorimotor control research? Further, can such a model be constructed parsimoniously, without the concatenation of many separate models (Nichols and Cope 2004)?

Eccentric tension, i.e., the force generated in response to extending a muscle, reflects the passive force response of both cross-bridge mechanisms and passive tissue to changes in length (Proske and Morgan 1999). Therefore, the encoding of intrafusal muscle tension by muscle spindles is an attractive, but not yet quantitatively tested hypothesis about the mechanical origins of history-dependent muscle spindle firing rates.

In this thesis, I use top-down approaches in which I infer mechanisms of muscle spindle mechanotransduction from experimental data (Chapters 2 & 3) and bottom-up approaches in which I use a hypothesized mechanism to predict experimental data (Chapters 3 and 4) to build a complete, novel model of muscle spindle function capable of nonlinear and history-dependent responses. In Chapter 2, I use data collected from muscle spindle Ia afferents and the triceps surae muscle in anesthetized cats to formulate a

phenomenological relationship between muscle force-related variables and history-dependent spike rates. In this chapter, I use a pseudolinear combination of recorded passive musculotendon force and its first time-derivative, yank, as proxies for the force and yank in the intrafusal fibers to describe and predict history-dependent Ia afferent firing rates in response to a range of stretch characteristics. In Chapter 3, I extend this descriptive model to use in the anesthetized rat by using an estimate of intrafusal muscle stress calculated using recorded musculotendon force and a simple model of the noncontractile tissues in the passive triceps surae. Additionally, I use the estimated intrafusal force as an input for a model neuron in order to simulate a range of afferent response phenotypes spanning healthy and diseased states. Finally, in Chapter 4, I use the theoretical mechanisms of history-dependent intrafusal cross-bridge cycling to construct a forward model of muscle spindle function. As is discussed in the chapter, this model is capable of not only history-dependent responses to stretch in a passive muscle, but also exhibits several emergent properties of muscle spindle responses previously written off as nonlinear sensitivities to muscle length and velocity. This model not only sheds light on the potential mechanisms behind nonlinear and history-dependent muscle spindle encoding, but also provides researchers with a tool that can be used at multiple scales of sensorimotor control.

CHAPTER 2. FORCE ENCODING IN MUSCLE SPINDLES DURING STRETCH OF PASSIVE MUSCLE

2.1 Attribution of efforts

The following chapter was published in the journal Public Library of Science (PLoS) Computational Biology with 3 co-authors: Boris Lamotte d'Incamps, Daniel Zytnicki, and Lena Ting (Blum, Lamotte D'Incamps, Zytnicki, and Ting 2017b). The data was collected by Lena Ting and Boris Lamotte d'Incamps in the laboratory of Daniel Zytnicki. Funding for the experiments was provided by Daniel Zytnicki.

2.2 Introduction

Proprioceptive sensory information is essential to movement, particularly in sensorimotor responses to external perturbations to the body–such as a push or bump–whether maintaining the posture of a limb, or during standing balance control (Macpherson and Horak 2013). Following a postural perturbation to standing balance, a transient pattern of corrective muscle activity follows the time course of the displacement, velocity, and acceleration of the body caused by the perturbation (Welch and Ting 2009; Safavynia and Ting 2013a; Safavynia and Ting 2013b) that is impaired after proprioceptive loss (Lockhart and Ting 2007; Stapley et al. 2002). Thus, the transformation between mechanical events in the body due to an external perturbation and the transient firing of proprioceptive afferents is critical to understanding sensorimotor control of posture and balance (Chiel et al. 2009; Ting et al. 2012). Muscle spindle proprioceptive receptors likely play a primary role in encoding the effects of perturbation on the body as they fire trains of action

potentials during muscle stretch that vary as a function of experimentally-imposed muscle length and velocity (P. B. C. Matthews 1963; P. B. C. Matthews and Stein 1969; P. B. C. Matthews and Stein 1969; Elek et al. 1990; Lewis and Proske 1972a; Lennerstrand and Thoden 1968). However, our current understanding and computational models of muscle spindle sensory encoding are insufficient to account for several transient and history-dependent properties of muscle spindle firing rates observed experimentally, and that also appear to be important in postural control.

Muscle spindle instantaneous firing rates (IFRs) in response to muscle stretch are not uniquely related to muscle length and velocity, but exhibit transient, history-dependent features in conditions relevant to detection and sensorimotor responses to postural perturbations. If a muscle is held at a constant length for a period of time before being stretched, two history-dependent features in muscle spindle IFRs appear that are absent if the muscle has been moving directly prior to stretch: 1) an initial burst of action potentials at the onset of stretch, and 2) an elevated firing rate during constant velocity ramps (Haftel et al. 2004). Because muscles are maintained at a constant length during control of posture and balance, these history-dependent features likely play a critical function in the detection of and sensorimotor response to perturbations. Moreover, both the initial burst of muscle spindle sensory signals and the initial burst of muscle activity evoked by postural perturbations have been shown to vary with perturbation acceleration (Welch and Ting 2008; Lockhart and Ting 2007; Schäfer 1967; Schäfer and Kijewski 1974). A third history-dependent feature called rate relaxation, or rate adaptation, is observed where the tonic firing rate of the muscle spindle decreases when the muscle is held at a constant length after being stretched (Boyd 1976).

Current muscle spindle computational models fail to predict some history-dependent characteristics of muscle spindle IFRs (Hasan 1983; Mileusnic et al. 2006; Lin and Crago 2002). The most commonly-used computational muscle spindle models use a muscle model to estimate stress in the intrafusal muscle fibers, found within muscle spindle sensory organs, based on measured changes in muscle length. The strain experienced by the sensory region of the fiber is then estimated with a linear model to predict responses to ramp-and-hold stretch perturbations (Hasan 1983; Lin and Crago 2002; Mileusnic et al. 2006). Such models are generally capable of reproducing firing patterns in response to ramp stretches either when the muscle has been at rest, or when it has been moving prior to stretch, but they cannot account for spindle firing rates during transitions in movement state, which occur frequently in mammalian behavior (Nichols and Cope 2004). For example, some muscle spindle models fail to capture the history-dependent nature of the initial burst based on the muscle state history (Haftel et al. 2004; Hasan 1983; Lin and Crago 2002), while others lack an initial burst altogether (Mileusnic et al. 2006).

It has been proposed that the transient, history-dependent properties of muscle spindle firing are due to history-dependent muscle forces arising from non-steady-state cross-bridge dynamics (Proske and Stuart 1985; Tsay et al. 2014; Proske and Gandevia 2009; Campbell and Lakie 1998; Campbell and Moss 2000; Campbell and Moss 2002). Thus, the lack of history-dependence in muscle spindle models may be due to the use of phenomenological muscle force models (e.g., Hill-type muscle models) that do not account for history-dependence (Hasan 1983; Lin and Crago 2002; Mileusnic et al. 2006). Experiments in muscle physiology have demonstrated history-dependence in muscle fiber forces, including a transient increase in force and the first time derivative of force (dF/dt)

when an isolated, permeabilized muscle fiber activated in a calcium solution is stretched after being held isometrically. In intact muscles, a similar his- tory-dependent transient force is observed when a muscle is stretched after being held isometrically, often referred to as short-range stiffness (Rack and Westbury 1974; Proske and Morgan 1999). This history-dependence is thought to arise from movement-dependent cycling of muscle cross-bridges (Campbell and Lakie 1998; Campbell and Moss 2000; Campbell and Moss 2002; Proske and Morgan 1999), and can be reproduced using models of cross-bridge kinetics (Campbell and Lakie 1998; Campbell and Moss 2000; Campbell and Moss 2002). Such muscle fiber force history- dependence has been implicated as a cause of history-dependent muscle spindle IFRs, but not yet demonstrated directly (Haftel et al. 2004; Nichols and Cope 2004; Proske and Stuart 1985; Proske and Morgan 1999). Classic studies of muscle spindles also remarked on qualitative parallels between muscle spindle firing rates and muscle force transients during stretch (Lewis and Proske 1972a; Proske and Stuart 1985). Moreover, transient features similar to force and dF/dt are evident in figures of rare recordings of receptor potentials in the encoding regions of muscles spindle afferents (Hunt and Ottoson 1975; Hunt and Wilkinson 1980). However, technical limitations of the day prevented direct and quantitative testing of the hypothesis that transients and history-dependence in muscle spindle IFR encode muscle fiber force, beyond highlighting qualitative similarities between the traces.

Thus, towards improved computational models of proprioceptive encoding relevant to postural control, we performed quantitative analyses of muscle spindle spike trains to identify transformations between muscle mechanical events that best predict transient and history- dependent features of muscle spindle firing rates during muscle stretch. We

directly tested the hypothesis that transient, history-dependent muscle spindle IFRs during stretch of a passive muscle encode information about muscle force. Here, we use "passive" to mean that the muscle is electrically-quiescent and lacks neural drive, as our experiments were conducted in deeply-anesthetized animals, but it is likely that muscle cross-bridge cycling is not completely absent. We collected muscle spindle firing rates across a wide variety of muscle stretch kinematic conditions in which a large range of initial burst amplitude, dynamic response, and rate relaxation characteristics were elicited. We tested whether pseudolinear combinations of muscle force-related versus length-related variables could better predict the temporal features of muscle spindle afferent IFRs including history-dependent firing characteristics. For each afferent recorded, we identified a unique set of parameters that best fit muscle state variables to spindle IFRs across all stretch conditions. Based on the goodness of fit and number of parameters, a model consisting of pseudolinear combinations of recorded muscle force and the first time derivative of force, dF/dt, was found to be the most likely model of muscle spindle IFRs across a wide range of passive muscle stretch conditions. To our knowledge, this is the first quantitative evidence that muscle spindle firing rates in transient, history-dependent conditions can be uniquely determined by muscle force. Our findings suggest that transient sensory information encoded by muscle spindle primary afferents in passive muscles is driven by transient mechanical properties of muscle cross bridges, as evidenced by history dependence in force- but not length-related variables.

2.3 Methods

2.3.1 Ethics Statement

In accordance with French legislation, the animal facility, experimental room, and investigators had valid licenses (75-789-R) to perform experiments on live vertebrates delivered by the Direction des Services Vétérinaires (Préfecture de Police, Paris, France). Animals in this study were anesthetized with sodium pentobarbital given intravenously and monitored continuously. Animals were sacrificed at the end of the experiments with a large bolus of sodium pentobarbital also given intravenously.

2.3.2 Data Collection

We collected data from muscle spindle Ia afferents in response to stretch perturbations of the isolated triceps surae musculotendon in anesthetized cats. Experiments were performed on 5 adult cats (2.8–3.3 kg) deeply anesthetized with sodium pentobarbital (Pentobarbital; Sanofi Recherche, Montpellier, France). Anesthesia was induced with an initial intraperitoneal injection (45 mg/kg). Animals were deeply anesthetized, with the level of anesthesia constantly assessed by monitoring the stability of the heart rate, blood pressure (measured through a carotid catheter), the maintenance of myotic pupils, and the absence of nociceptive reflex. It was supplemented whenever necessary (usually every 2 h) by intravenous injections (3–6 mg/ kg) of pentobarbital. The anesthesia was deep enough to prevent any pain as indicated by the fact that noxious stimuli (induced by pinching the ear or the foot paw) did not elicit any heart acceleration or blood pressure changes. Animals were paralyzed with Pancuronium Bromide (Pavulon; Organon, Puteaux, France) at a rate of 0.4 mg/h and artificially ventilated (end-tidal P_{CO2} maintained at *4%). This allowed us to perform a bilateral pneumothorax in order to prevent movements of the rib cage during the recordings. At the onset of experiment, amoxicillin (500 mg; Clamoxyl; Merieux, Marcy l'Etoile, France) and methylprenidsolone (5 mg; Solu-Medrol; Pfizer,

New York, NY) were given subcutaneously to prevent the risk of infection and edema, respectively. The central temperature was kept at 38℃ with the help of a thermo- controlled blanket. Blood pressure was maintained above 90 mmHg by perfusion of a 4% glucose solution containing $NaHCO_3$ (1%) and gelatin (14%; Plasmagel, Roger Bellon Laboratories, Neuilly, France) at a rate of 3–12 ml/h. A catheter allowed evacuation of urine from the bladder. At the end of the experiments, animals were given a lethal intravenous injection of pentobarbital (250 mg).

The dorsal aspect of lumbar segments (L1-L6) was exposed to allow electrode access to the dorsal columns. The triceps nerve was dissected without alteration of its continuity with the muscle and mounted on a bipolar stimulation electrode. The Achilles tendon was detached from the calcaneus and the isolated bone fragment attached to the tendon was affixed to a muscle puller (Aurora 310B LR, Aurora, ON, Canada) to control the elongation of the attached muscle and to measure the force developed at the tendon. The initial length of the triceps was set to maintain a low level of resting tension (typically 0.1 N) but could be adjusted to reach a low resting firing of the afferents. A pool filled with mineral oil heated at 38℃ was made around the triceps surae and its nerve.

A sharp microelectrode (KCl 3M, Resistance 11.5–20 MO) was driven into the dorsal horn of the spinal cord at the location of the largest afferent volley upon electrical stimulation of the triceps nerve. The high electrical resistance of the electrode allowed us to isolate a single afferent that displayed an all-or-none spike in response to nerve stimulation. Identified afferents were classified as Ia based on axonal conduction velocity 74 m/s and on response to the rising phase of a small stretch. To facilitate spike detection,

voltage recordings were high-pass filtered at 500 Hz to remove drift. Recordings lasted as long as the signal-to-noise ratio allowed us to differentiate spikes from background noise.

Musculotendon length, velocity, and tension were sampled at 2 kHz and used to calculate acceleration and the first time-derivative of tension. Low-pass filters were applied to velocity (40 Hz), acceleration (40 Hz), Force (50 Hz), and dF/dt (100 Hz).

Custom musculotendon stretch profiles were designed in Spike2 software to dissociate the effects of velocity and acceleration on the response of the afferent. Multiple stretch perturbation waveforms ranged from 1–4 mm in peak length, 4–50 mm/s in peak velocity, and 200–3500 mm/s in peak acceleration. Rest periods of at least 5 seconds were included between all perturbations (in repeated ramp-release stretches, rest periods of at least 5 seconds were used in between sets of 5 stretches).

2.3.3 Sample Size

No explicit *a priori* power analysis was performed to determine sample size. Experiments were performed over the course of 5 months. At the conclusion of this period, data were screened for quality and it was determined that the available sample of recorded afferents was commensurate with a previous study with similar methodology (Prochazka and Gorassini 1998a).

2.3.4 Data inclusion and exclusion

Analyses treated individual recorded afferents and individual recorded stretch trials as biological replicates and as technical replicates, respectively. To ensure sufficient information for statistical measures, we required that stretch trials have at least 50 recorded

action potentials in order to be included in statistical analyses. Stretch trials with low signal to noise ratio based on visual inspection were excluded. To ensure that each individual recorded afferent had sufficient observations to enable cross-validation during model fitting (below), we required that afferents have at least 40 acceptable stretch trials. This guaranteed at least 30 observations of testing data for each afferent. These criteria yielded suitable datasets for 10 individual afferents. Data available from the Dryad Digital Repository: http://dx.doi.org/10.5061/dryad.pd40m (Blum, Lamotte D'Incamps, Zytnicki, and Ting 2017a).

2.3.5 Initial burst correlations

For correlating the peak initial burst amplitudes with preceding peaks in transient force- and length-related variables (dF/dt and acceleration, respectively), we performed simple least squares linear regressions in Matlab that found a linear function relating peak dF/dt or acceleration to initial burst amplitude,

$$\hat{y} = b_1 x + b_2 \tag{1}$$

where $\hat{y}$ is the estimated initial burst amplitude predicted by x (either peak dF/dt or acceleration). To measure the amount of variance in peak initial burst amplitude explained by peak dF/dt and acceleration, we computed the coefficient of determination

$$R^2 = 1 - \frac{\sum_i (y_i - \hat{y}_i)^2}{\sum_i (y_i - \bar{y})^2} \tag{2}$$

where y is the recorded value of initial burst amplitude, $\hat{y}$ is the predicted initial burst

amplitude, $\bar{y}$ is the arithmetic mean of the recorded initial burst amplitudes, and i denotes the ith data point.

2.3.6 Candidate models

For testing the information encoded by muscle spindle Ia afferent IFRs, we developed 6 candidate models. Candidate models were pseudo-linear in that they used weighted sum of measured variables subjected to a half-wave rectification to account for the unidirectional effects of muscle stretch on muscle spindle spiking behavior. The primary candidate models consisted of linear combinations of musculotendon length-related and force-related variables. Based on previous observations, we tested a model that allowed for muscle velocity to be raised to a fractional power (Hasan 1983; Prochazka and Gorassini 1998b; Houk, Rymer, and Crago 1981). In addition, we also tested the efficacy of length-related variables based on estimated muscle fascicle length using both high and low ten- don stiffness values.

For certain afferents, force and dF/dt components were modeled as competing influences on the IFR, as done previously by Lin and Crago (Lin and Crago 2002). At time points where simultaneous contributions of force and dF/dt were significant, we used an iterative process to set the values of the smaller-magnitude component to zero. The two components were then summed as in the original force-related model. We used the competing model if the mean R2 achieved across all observations was higher than for the original model. This was the case in 4 out of 10 afferents (1, 2, 3, and 6), which also had the largest contributions of dF/dt to the IFR. Although the mechanism of the competition is not clear, it could result if the effects of force and dF/dt components arise from different

branches of the muscle spindle primary afferent endings. Dynamic sensitivity of the muscle spindles is controlled by terminals innervating the bag1 intrafusal fiber, whereas the static response is controlled by the terminals innervating the bag2 and chain intrafusal fibers (Banks et al. 1997).

2.3.7 Fascicle length-related variable estimates

To estimate muscle fascicle length-related variables, we assumed an exponential elastic tendon, based on experiments by Rack and Westbury (Rack and Westbury 1984), to be serially aligned with the muscle fascicle such that the force was equal in the fascicles and the tendon. Using measured musculotendon force, we estimated tendon elongation during stretch and subtracted it from measured musculotendon elongation to estimate fascicle length. We assumed that the pinnation angle of the muscle fascicles remained constant throughout the range of stretches applied to the musculotendon in these experiments. Because a constant pinnation angle would only decrease the fascicle lengths by a constant factor, and because this factor would be eliminated when the muscle fascicle length-related variables were scaled and offset in the model, we ignored the effects of pinnation altogether. We calculated fascicle velocity and acceleration using numerical differentiation of estimated fascicle length.

2.3.8 Time lags and parameter search limits

In order to determine appropriate time lags and parameter search limits for each candidate model, we fit the estimated IFR for each of the 6 candidate models to the IFR of the afferent for a selection of stretch perturbations applied to the muscle. The candidate model parameters, consisting of a weight (k_i) and offset (b_i) for each force-related or

kinematic variable included in the sum, were found via least-squares regression using Matlab's optimization toolbox (*fmincon.m*) and custom scripts. A lumped neuromechanical delay (λ_j) was determined by shifting the timestamp of the muscle variables (e.g. length, force) forward relative to the IFR data to be fit. The form of the models was:

$$IFR_j(t) = \left(\sum_{i=1}^{n} k_i \cdot \left(\lfloor x_i(t - \lambda_j) \rfloor + b_i \right) \right) + e(t) \quad (3)$$

where the IFR of the *j*th model was estimated by a sum of n force- or length-related variables, each of which was temporally shifted by a neuromechanical delay, λ_j (held constant for each model for a given trial), offset by a single value, b_i, and scaled by a gain, k_i. $\lfloor \rfloor$ denote positive values of the argument. Error, $e(t)$, was minimized by finding the set of parameters for each model that minimizes a measure related to $e(t)^2$ (see Data Fitting). In all, the optimization swept through 16 values of λ_j, in 1 ms increments from 0 to 15 ms. Then, the lag value for each trial which yielded the most explained variance (highest R^2 value) were averaged to determine a single lag value for each afferent. This value was also used later for prediction and cross-validation analyses. The weights and offsets (i.e. k_i and b_i) found in this analysis were used to appropriately restrict the parameter search in the prediction and cross-validation analyses of the complete afferent datasets. No statistical tests were performed on the parameters estimated from this analysis.

2.3.9 Cross validation

We used an iterative cross-validation procedure to robustly estimate the fit of each model to recorded IFR data of each afferent. For each model and each afferent, we performed cross-validation as follows. All available stretch perturbations were randomly divided into training (≈75%) and test (≈25%) sets. Using the training dataset, model parameters were identified that minimized the cost function

$$J = \frac{\sum_i (y_i - f_i)^2}{\sum_i (y_i - \bar{y})^2} = \frac{SSE}{SSM} \tag{4}$$

where the numerator represents the sum of squared errors (SSE) between the afferent IFR (y) and the model estimate of IFR (f), and the denominator represents the total sum of squares of the IFR about its mean (SSM). Model fit (R^2) was then assessed using the test IFR dataset. Mean ± SD R^2 values were calculated over a set of 100 iterations of this cross-validation procedure for each model and each afferent.

2.3.10 Model selection

We used the approach of Burnham and Anderson (Burnham and Anderson 2003) to determine which model among our candidate models performed best at predicting recorded muscle spindle spike data. Test set AICc (Akaike Information Criterion, corrected for finite sample sizes) was calculated for each model for each afferent as:

$$AICc = 2\left(k - \ln\left(\hat{L}\right) - \frac{k(k+1)}{n-k-1}\right) \tag{5}$$

where k is the number of estimable parameters in the model, $\hat{L}$ is the maximum value of the likelihood function for the model (here, estimated as J^{-1} of the test set), and n is the number of recorded stretch trials in the test set. Differences in AICc between models for each afferent were calculated as:

$$\Delta_j = AICc_j - \min\{AICc_1 \dots AICc_6\} \tag{6}$$

where Δ_j is the difference in AICc between the *j*th model and the minimum AICc from the set of candidates. AICc differences were used to calculate a set of Akaike weights:

$$w_j = \frac{\exp\left(-\frac{1}{2}\Delta_j\right)}{\sum_{r=1}^{6}\exp\left(-\frac{1}{2}\Delta_r\right)} \tag{7}$$

where w_j is the normalized likelihood of the *j*th model being the best in the set.

To assess the models' abilities to predict the afferent population IFRs, we used similar statistical methods as for the individual afferents. To measure goodness of fit for the entire afferent population, we took the average model R^2 values for each afferent from the 100 optimization procedures and averaged them together, resulting in a single R^2 value for the population. Then, we used a similar averaging procedure to obtain a single AICc value for each model. From these values, we calculated w_j for the entire population as described above.

2.4 Results

2.4.1 Response of muscle spindles Ia afferents to stretch

All muscle afferents were confirmed to be muscle spindle primary afferents using classical criteria, i.e. axonal conduction velocity >74 m/s, resting discharge, and dynamic response to muscle stretch (P. B. Matthews 1963). In five deeply anesthetized adult cats (2.5–3.5 kg), the distal extremity of the triceps surae muscles was isolated, mounted on a length servomotor, and force was monitored (see Methods for further details). Stable recordings across a full protocol of diverse stretch perturbations were achieved in 12 afferents using sharp glass microelectrodes. Peak length, velocity, and acceleration were varied independently to elicit a variety of muscle force and muscle spindle firing responses.

Muscle spindle IFRs showed striking similarities to musculotendon force-related variables, i.e., force and the first time derivative of force (dF/dt), over the entire time course of each stretch perturbation (Figure 2-1A). IFRs exhibited history-dependent features, i.e., initial bursts and dynamic responses during ramp stretches, and rate relaxation during hold periods. These features were associated with changes in length- and force-related variables (Figure 1A red and blue traces, respectively), though the transient behaviors more closely resembled recorded force-related variables. During stretch, the initial burst and dynamic response closely resembled dF/dt. During post-lengthening hold, rate relaxation closely resembled musculotendon force (Figure 2-1B).

2.4.2 Relationship of muscle spindle Ia initial burst magnitude to force- and length-related transients

To test potential variables encoded by the initial burst of spikes at stretch onset, we regressed maximum initial burst amplitude on corresponding peaks in force- and length-

related transients, i.e. whole-muscle dF/dt and acceleration. For 6 afferents exhibiting consistent initial bursts (afferents 1, 2, 3, 5, 11, and 12), we performed a linear regression between the preceding peak in dF/dt or acceleration and peak initial burst amplitude across a minimum of 12 stretch trials in which muscle acceleration was varied systematically.

In these afferents, the peak initial burst amplitude (IBA: peak IFR during the initial burst) increased linearly with either dF/dt or acceleration (Figure 2-2). Either peak dF/dt or acceleration predicted similar amounts of variance in the initial burst amplitudes across all

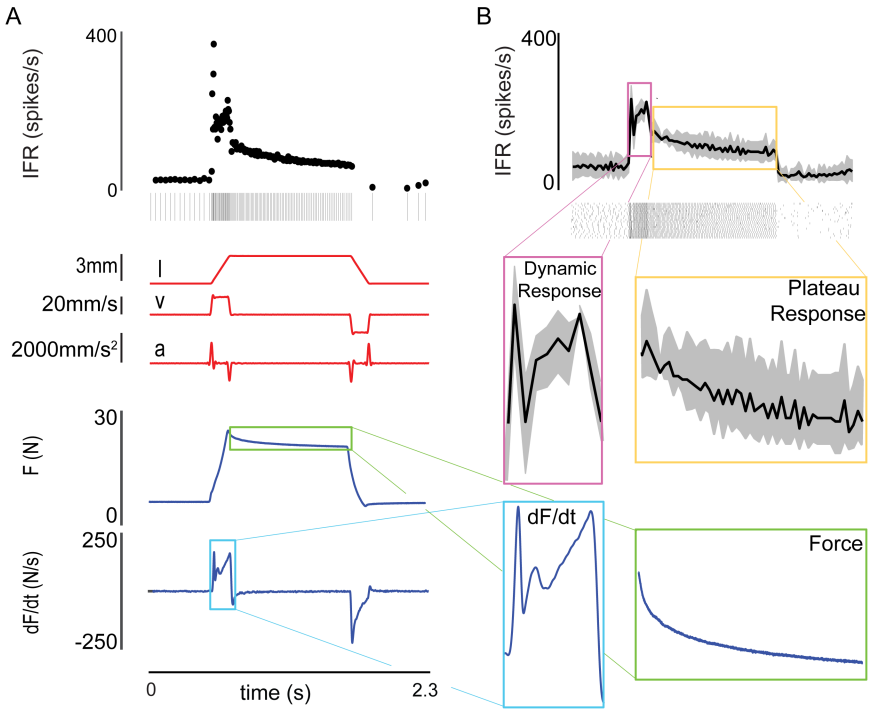

Figure 2-1 – Similarity of muscle spindle IFRs and musculotendon force-related variables during stretch. **(A)** An example ramp-hold-release length profile applied to the triceps surae at the calcaneus, and response of the musculotendon force and muscle spindle primary afferent spiking. The spike train from a single trial and corresponding instantaneous firing rate (IFR) are shown in black at the top as an example of a typical response. Perturbation kinematics (i.e. muscle length, velocity, and acceleration) are shown in red. The musculotendon response to this stretch (i.e. force and dF/dt) is shown in blue. **(B)** The similarities between muscle spindle IFR shown in black at the top (ensemble average of 20 trials with bin size of 20 ms) and the muscle force-related variables shown in A. Specifically, note the similarities between force (green box) and the plateau response of the muscle spindle (yellow box), and between rate change in force (light blue box) and the

dynamic response of the muscle spindle afferent (magenta box). The examples shown are from afferent 2.

6 afferents (R^2 = 0.76 ± 0.08 with dF/dt; R^2 = 0.71 ± 0.09 with acceleration). Peak initial burst firing rate increased with either dF/dt or acceleration in each of the 6 afferents ($p < 0.05$). Although peak acceleration amplitude predicted peak firing rate of the initial burst to a similar degree as peak dF/dt amplitude, acceleration exhibited a second peak during the return of the musculotendon to its initial length (e.g. Figure 2-1A) that did not have a corresponding peak in muscle spindle IFR nor whole muscle dF/dt.

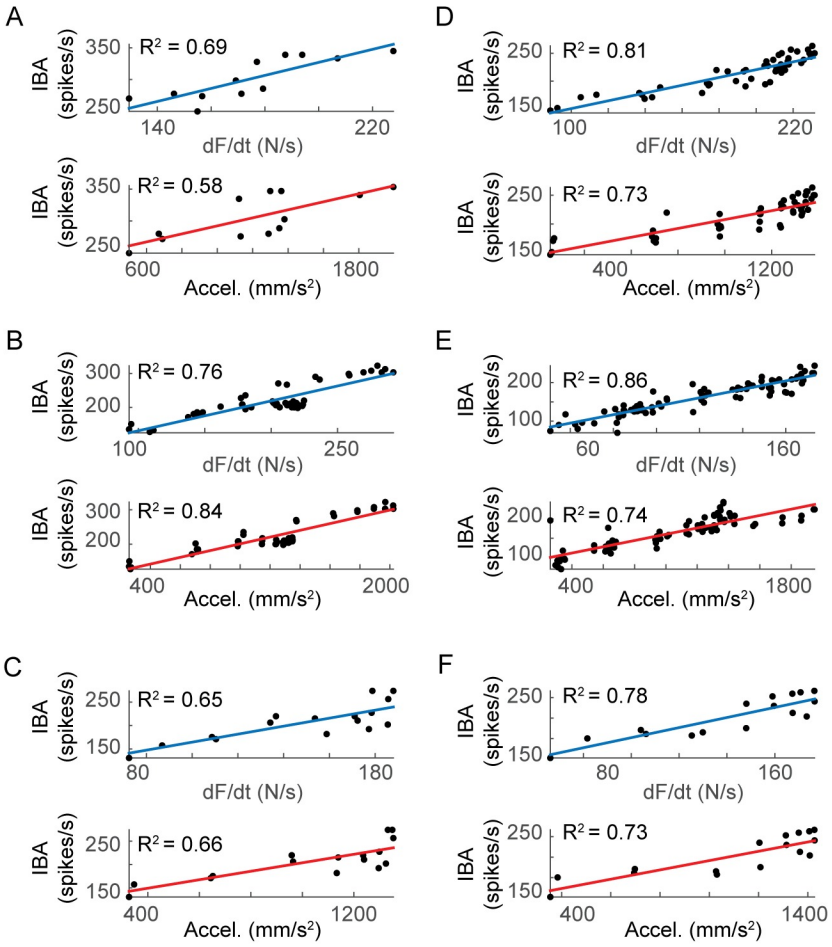

Figure 2-2 – Linear regression of perturbation acceleration and muscle dF/dt to muscle spindle initial burst amplitude in 6 afferents. **(A-F)** Black dots represent the initial burst amplitude (IBA) versus either dF/dt or acceleration. Blue traces indicate linear regression of IBA on corresponding peaks in dF/dt. Red traces indicate linear regression of IBA on

corresponding peaks in acceleration for the same trials. For all 12 cases (6 afferents, 2 regressions each), $p < 0.05$.

2.4.3 Relationship of muscle spindle Ia IFRs to musculotendon length- and force-related variables

To test which musculotendon mechanical variables best reproduced transient, history-dependent muscle spindle IFRs, we developed 2 primary candidate models (Figure 2-3A). The first was a pseudo-linear combination of musculotendon force and dF/dt (Figure 2-3A, blue traces). The second was a pseudo-linear combination of musculotendon length, velocity, and acceleration (Figure 2-3A, red traces). In each model, only positive changes above a threshold value were retained and compared to recorded IFRs. To account for neuromechanical delays, a common lag was applied to each group of variables. For our initial analysis, we estimated parameters of each candidate model and computed the goodness of fit (coefficient of determination, R^2) to recorded IFRs for each afferent on a per-stretch basis (Figure 2-3A). Here, we first present a few examples comparing force-related and length-related model fits to individual stretch responses. In a subsequent analysis, we provide more comprehensive comparisons of several models based on their ability to predict all stretches for each afferent using a single set of parameters.

2.4.4 Force-related but not length-related variables reproduce rate relaxation in fast stretches

While both force- and length-related models could reproduce some features of muscle spindle IFRs, force-related variables better accounted for the details of the IFRs, especially at faster stretch velocities (Figure 2-3B). Both models qualitatively captured IFR

features during a 10 mm/s stretch, with R^2 of 0.93 and 0.79, respectively (Figure 2-3B, left column). As stretch velocity increased to 20 and 40 mm/s, the force-related model reproduced IFRs with high fidelity (Figure 2-3B, blue traces; R^2 = 0.93, 0.94), whereas the length-related model had greatly reduced good- ness of fit (Figure 2-3B, red traces; R^2 = 0.55, 0.57).

Specifically, as the stretch velocity increased, rate relaxation increased during the hold period in concert with a decline in muscle force (Figure 2-3B, light blue traces). Whereas the dynamic response during the ramp stretches could be accounted for by either musculotendon dF/dt or velocity and acceleration (but underestimated by length-related variables for the 40 mm/s stretch; Figure 2-3B), the differences in musculotendon length and force were highly evident during the hold period. Over the hold period, muscle force (Figure 2-3B, light blue traces) decreased with a similar time course as the muscle spindle IFRs. As musculotendon length was constant, the length-related model first under-estimated, and then over-estimated IFRs during the hold (Figure 2-3B, red traces).

2.4.5 Rate change in force, dF/dt, reproduces the initial burst and dynamic response to stretch

The initial burst IFRs increased when ramp accelerations were increased while keeping stretch length and velocity the same (Figure 2-3C) and was accounted for by both models. The initial burst IFRs were similarly accounted for by either dF/dt in the force-related model, or acceleration in the length-related model.

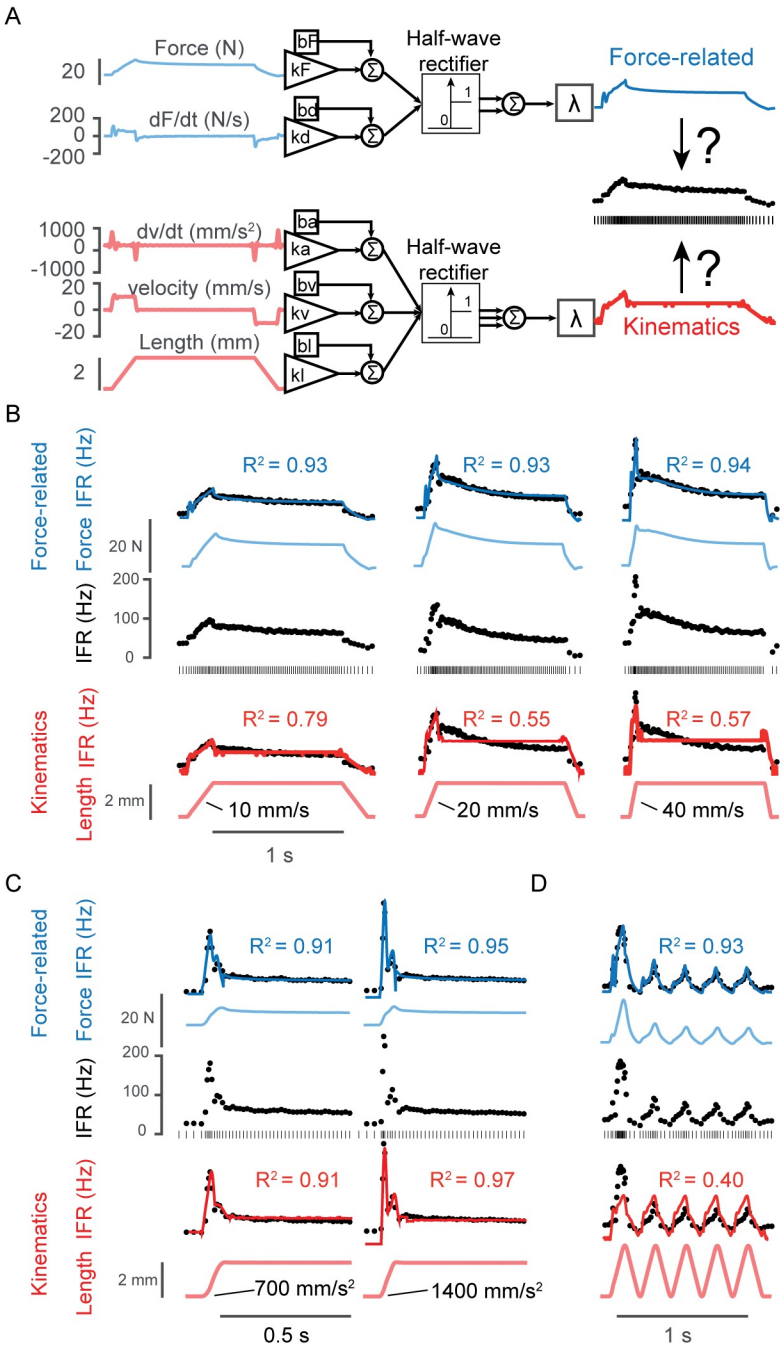

Figure 2-3 – Reconstruction of muscle spindle firing rates by two candidate models. **(A)** Two main candidate models for predicting IFRs are shown: the force-related model used a combination of the force developed in the musculotendon and its first time-derivative as input (linearly combined, inputs and model prediction in blue); the length-related model used a linear combination of the muscle length, velocity, and acceleration (inputs and model prediction in red). The instantaneous firing rate of the afferent (black dots) was used to compute the error to optimize model parameters. **(B)** Three examples of muscle stretch with different stretch speed are shown (10, 20, and 40 mm/s). The stretch was sustained for 1s before being released. From top to bottom, the force-related model output (blue line) is overlaid on the instantaneous firing rate during the stretch; the recorded force (light blue)

and the response of the afferent (black dots and raster) are shown directly below the force-related model output; the length-related model output (red line) is overlaid on the instantaneous firing rate and shown with the controlled musculotendon length (light red) below the response of the afferent. **(C)** The muscle was stretched to the same final length and at the same velocity, but with different initial accelerations (700 and 1400 mm/s2, respectively). **(D)** The muscle was stretched with sawtooth patterns, where stretches were not sustained but immediately released and repeated. In all cases, the force- related model fits were as good or better than the length-related model fits, as indicated by the R2 value. The examples shown are for afferents 4 (A-B, D) and 5 (C).

However, during a series of ramp-release muscle stretches, the dynamic response was better reproduced in the force-related vs. length-related model (Figure 2-3D). The differences in musculotendon force and length during repeated stretch and release, or "sawtooth" perturbations, were most evident when comparing the first stretch and release to the subsequent ones (Figure 2-3D, blue vs red traces). In an example afferent, musculotendon length changes were the same across all five stretches, whereas musculotendon force and muscle spindle IFRs were greater in the first stretch (Figure 2-3D), resulting in much better goodness of fit in the force-related versus length-related model.

2.4.6 Muscle fascicle length-related variables do not reproduce muscle spindle Ia IFRs

To rule out the hypothesis that muscle spindles encode muscle fascicle and not musculotendon length-related variables, we refined our length-related model to include the effects of tendon elasticity. The inclusion of a tendon model allowed us to compare predicted IFRs based on musculotendon versus muscle fascicle length. We estimated muscle fascicle length changes by subtracting the stretch of the modeled tendon from recorded musculotendon length (Figure 2-4A). We did not explicitly consider pinnation angle; assuming a constant pinnation angle of the fascicles through the range of stretches would scale the length change by a constant factor and would not change our results.

Tendon stretch was estimated by applying musculotendon force (Figure 2-4B) to an exponential model of Achilles' tendon stiffness, based on the linear increase in tendon stiffness with muscle force shown in anesthetized cat tendon (Rack and Westbury 1984). Based on two values of tendon stiffness, we estimated muscle fascicle length, velocity, and acceleration (Rack and Westbury 1984; Proske and Morgan 1987)(6 mm^{-1}, 2 mm^{-1}, representing upper and lower limits of stiffness, respectively). Models based on muscle fascicle length-related variables typically produced worse goodness of fit values than whole-musculotendon length-related variables (Figure 2-4C). Specifically, of 1185 stretch perturbations across 10 afferents, goodness of fit based on muscle fascicle length-related variables were only higher in 5.2% and 19.1% instances for the high and low tendon stiffness estimates, respectively. Over all afferents, mean R^2 values (± standard deviation) did not improve when using length-related variables based on muscle fascicle estimates (0.75 ± 0.13, and 0.70 ± 0.18 for high vs low tendon stiffness, respectively) versus those recorded from the whole musculotendon unit (0.77±0.12).

2.4.7 Force-related model parameters are consistent across stretch velocity in all recorded afferents

We used dynamic index (DI) to characterize the variations in dynamic sensitivity of the 10 analyzed muscle spindles to muscle stretch (Figure 2-5A). DI is a classical metric in which the IFR during the hold phase (Matthews 1963), measured 0.5 s after the end of the ramp phase, is subtracted from peak IFR at the end of the ramp phase (Figure 2-5A). Higher DI values characterize muscle spindles exhibiting relatively large initial bursts and dynamic response; these are typically

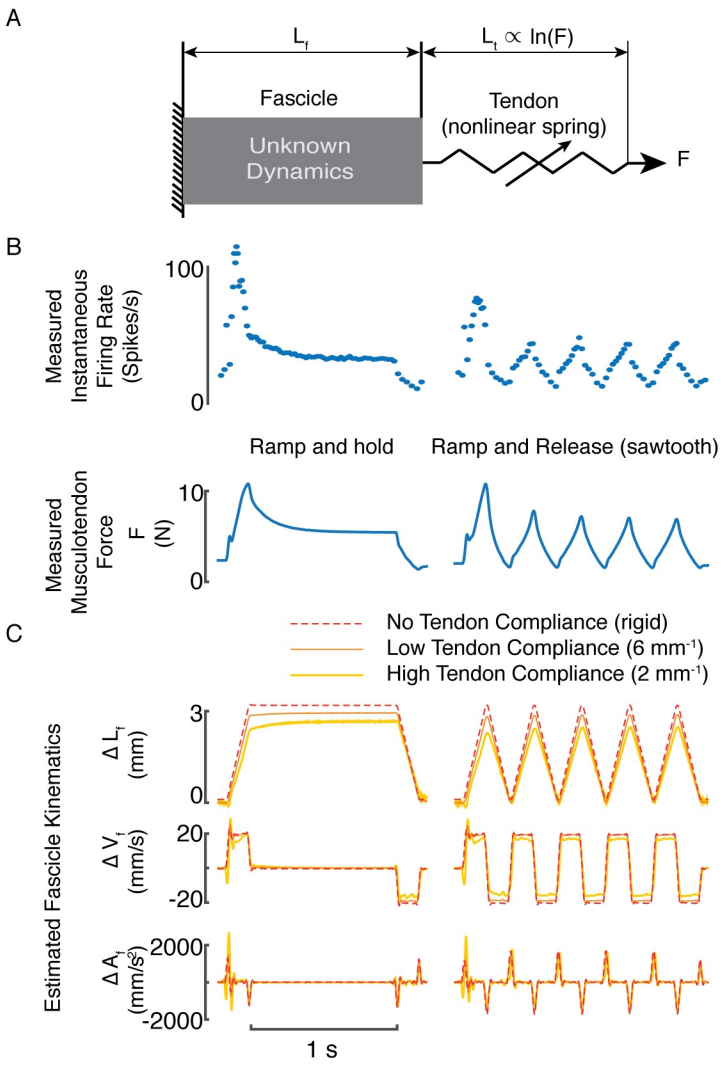

Figure 2-4 – Estimated muscle fascicle length. **(A)** The Achilles tendon was assumed to be arranged in series with the triceps surae muscle fascicles. The measured musculotendon force was used to estimate tendon elongation. Muscle fascicle length was found by subtracting estimated tendon length from measured musculotendon length. A rigid tendon assumes changes in muscle fascicle length are equal to measured changes in musculotendon length. **(B)** Recorded IFR and measured musculotendon force in response to ramp-and-hold (left) and ramp-and-release stretches. Musculotendon force was used to compute estimated tendon elongation. **(C)** Example of estimated muscle fascicle length-related variables for ramp-and-hold stretch (left) and repeated ramp-and-release stretch (right). Top row is measured change in musculotendon length (red dashed trace) and two estimates of change in muscle fiber length (high tendon compliance = 2 mm^{-1}: yellow; low tendon compliance = 6 mm^{-1}: orange). The second and third rows are velocity and acceleration estimates, respectively, using the same coloring convention as for length.

attributed to large contributions to firing rates from terminals on bag 1 intrafusal fibers (e.g. Figure 2-3C). More dynamic afferents are also characterized by

increasing DI with stretch velocity (P. B. Matthews 1963) (Figure 2-5A, left: colored bars). Lower DI values describe muscle spindles that respond less to ramp stretches but maintain higher firing rates during the hold period (e.g. Figure 2-3B); these are typically attributed to large contributions to firing rates from terminals on bag2 and chain intrafusal fibers.

The recorded muscle spindle Ia afferents spanned the range from highly dynamic to static (Figure 2-5A, left to right). Where the datasets allowed, we calculated DI across stretch velocities (4–50 mm/s). As expected, for each afferent with trials at different stretch velocities, DI increased with stretch velocity (Figure 2-5A). Four afferents exhibited mean DIs of larger than 50 imp/s for 20mm/s stretch velocity (Figure 2-5A, blue error bars, afferent numbers 1–4; conduction velocities shown in Figure 2-5D), the only stretch velocity tested in every afferent. Two afferents exhibited mean DIs less than 30 imp/s at 20mm/s stretch velocity, which was unexpected given their conduction velocities (Figure 2-5A, blue error bars, afferent numbers 9–10; conduction velocities shown in Figure 2-5D). The remainder of afferents exhibited mean DIs between 30 and 50 imp/s at 20mm/s stretch velocity (Figure 2-5A, blue error bars, afferent numbers 5–8; conduction velocities shown in Figure 2-5D). A direct comparison of our DI measurements to the original measures of Matthews (P. B. Matthews 1963) could not be made because our estimates of DI were computed based on 3mm stretches, a lower amplitude than used by Matthews (P. B. Matthews 1963).

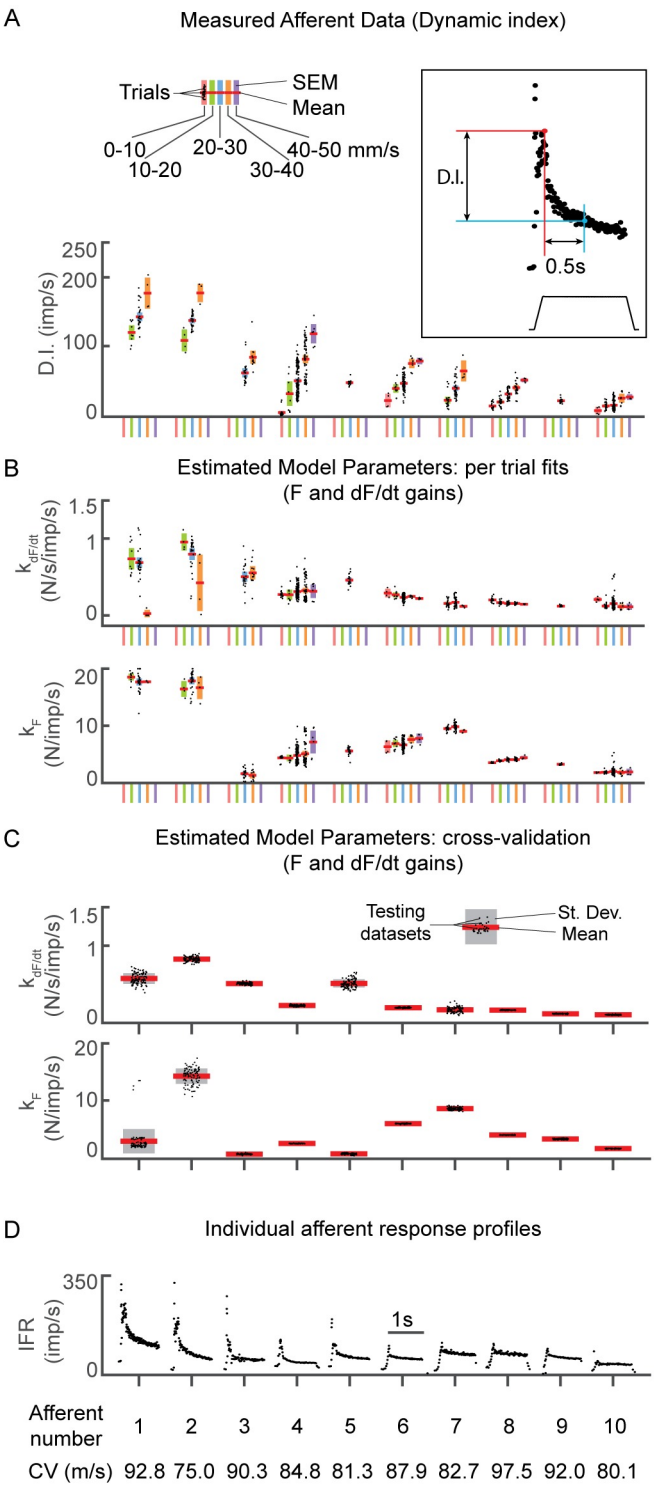

Figure 2-5 – Single muscle spindle afferent statistics and model parameter estimates. **(A)** Dynamic index measured for each ramp-and-hold stretch trial for every afferent, organized in descending order from left to right. For the 10 afferents analyzed, stretch trials were separated based on the velocity (indicated by colors) imposed on the muscle for that trial (divided into 5 10 mm/s velocity bins ranging from 0–50 mm/s). Bins with fewer than 4 trials were excluded from this figure. Horizontal red lines represent the mean, the colored

bars represent the standard error of the mean (SEM), and the black dots represent individual trial values. **(B)** In contrast to DI, force-related model weights were relatively constant with increasing stretch velocity. The color scheme is the same as in A. The upper plot is model weight on dF/dt and the lower plot is the model weight on force. **(C)** Force-related model weights and distributions for 100 randomized testing datasets (fitting one set of parameters for the entire dataset) for each afferent. For each afferent, a range of stretch perturbations (e.g. varying length, velocity, acceleration and stretch type) were included in the testing dataset. Red lines represent the means, grey bars represent standard deviations, and the black dots represent values for each testing dataset. As in B, model weights on dF/dt are shown in in the upper plot and model weights on force are shown in the lower plot. **(D)** Responses to a ramp-and-hold stretch at 3mm hold length, and 20mm/s stretch velocity for each afferent. Bottom row indicates conduction velocity for each afferent included in this analysis.

In contrast to DI, force-related model parameters for each afferent were similar across stretch velocities (Figure 2-5B). Weights for both dF/dt and force (kdF and kF) were relatively consistent across trials (Figure 2-5B vs. Figure 2-5A, colored blocks for each afferent) and were highest in the most dynamic afferents (Figure 2-5B, left).

2.4.8 The most likely model of muscle spindle IFRs uses musculotendon force-related variables

We systematically assessed the ability of six candidate models to predict information contained in 10 muscle spindle IFR datasets. Briefly, for each afferent we randomly sorted the entire set of stretch perturbations into a training and testing dataset based on the number of available trials. For each model, we identified model parameters from the training dataset and then used them to predict IFRs in the testing dataset. To reduce potential data selection biases, this process was repeated on 100 randomized training and testing datasets.

A single set of force-related model parameters were identified that reproduced IFRs in each afferent across all stretch conditions (Figure 2-5C). As when fitting individual stretches, weights corresponding to dF/dt were typically highest in the most dynamic

afferents (Figure 2-5C, left). Based on DI, weights corresponding to dF/dt for afferent 5 were higher than expected, but this afferent exhibited a relatively high initial burst, which is not captured by DI (same afferent as shown in Figure 2-3C).

In addition to the force-related model, the other 5 candidate models included combinations of musculotendon and muscle fascicle length-related variables. Candidate models included combinations of musculotendon length-related variables (Figure 2-6, red bars) described above (Figure 2-3A). Based on prior muscle spindle models, we also tested a model that allowed velocity to be raised to a fractional power (Hasan 1983; Houk, Rymer, and Crago 1981; Prochazka and Gorassini 1998a) (Figure 2-6, pink bars). We included models using muscle fascicle length-related variables estimated using low and high tendon compliance (Figure 2-6, orange and yellow bars). Finally, we tested a combination of all predictor variables (Figure 2-6, purple bars).

We compared the likelihood that each candidate model best predicts the information contained in the recorded muscle spindle IFRs while accounting for over-fitting. We report the fraction of times each model was selected as the best candidate (Figure 2-6, top row) out of 100 randomized iterations of training and testing our models. Based on the Akaike information criterion (AICc, including a correction for finite sample sizes), we also computed the normalized likelihood, w_i, that each model best reproduced the data, while taking into consideration the number of model parameters (Fig 6, middle row). For reference, goodness of fit was quantified using the coefficient of determination, R^2 (Figure 2-6, bottom row).

The force-related model was selected as the best candidate for each afferent when analyzed individually. The force-related model was selected as the best model in most of the 100 iterations for each afferent (Figure 2-6A top row; selection frequency = 0.59 for afferent 1, selection frequency = 1.0 for every other afferent). The normalized likelihood

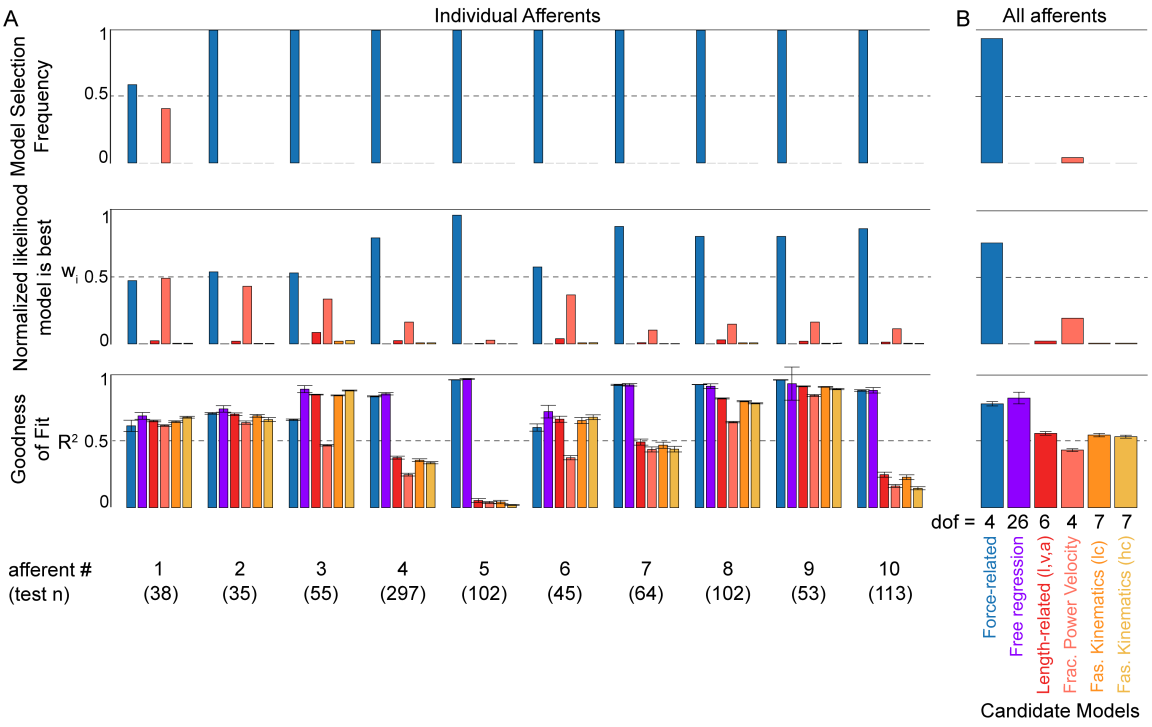

Figure 2-6 – Comparison of candidate models' abilities to predict muscle spindle Ia afferent IFRs. **(A)** Testing dataset model results for 10 afferents with 6 candidate models. The candidate models include one containing only force-related variables (force and its first time- derivative, dF/dt: blue), length-related variables (length, velocity, and acceleration: red), length-related variables with velocity raised to a fractional power (light red), muscle fiber length-related variable estimates (fiber length, velocity, and acceleration estimated with low and high tendon compliance: orange and light orange, respectively), and a free regression with all predictor variables from the other candidate models (purple). Top row: model selection frequency (number of times model was selected as the best candidate) for each model for 100 randomized testing datasets. Middle row: mean normalized likelihood (or Akaike weights, wi) that a given model is the best predictor of information in the IFRs, based on corrected Akaike Information Criterion (AICc) for regressions of the 100 randomized testing datasets. This is the relative weight of evidence in favor of a model being the best, given the set of candidate models. The sum of all 6 Akaike weights is equal to 1. Bottom row: mean R2 (coefficient of determination) calculated between afferent instantaneous firing rate and model prediction for 100

randomized testing datasets. Error bars represent 1 standard deviation. **(B)** Similar statistics to (A), but calculated for all 1000 randomized datasets (100 randomizations for 10 afferents). Top row: total model selection frequency for each model out of 1000 randomized datasets. Middle row: relative likelihood that each model is the best model in the set. This was calculated from the mean AICc values of all 10 afferents in (A). Bottom row: mean R2 across all 10 afferents in (A) for each model. Error bars represent 1 standard deviation.

of the force-related model as the best candidate was at least 0.5 for all afferents except one (Figure 2-6A middle row); the lowest values were found in afferents in which smaller data sets were available (Figure 2-6A; "test n" displayed below afferent number), indicating relatively stronger force-related model performance (when compared to length-related models) where more stretch conditions were applied to the muscle. The model containing all predictor variables yielded the highest R2 for every afferent (Figure 2-6B, bottom row purple bars). In 6 of the 10 muscle spindle afferents, mean R2 of the force- related model was much higher than the remaining models (Figure 2-6A, bottom row blue bars).

The force-related model was also selected as the best candidate for the entire set of muscle spindle afferents. The force-related model was always the best predictor of information in the IFRs of the testing dataset (Figure 2-6B). As in the individual afferent analysis, the force-related model was the most frequently-selected model across the population of afferents (Figure 2-6B, top row; selection frequency = 0.959). When considering the entire population of afferents, the normalized likelihood (w_i) of a model being the best within the set of candidates was greatest for the force-related model because it used fewer parameters than the model containing all predictor variables, but still predicted most of the information contained in the IFRs (Figure 2-6B, middle row; w_{force} = 0.77). Goodness of fit was highest in the model containing all 11 predictor variables (Fig

6B, bottom row, purple bar; R2 = 0.86 ± 0.046). Across all other models, mean R^2 across afferents was highest for the force-related model (Figure 2-6B blue, $R^2 = 0.82 \pm 0.017$ for force-related model; red, $R^2 = 0.58 \pm 0.014$ for length-related model); $R^2 < 0.58$ for other length-related models).

2.5 Discussion

To our knowledge, this is the first demonstration of muscle spindle Ia afferents firing in direct proportion to muscle force and the first time-derivative of force, dF/dt, when passive, i.e. electrically-quiescent, muscles are stretched. While qualitative comparisons have been made previously between intrafusal tension transients and muscle spindle receptor potentials (Hunt and Wilkinson 1980), this is the first quantitative description of a relationship between the spindle and muscle force response to stretch. The whole-muscle forces we recorded closely resembled transient force properties in stretched isolated muscle fibers that are attributed to calcium-dependent muscle cross-bridge interactions, including short-range stiffness and other history-dependent proper- ties, despite the absence of measurable electrical potentials in the muscle. Our analyses show that muscle force and dF/dt parsimoniously define a unique transformation between muscle mechanical events and muscle spindle firing rates during passive muscle stretch. Therefore, consideration of history-dependent muscle forces could improve current muscle spindle models, which do not predict history dependent firing rates. Further, muscle spindles exhibiting a more dynamic response had higher sensitivity to dF/dt, while more static muscle spindles were primarily sensitive to muscle force. The initial bursts at the onset of stretch were proportional to dF/dt and acceleration, and likely play a functional role in sensorimotor responses to external perturbations, particularly during posture and balance (Welch and

Ting 2008; Safavynia and Ting 2013a; Lockhart and Ting 2007; Lee and Tatton 1975; Shemmell, Krutky, and Perreault 2010). The transient spiking features we analyzed were similar to those reported in the classic literature in muscle spindles (P. Matthews 1981); our unique approach was to dissociate muscle force and length by recording a large, diverse set of muscles stretch conditions from each afferent, including variations in muscle acceleration that was independent of velocity. Further work is warranted to test whether encoding of muscle force will extend to active conditions, when fusimotor and skeletofusimotor motoneurons are firing, and its potential to explain load sensitivity and the non-unique relationships of muscle spindle firing rates to muscle length shown recently in humans (Dimitriou 2016; Dimitriou 2014).

Our experimental measures of whole muscle force were likely correlated to intrafusal muscle fiber forces within the encoding regions of muscle spindles arising from muscle cross-bridge mechanics. It is unlikely that the forces from intrafusal fibers made a significant contribution to the recorded force or, conversely, that the extrafusal force had a significant contribution to the intrafusal fiber forces. Our assumption is that intrafusal and extrafusal forces exhibited similar history-dependent effects when stretched. Thus, we used the whole muscle force as a surrogate for intrafusal force, which is reasonable under anesthetized conditions, and consistent with our ability to predict fine details of muscle spindle IFR based on extrafusal muscle force. Our whole muscle forces during stretch closely resembled forces from experiments of single, permeabilized muscle fibers, suggesting little contribution of non-contractile tissue to whole muscle force in this experimental condition. Similar to our whole muscle recordings, isolated muscle fiber forces exhibit short-range stiffness when stretched after being held isometrically,

characterized by a rapid rise in force at the onset of stretch, where the first time-derivative of force, dF/dt, increases transiently (Campbell and Lakie 1998; Campbell and Moss 2000; Campbell and Moss 2002; Campbell 2014; Getz, Cooke, and Lehman 1998). Both our whole muscle and isolated muscle fibers also exhibit history-dependent characteristic of dynamic response to ramp stretch and post-stretch rate relaxation. These history-dependent force transients are only present in isolated muscle fibers when attachment and detachment of muscle cross-bridges is possible due to the presence of low concentrations of Ca2+ (Campbell and Moss 2000; Campbell and Moss 2002; Proske and Morgan 1999). Thus, even in passive, i.e. electrically-quiescent muscles, we see evidence of these transients in whole muscle force and dF/dt predict history-dependent muscle spindle initial bursts, dynamic response, and rate-relaxation after being held isometric, suggesting that muscle cross-bridge cycling is present at low levels. There may be differences that we did not account for due to the potential different myosin isoforms expressed in intrafusal and extrafusal muscle fiber (Liu, Eriksson, Thornell, and Pedrosa-Domellöf 2002a). Nevertheless, in the anesthetized conditions of our experiments, it seems reasonable to assume that whole-muscle force transients were similar to *in vivo* muscle fiber force, including intrafusal muscle fibers within muscle spindle sensory organs. Indeed, the initial burst of muscle spindle firing at the onset of muscle stretch has been described as "an intrafusal manifestation of the passive short-range stiffness of the extrafusal muscle" (Proske and Stuart 1985).

Our results show that muscle force-related variables define a unique transformation between muscle mechanical events and muscle spindle firing rates during stretch of passive muscle. Muscle force and its first time-derivative could reliably predict previously-

observed history-dependent features of muscle spindle IFRs such as the initial burst, dynamic response, and rate relaxation that cannot be explained by muscle length-related variables. Moreover, a single set of model fit parameters produced high-fidelity predictions of muscle spindle IFRs across a wide range of stretch conditions. Our data quantitatively support the hypothesis that muscle spindles encode muscle fiber force (Lewis and Proske 1972a; Proske and Stuart 1985), which could not previously be tested due to technical limitations. Further, recordings of receptor potentials in muscle spindle encoding regions are qualitatively similar to the history-dependent transients in muscle force and dF/dt that we used to predict muscle spindle firing rates (Hunt and Wilkinson 1980). The role of anatomically-distinct encoding regions of the muscle spindle, i.e. bag1, bag2, chain regions (Boyd 1976; Banks, Barker, and Stacey 1979; Jami and Petit 1979) as well as rap- idly- and slowly-adapting force sensitive ion channels (Bewick and Banks 2015; Xiao and Xu 2010; Delmas and Coste 2013) in encoding force-related information in muscle spindles remains to be fully explained, although contributions of distinct encoding sites to muscle spindle afferent firing rates have been demonstrated (Banks et al. 1997).

Our results suggest that adding muscle cross-bridge kinetics to computational models of muscle spindles would produce history-dependent muscle spindle firing rates. Sarcomere- level muscle models of cross-bridge kinetics can predict all of the history-dependent features of muscle fiber force described above, but generally require significant computation time (Campbell and Lakie 1998; Campbell and Moss 2000; Campbell and Moss 2002). Moreover, several muscle spindle models assume that force and dF/dt of intrafusal muscle fibers give rise to muscle spindle firing rates, but use more computationally-efficient phenomenological muscle models, e.g. Hill-type models, to

estimate intrafusal muscle fiber force based on muscle length (Hasan 1983; Lin and Crago 2002; Mileusnic et al. 2006). Hence, prior models do not reproduce the history-dependent features of muscle spindle IFRs that we studied. Computationally efficient simulation of muscle forces based on cross-bridge kinetics is thus critical for reproducing muscle spindle history- dependence, particularly sensorimotor responses to perturbations, where Hill-type muscle models lack necessary history-dependent properties to explain experimental results (Cui et al. 2008).

Muscle spindle subtypes may be characterized based on their individual sensitivities to force (k_F) and the first time-derivative of force ($k_{dF/dt}$). Classic measures of dynamic index are specific to stretch condition and only compare peak and steady-state firing rate during specific time windows of muscle ramp stretches. In contrast, constant parameters characterizing sensitivity to force and dF/dt take into account the entire time course of muscle spindle spiking activity. In our study, slowly-adapting, or "static" muscle spindles that had a low dynamic index lacked an initial burst and responded primarily to muscle force. Rapidly-adapting, or "dynamic" muscle spindles with a high dynamic index, exhibited initial bursts due to higher sensitivity to the transients in the first time-derivative of force, dF/dt, and were also sensitive to muscle force. While dynamic index varied with stretch velocity, sensitivity to force and dF/ dt was invariant across different stretch conditions, making it a robust metric allowing comparisons across different stretch types. Further, the invariance of sensitivity to force and dF/dt within each afferent underscores the potential mechanistic relationship between muscle fiber forces and muscle spindle firing rates, providing a quantitative parameter of static and dynamic sensitivity. It remains to be seen whether the effects of alpha-gamma co-activation, which can enhance muscle

spindle sensitivity in a subpopulation of afferents (Kakuda, Miwa, and Nagaoka 1998) can also be quantified in terms of sensitivity to force and dF/dt. Tuning the sensitivity of muscle spindle afferents could be a mechanism for tuning the net population firing rate arising from muscle spindle afferents during external perturbation.

Muscle spindle initial bursts that scale with stretch acceleration have been shown previously and can be explained by sensitivity to the first peak in dF/dt. Initial bursts have been observed in both acute animal experiments and in human microneurography in awake participants (P. B. Matthews 1963; Haftel et al. 2004; Nichols and Cope 2004; Dimitriou 2014; Kakuda, Miwa, and Nagaoka 1998; Cordo et al. 2002) and have been largely attributed to stretch acceleration (Schäfer 1967; Schäfer and Kijewski 1974; Houk, Rymer, and Crago 1981). In our experiments, the initial burst scaled equally well to initial stretch acceleration or the peak in dF/dt, although later transients were only described by dF/dt. Although the number of spikes may be low in animal experiments using relatively fast stretches, in human microneurography studies using slow stretch velocity, as many as 20 spikes have been observed (Cordo et al. 2002; Vallbo, AB 1974). More- over, visual inspection of joint torque traces presented by Cordo and colleagues (Cordo et al. 2002) reveal similarities in muscle spindle initial bursts and joint torque transients.

Muscle spindle initial bursts are likely critical in generating rapid and predictive corrective sensorimotor responses to external perturbation. Our prior experimental work demonstrates that corrective muscle activity elicited in long-latency responses to standing balance perturbation exhibit an initial burst of activity that scales with perturbation acceleration (Welch and Ting 2009; Welch and Ting 2008; Safavynia and Ting 2013a; Safavynia and Ting 2013b; Lockhart and Ting 2007). More- over, the initial burst in muscle

activity is lost in animals with large fiber sensory neuropathy in which muscle spindle Ia afferents are destroyed; these animals also exhibit balance impairments (Lockhart and Ting 2007; Stapley et al. 2002). As muscles are near isometric during quiet standing (Loram, Maganaris, and Lakie 2004), muscle spindles within those muscles are likely to exhibit initial bursts at the onset of a perturbation due to transients in muscle force and dF/dt. Indeed, our simulation studies demonstrate that short-range stiffness is necessary to account for measured joint torque-angle relationships during perturbation to standing (De Groote, Allen, and Ting 2017). Further, theoretical studies show that delayed feedback based on acceleration or force can preemptively evoke a corrective response before large displacements occur, acting as a predictive controller (Insperger, Milton, and Stépán 2013). It is currently unclear whether the sensory feedback required for these postural responses arises from active or passive muscles, or both. Though our study does not directly test the generalization of force encoding to active muscle, there is evidence that initial bursts persist with gamma activation (Boyd et al. 1977) and that acceleration-dependent sensorimotor bursts occur in active muscle during postural perturbations (Welch and Ting 2009; Welch and Ting 2008; Safavynia and Ting 2013a; Lockhart and Ting 2007; Welch and Ting 2014). Thus, the initial burst of muscle activity that scales with acceleration is likely due to muscle spindle initial bursts and may explain why peak activity of postural muscles occurs prior to peak displacement (Welch and Ting 2008; Loram, Maganaris, and Lakie 2004).

We speculate that force encoding in muscle spindles could underlie other non-unique relationships observed between joint motion and perceived limb position, and between muscle force generation and muscle spindle firing rates (Proske and Gandevia 2012).

Muscle spindles play a role in both conscious and unconscious motor control (Proske and Gandevia 2012). To a degree, the CNS is likely capable of compensating for any shortcomings of the spindle as a length transducer with contributions from other sensory modalities (e.g. cutaneous receptors, which have an important contribution to proprioception). However, there are important circumstances in which history-dependent muscle spindle behavior such as thixotropy can impair the position sense provided in part from muscle spindles. When the limbs are passively manipulated, perceived joint position exhibits similar history-dependence to muscle spindle firing, causing an illusion in joint angle if the muscle is first stretched versus activated prior to stretch (Proske, Tsay, and Allen 2014; Proske and Gandevia 2009). Muscle spindle sensory information is distinct from that provided by Golgi tendon organs, which encode a combination of force and the first derivative of muscle *contractile* force due to efferent drive to muscles (Jami et al. 1985) (Jami 1992), but are generally silent during passive stretch and lack an initial burst (Jami 1992). Recent work demonstrates that muscle spindle firing is not uniquely related to muscle length during active muscle contractions; instead, the rate of firing depends on magnitude and direction of external load, not joint kinematics (Dimitriou 2014). Human muscle spindle primary afferents have also been shown to fire distinctly during different stages of learning regardless of similar movement kinematics (Dimitriou 2016). Another recent study showed that firing rates in human muscle spindle primary afferents in response to sinusoidal changes in ankle angle are only predicted by muscle length at steady-state and not during transient firing at the onset of imposed movements (Day et al. 2017). Our findings predict that history-dependent muscle forces, which are difficult to measure *in vivo*, would predict steady-state as well as transient firing in muscle spindle afferents.

During alpha-gamma coactivation, such as during voluntary muscle contractions (Dimitriou 2014; Kakuda, Miwa, and Nagaoka 1998) and perceived postural threat (Horslen et al. 2013), intrafusal muscle spindle fibers that lie in parallel with extrafusal muscle fibers are also activated; we speculate that this increase in muscle activity would increase the sensitivity of the muscle spindle to errors in muscle force and rate change in force due to unanticipated environmental interactions, relative to the anesthetized conditions here that lack efferent drive. Indeed, alpha-gamma co-activation has been shown to modulate muscle spindle primary afferent dynamic sensitivity based on loading of the spindle-bearing muscle in response to external perturbations (Kakuda, Miwa, and Nagaoka 1998). This interpretation is consistent with the idea that muscle spindles inform internal models for movement, providing estimates of sensory error based on efference copy (Hwang, Smith, and Shadmehr 2005). However, much further study is necessary to test whether the encoding of whole-muscle force in passive muscle spindles generalize to conditions involving active muscle contraction. As muscle force is a good proxy for muscle length in many conditions, we hypothesize that that the biophysical transformation from passive muscle stretch to muscle spindle firing is based on muscle force transients but potentially interpreted perceptually in terms of joint position and velocity.

CHAPTER 3. MUSCLE SPINDLE IA AFFERENT RESPONSES TO STRETCH ARE ROBUSTLY EXPLAINED BY DIFFERENTIAL SENSITIVITY TO FORCE AND YANK

3.1 Attribution of Efforts

This chapter relies on data that was collected by myself and members of Timothy Cope's laboratory. I had assistance with the *in vivo* experiments I collected data in from Paul Nardelli. I also used data collected by another current student, Nicholas Housley, and by a former student, Katie Bullinger.

3.2 Introduction

Muscle spindle proprioceptive signals are classically understood to encode muscle length and velocity (Houk, Rymer, and Crago 1981; Stein et al. 2004; P. Matthews and Stein 1969; P. B. Matthews 1963), facilitating both conscious and unconscious corrective sensorimotor responses to mechanical perturbation (Lockhart and Ting 2007; Welch and Ting 2009; Welch and Ting 2008; London and Miller 2013; London et al. 2008). Decades of reports demonstrate strong correlations between *steady-state* muscle spindle firing rates to muscle length and velocity, however, these correlations are not unique as they are altered by background muscle force (Bullinger, Nardelli, Wang, et al. 2011; Cordo et al. 2002), perturbation characteristics (Hasan and Houk 1975; P. B. C. Matthews 1964; P. Matthews 1981; P. B. Matthews 1959; Haftel et al. 2004; Stein et al. 2004; P. B. Matthews and Stein 1969; P. Matthews and Stein 1969; Honeycutt et al. 2012), muscle activation levels (Prochazka and Gorassini 1998a; Prochazka and Gorassini 1998b; Kakuda, Miwa, and

Nagaoka 1998; Kakuda and Nagaoka 1998; Dimitriou 2014), external load (Dimitriou 2014), and reciprocal inhibition (Dimitriou 2014). Further, *transient instantaneous* muscle spindle firing rates during muscle stretch perturbations exhibit non-unique relationships between muscle length and velocity that change as a function muscle movement history (Haftel et al. 2004) that can be explained by history-dependent changes in muscle stiffness (Blum, Lamotte D'Incamps, Zytnicki, and Ting 2017b). Additionally, lesions or perturbations to sensory afferents can alter the relationships between steady-state and instantaneous muscle spindle firing rates elicited by stretch of passive muscle (Bullinger, Nardelli, Wang, et al. 2011; Carrasco, Vincent, and Cope 2017). Current notions about muscle spindle function often fail to account for non-unique relationships between muscle length and velocity and muscle spindle firing patterns. Even in stretch of passive muscle, we currently lack mechanistic hypotheses about muscle spindle function that could robustly predict non-classical muscle spindle relationships to muscle length and velocity. A common set of descriptor variables robust to inter- and intra-afferent variations in history-dependent changes to sensitivity would greatly enhance our understanding of proprioceptive encoding. In this study, we aim to test the feasibility of a recently identified set of mechanical descriptor variables to predict muscle spindle firing rates across a range of perturbations to the muscle and neuron (Blum, Lamotte D'Incamps, Zytnicki, and Ting 2017b).

Muscle fiber force could be a mediating mechanical variable to explain both classical and non-classical relationships between muscle spindle firing rates and muscle length and velocity (Proske and Morgan 1999; Proske and Stuart 1985; Proske, Morgan, and Gregory 1992; Lewis and Proske 1972b; Campbell and Moss 2000; Campbell and Moss 2002;

Campbell and Lakie 1998). Recently, we showed that whole muscle force and its first time derivative, yank, robustly predict both steady-state and transient instantaneous muscle spindle firing rates across stretch conditions, including changes in firing rate due to prior movement history (Blum, Lamotte D'Incamps, Zytnicki, and Ting 2017b). But, we were unable to dissociate whole muscle force from muscle fiber force in the experimental protocol we used, conflating the specific information encoded by the spindle receptors. Further, it is not known whether the transient and steady-state firing rate are independently or jointly encoded by the spindle. Finally, we lack predictive models that can generate the classical and non-classical muscle spindle firing behaviors (Lin and Crago 2002; Prochazka and Gorassini 1998b; Prochazka and Gorassini 1998a; Houk, Rymer, and Crago 1981; Mileusnic et al. 2006; Hasan 1983).

We hypothesized that muscle spindle firing rate during passive muscle stretch is encoded by two independent mechanisms encoding intrafusal muscle fiber force and yank. Here, we applied muscle stretch perturbations spanning. a large range of length and velocity to the isolated triceps surae of rats. We analytically dissociated muscle fiber and whole muscle force and tested whether Ia afferent IFRs could be reconstructed based on pseudolinear combinations of estimated fiber force and yank in classical and non-classical conditions. We focused on a variety of applied stretch length and velocity for each afferent to test whether the same force and yank variables could account for inter- and intra-afferent variability in stretch sensitivity (P. B. Matthews 1963; P. B. Matthews and Stein 1969; Lennerstrand and Thoden 1968; Schäfer 1967; Schäfer and Kijewski 1974). We also tested whether these descriptor variables would predict history-dependent spiking responses in the same afferents by applying repeated stretch stimuli (Haftel et al. 2004). Next, we

compared reconstruction of IFRs during two types of perturbations to sensory afferents: electrical stimulation of the axon and pharmacologically-induced channelopathy (Bullinger, Nardelli, Wang, et al. 2011). Finally, we generated a family of firing rates using a spiking neuron model using independent currents that were scaled to estimated intrafusal fiber force and yank. Our results show that independent mechanisms encoding force and yank can explain a wide range of classical and non-classical muscle spindle firing behaviors in both normal and perturbed conditions.

3.3 Methods

3.3.1 Animal care

All procedures and experiments were approved by the Georgia Institute of Technology's Institutional Animal Care and Use Committee. Adult female Wistar rats (250–300 g) were studied in terminal experiments only and were not subject to any other experimental procedures. All animals were housed in clean cages and provided food and water ad libitum in a temperature- and light-controlled environment in Georgia Institute of Technology's Animal facility.

3.3.2 Terminal physiological experiments

Experiments were designed to measure the firing of individual muscle afferents in response to muscle stretch in vivo with electrophysiological techniques. Rats were deeply anesthetized (complete absence of withdrawal reflex) by inhalation of isoflurane, initially in an induction chamber (5% in 100% O_2) and for the remainder of the experiment via a tracheal cannula (1.5–2.5% in 100% O_2). Surgical and recording preparation followed by

data collection lasted for up to 10 h. Subcutaneous injections of lactated Ringer solution were given to support fluid levels and blood pressure. respiratory rate, Pco_2, and core temperature were monitored via a rectal probe, and maintained between 36 and 38 °C with heated water pads and a heat lamp. Pulse rate and Po_2 were monitored intermittently. At the conclusion of data collection, rats were killed by exsanguination preceded either by overdose with isoflurane inhalation (5%). Surgical preparation for data collection were described in earlier reports from this laboratory (Bullinger, Nardelli, Wang, et al. 2011; Bullinger, Nardelli, Pinter, et al. 2011; Vincent et al. 2017).

Briefly, the triceps-surae muscles nerves were dissected free of surrounding tissue in the left hindlimb. All other nerves in the left hind limb were crushed to avoid (1) cross-talk with stimulation and (2) to reduce total afferent feedback to the recorded dorsal root. The rats were fixed in a rigid frame at the snout, vertebral bodies, distal tibia, and distal femur (knee angle 120°). The tendon of triceps-surae was then cut at its insertion and attached to the lever arm of a force and length-sensing servomotor (Model 305B-LR, Aurora Scientific Inc.), which provided for application of controlled muscle stretch while recording muscle length and force. (dual-mode lever arm system, Aurora Scientific) used to control muscle length and measure force. Initial muscle length was set at $L_{r(rest)}$. Dorsal roots exposed by laminectomy were placed on bipolar electrodes. Triceps-surae nerves were loosely positioned in continuity on a unipolar silver stimulating electrode. Exposed tissues were covered with warm mineral oil in pools formed by attaching the edges of severed skin to the recording frame.

Either ramp-hold-release (e.g. Figure 3-1A) or repeated ramp release (e.g. Figure 3-1B) were applied to the muscle with the servomotor to evoke history-dependent stretch

responses from the Ia afferents. In the 11 afferents for which the initial pseudolinear model analyses were performed, a range of 6-99 stretch trials with varying maximum length and velocity were achieved depending on the recording stability.

3.3.3 Sample size

No explicit a priori power analysis was performed to determine sample size. Experiments were performed over the course of 36 months. At the conclusion of this period, data were screened for quality and it was determined that the available sample of recorded afferents was commensurate with a previous study with similar methodology (Blum, Lamotte D'Incamps, Zytnicki, and Ting 2017b).

3.3.4 Data inclusion and exclusion

Analyses treated individual recorded afferents and individual recorded stretch trials as biological replicates and as technical replicates, respectively. To ensure sufficient information for statistical measures, we required that stretch trials have at least 50 recorded action potentials in order to be included in statistical analyses. Stretch trials with low signal to noise ratio based on visual inspection were excluded. Additionally, technical replicates for which our model optimizations would not converge to a solution were excluded from analyses. These criteria yielded suitable datasets for 11 individual afferents from 5 animals for the parameter analyses, and 6 individual afferents from 5 animals for the axonal stimulation analyses. We also included 3 afferents from 3 animals from a previous study in which the animal was treated with oxaliplatin (Bullinger, Nardelli, Wang, et al. 2011).

3.3.5 Muscle fiber force estimation

To isolate the component of recorded musculotendon force arising from the muscle fibers (used as a proxy for intrafusal muscle force), we assumed an idealized musculotendon mechanical arrangement (Figure 3-1A). In summary, we assumed there was noncontractile passive connective tissues arranged in mechanical parallel with the musculotendon. We thus hypothesized that the contribution of this tissue to the recorded force at the calcaneus could be analytically removed by 1) assuming these tissues were purely elastic (i.e., the force developed by stretching these tissues was only length-dependent), 2) assuming these tissues have a specific nonlinear force-length relationship which was uniform along the length of the musculotendon (Hill 1953) (Figure 3-1B),

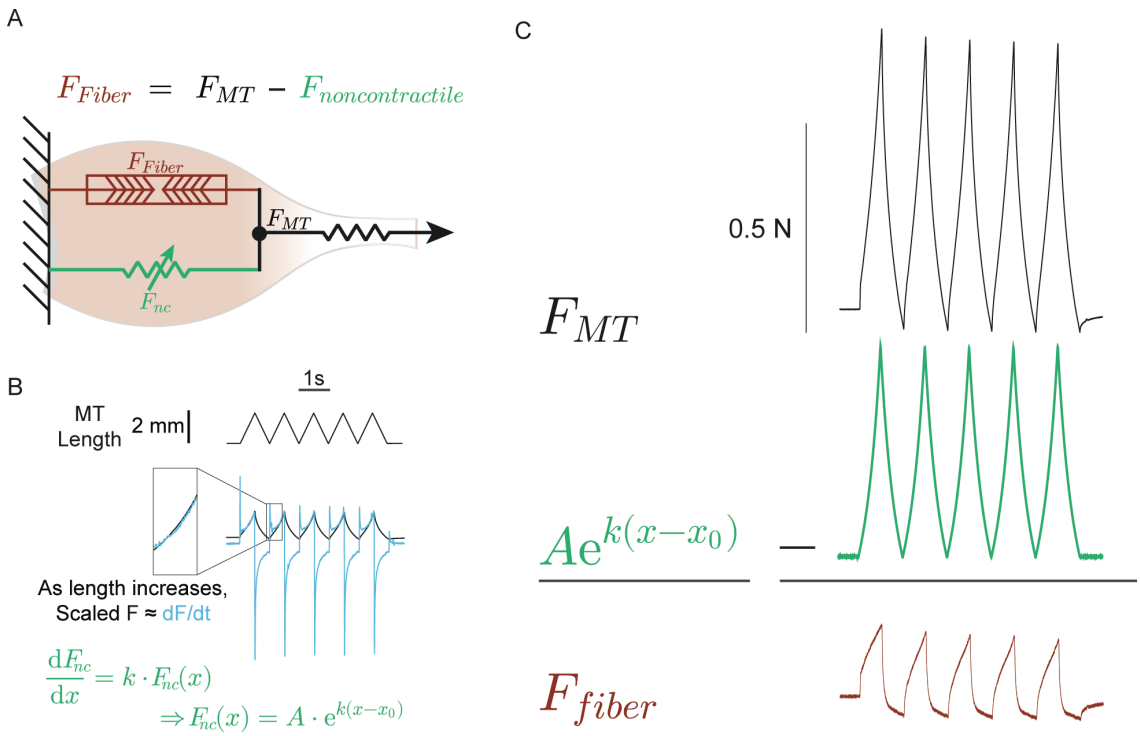

Figure 3-1 – Muscle fiber force estimation from recorded data. **(A)** Simplified assumption of musculotendon mechanical arrangement. We assumed that the muscle fibers (red) and tendon (black) are aligned in mechanical parallel with an unknown amount of noncontractile tissue (green), which could be subtracted from the recorded musculotendon

force if known. **(B)** Anecdotal evidence that noncontractile tissues behave similarly to an exponential spring. As applied musculotendon length increases, force (black) and yank (cyan) are approximately linearly related implying an exponential relationship between force and length is dominating the recorded musculotendon force. **(C)** Assuming noncontractile tissue force (green) behaves as a perfect exponential spring, muscle fiber force (red) is estimated by subtracting the estimated noncontractile force component from the recorded musculotendon force (black), revealing a history-dependent muscle fiber force estimate.

and 3) using the applied length to estimate the force contribution of these tissues, and subtracting it from the recorded force (Figure 3-1C).

We chose to assume the noncontractile tissues had a combination of exponential and linear stiffness. We observed that during repeated ramp-release stretches, recorded force and change in force with respect to length (dF/dx) were linearly related for the majority of the stretch (Figure 3-1B), which is a property of exponential springs. We added a linear spring component to the noncontractile tissue model as a contingency to account for the possibility of inconsistent or more complex tissue mechanics. These parameters were allowed to be 0 in the optimization procedure, so they were only included in the noncontractile estimates when the optimization deemed it beneficial to the quality of fit (see parameter selection for force related model).

Once parameters were selected by the optimization procedure, the estimated noncontractile tissue forces were subtracted from the recorded force to estimate the muscle fiber force, which was fit to the IFRs.

3.3.6 Pseudolinear models for predicting firing responses

We predicted spiking responses using pseudolinear combinations of either recorded musculotendon length-related (length, velocity, and acceleration) or force-related

(estimated muscle fiber force and yank) variables. The relative weights and offsets for each variable in a model were optimized to minimize the squared error between the model prediction and Ia spike rates on a per-trial basis. The optimization procedure for the force-related model was done in several steps and is explained in greater detail later.

For both the force- and length-related models, we fit the estimated IFR for each model to the IFR of the afferent for each stretch trial included in our analyses (for all 20 afferents presented in this study). The model parameters, consisting of a weight (k_i) and offset (b_i) for each force- or length-related variable included in the sum, were found via least-squares regression using Matlab's optimization toolbox (*fmincon.m*) and custom scripts. A time delay (λ_j) was determined by shifting the timestamp of the variables forward relative to the IFR data to be fit (note: this time delay was 0 for all variables except yank, to account for the apparent delay between the onset of muscle force response and the onset of the spiking response). The general form of the models was:

$$IFR_{j,n}(t) = \left(\sum_{i=1}^{n} k_i \cdot \left(\lfloor x_i(t - \lambda_j) \rfloor + b_i \right) \right) \tag{8}$$

where the IFR estimate of the jth model for the nth perturbation was estimated by a sum of n force- or length-related variables, offset by a single value, b_i, and scaled by a gain, k_i. $\lfloor \rfloor$ denote positive values of the argument. Model estimates for IFR were related to the recorded IFR of the mth afferent by the equation:

$$IFR_{j,n}(t) + e(t) = IFR_{m,n}(t) \tag{9}$$

Error, $e(t)$, was minimized by finding the set of parameters for each model that minimizes

a measure related to $e(t)^2$. The weights and offsets (i.e. k_i and b_i) found as a result of this analyses are presented in Figure 3-5. No statistical tests were performed on the parameters estimated from this analysis.

3.3.7 Parameter estimation for force-related model

Because of the difficult nature of the nonlinear optimization problem presented by estimating the noncontractile tissue parameters, calculating the resulting estimated fiber force and yank, and fitting these variables to the recorded firing rate for every afferent, the parameter selection for the force-related model was performed in four steps. In the first step, muscle fiber force was estimated by the method described above, where the noncontractile tissue parameters and the gain and offset for the resulting estimated fiber force were optimized to minimize the error between only the fiber component plus a constant and the IFR for that trial. The second step of parameter selection allowed for the optimization from the first step to re-optimize within the bounds of +/- 10% of the final parameter values found in step 1. In the third step, all parameters from the second step were fixed, and yank gain, offset, and time-delay were optimized via least squares regression. In the final step, all parameters were allowed to vary by +/- 20% to help the optimization algorithm find a local minimum near the forced solution from the third step.

By allowing the model parameters to vary trial-to-trial, we were able to examine the capability of the noncontractile tissue model to estimate the component of musculotendon stress that was extraneous to the muscle spindle firing rates. One-way analysis of variance (ANOVA) was performed on the sum of squared model errors between

the force- and length-related models. Only the significance between model errors was considered here.

3.3.8 Axonal stimulation dataset

To test whether the force and yank components could arise from separate mechanosensitive mechanisms, another set of experiments was performed on 6 additional afferents in 4 animals. Each afferent dataset consisted of three trials in which the muscle was perturbed mechanically (3 mm, 20 mm/s). The first and third trials for each afferent served as bookend controls: alternating between control and intra-axonal current injection trials allowed assessment of the response through the course of extended single cell recordings. In the second of the three trials, we applied a depolarizing current (30nA for 500ms) which led to a train of antidromic action potentials traveling down the axon, which ceased immediately before applying a mechanical perturbation (3mm, 20mm/s), to which the firing response of the Ia afferents was dramatically reduced.

For each trial in these 6 afferents, we found the best-fit prediction for the force-related model using the parameter optimization described earlier. For the pre- and post-stimulation control trials, we first fit the model without a yank component, and then refit the model with a yank component. For the trials in which the electrical stimulus was applied, the yank component was set to be zero and the force and constant components were optimized as described before.

We performed one-way ANOVA on model performance (R^2), yank sensitivity (k_Y), force sensitivity (k_F), and the constant component (C) across 5 groups of model fits: pre-stimulus control trials without (1) and with (2) yank sensitivity, stimulus trials (3), and

post-stimulus trials without (4) and with (5) yank sensitivity. We used the Tukey-Kramer method to examine all pairwise comparisons between groups.

3.3.9 Oxaliplatin dataset

We used data collected previously to test whether force and yank components were altered by oxaliplatin chemotherapy (Bullinger, Nardelli, Wang, et al. 2011). For this analysis, we selected three afferents from different animals and fit the muscle fiber force-related model (described above) to three stretch trials for each afferent (3mm, 20 mm/s). We performed one-way ANOVA on model performance (R^2) between model fits with and without yank for each afferent to test the significance of the yank component on model performance.

3.3.10 Applying estimated fiber force-related currents to model neuron

To test the feasibility of the force, yank, and constant components of the muscle fiber force-related model as mechanical signals encoded by the muscle spindle receptor, we applied a range of combinations of components to a conductance-based model neuron (based on the Connor-Stevens model; see next section) and examined the resulting firing rates. We first estimated the muscle fiber force and yank, as described previously, and varied the relative gains of these signals before adding them with a constant component. Once the components were added together, they were half-wave rectified, and applied to the model neuron as a stimulus current.

Model neuron sensitivities to these components were hand-tuned until the model instantaneous firing rate was reasonably similar to the firing rate of the Ia afferent for a

chosen trial (initial burst, dynamic response, and final plateau firing magnitudes were each within 10 spikes/s for each characteristic). We treated the parameter values which produced this response as the nominal values for the model. The relative sensitivities of the model neuron to force and yank component were then swept from 25-400% and 25-200% of their respective nominal values. We then compared the resulting changes in predicted firing rates with different phenotypical muscle spindle responses observed from these and other experiments.

3.3.11 Conductance-based model neuron for reproducing spiking activity

To demonstrate the plausibility of force- and yank-related ionic currents caused by stretch, we used a modified Connor-Stevens conductance-based model neuron to model the transformation of graded receptor potentials into action potentials by the afferent (Connor and Stevens 1971). The model neuron contained a fast sodium, delayed rectifier potassium, transient potassium, and leak conductances implemented in Simulink using built-in differential equation solvers (*ode23s.m)*. The governing current equation for the model is of the following form:

$$I(t) = C_m \frac{dV}{dt} + \bar{g}_L(V(t) - E_L) + \bar{g}_{Na} m^3 h(V(t) - E_{Na}) + \bar{g}_K n^4(V(t) - E_K) + \bar{g}_A a^3 b(V(t) - E_A) \quad (10)$$

where $I(t)$ is the current per unit area, C_m is the electrical capacitance of the membrane per unit area (1 μF/cm^2 in this model), $\overline{g}_n$ is the maximal value of the conductance for a given ion (or leak current), E_n is the reversal potential for a given channel. n, m, h, a, and

b are associated with delayed rectifier potassium channel activation, fast sodium channel activation, fast sodium channel inactivation, transient A-type potassium activation, and transient A-type potassium inactivation, respectively. Transient A-type potassium gating variables (a and b) in the current equation are governed in the model by the differential equation of the form:

$$\tau_z(V)\frac{dz}{dt} = z_\infty(V) - z \tag{11}$$

where z denotes a generic gating variable. This form was chosen because the A-type potassium current was originally described in terms of the functions $z_\infty(V)$ and $\tau_z(V)$, which were derived from experimental data (Connor and Stevens 1971). The other gating variables were expressed in terms of their opening and closing rates $\alpha_z(V)$ and $\beta_z(V)$:

$$\frac{dz}{dt} = \alpha_z(V)(1 - z) - \beta_z(V)z \tag{12}$$

All neural model parameters governing the gating equations were chosen as presented by Dayan and Abbott (Dayan and Abbott 2001). Unit ionic conductances and reversal potentials are shown in Table 3-1.

Table 3-1 Unit Ionic Conductances and Reversal Potentials used in model neuron

Parameter	Value
$\overline{g}_L$	0.3 mS/cm^2
$\overline{g}_{Na}$	80 mS/cm^2
$\overline{g}_K$	20 mS/cm^2
$\overline{g}_A$	50 mS/cm^2
E_L	-75 mV
E_{Na}	70 mV
E_K	-90 mV
E_A	-90 mV

3.4 Results

3.4.1 Responses of muscle spindle Ia afferents to stretch

Consistent with prior studies, all Ia afferents exhibited initial bursts at onset of applied stretch, followed by a dynamic response during constant velocity stretch, and a period of rate adaptation during the subsequent isometric hold period (Figure 3-2A-B). When repeated ramp-release stretches were applied to the muscle, an initial burst and dynamic response was present during the first ramp, but the initial burst was absent and dynamic response was reduced during subsequent stretches (Figure 3-2C) – a phenomenon in Ia afferents known as history-dependence (cf. Haftel et al. 2004).

The population of 11 Ia afferents considered for the first analysis varied in sensitivity to stretch length, velocity, and acceleration. More dynamic afferents, as quantified by

dynamic index (P. Matthews 1963) typically had relatively large spike responses during positive velocity stretch (Figure 3-2D). More static afferents exhibited more firing during the plateau phase of stretch, with relatively smaller dynamic indices (Figure 3-2D). The population of afferents also exhibited a range of initial burst amplitudes in response to stretch (Figure 3-2E). There was no clear relationship between the dynamic index and initial burst amplitudes for a given afferent. Despite the differences in sensitivity amongst the afferent population, the waveforms of afferent responses to the same stretch stimuli contained the same features (i.e. all afferents exhibited initial bursts, dynamic responses, and rate adaptation to varying degrees).

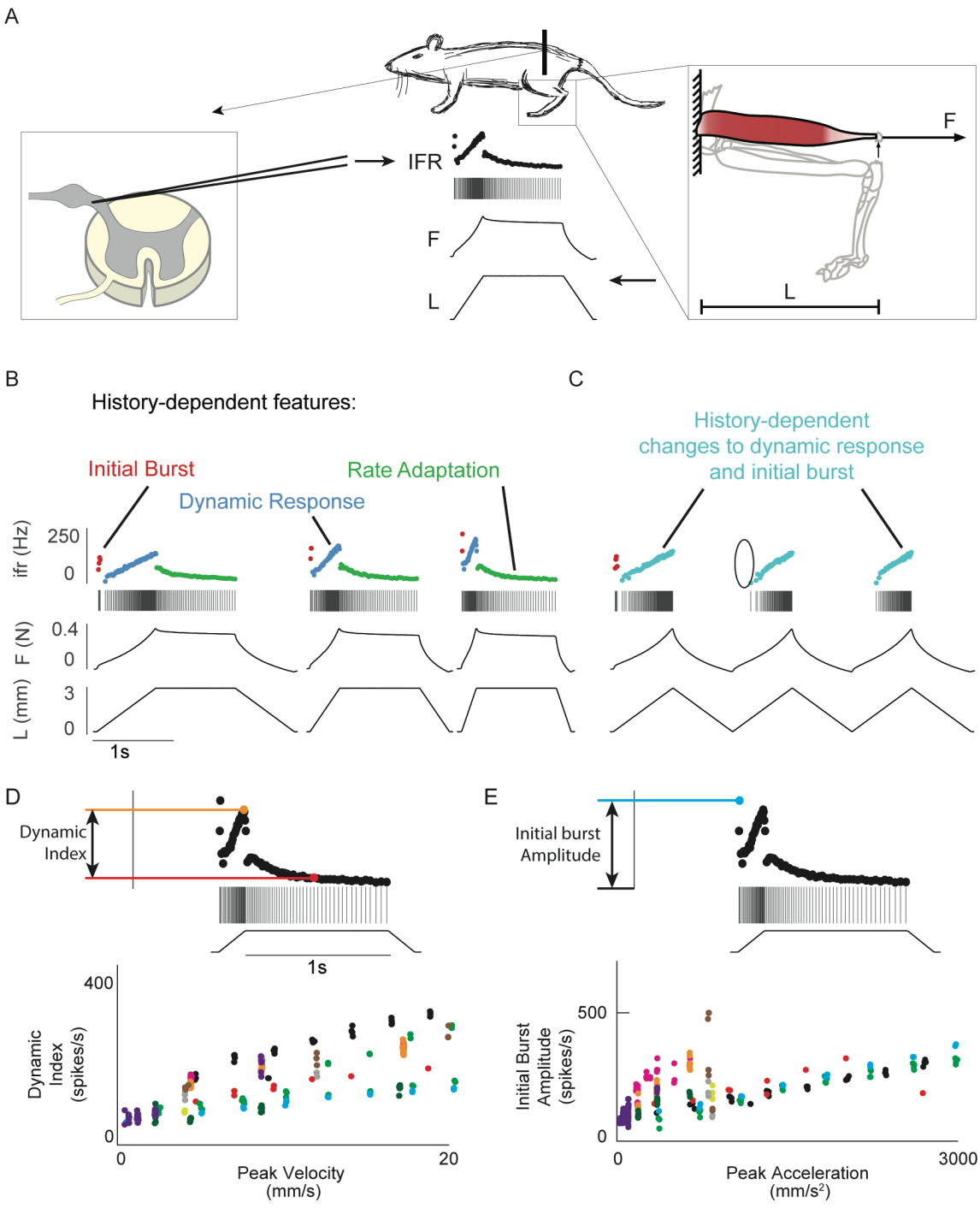

Figure 3-2 – Responses of muscle spindle Ia afferents to stretch. **(A)** Overview of data collection. When applying length changes (L) to the muscle, we recorded musculotendon force (F) and the muscle spindle Ia spiking response (IFR). **(B)** Muscle spindle Ia afferents fired with history-dependent IFR features in response to applied muscle stretch including initial bursts of firing (red) at stretch onset, dynamic response (blue) during the positive velocity ramp phase of stretch, and rate adaptation (green) during isometric hold after positive velocity stretch. **(C)** Ia afferent IFRs were history-dependent. When an identical

stretch stimulus was applied repeatedly, the Ia afferent exhibited larger initial bursts and dynamic responses during the first stretch compared to subsequent stretches. **(D)** The population of afferents exhibited a range of dynamic indices with respect to stretch velocity. Each color represents data from a different afferent. **(E)** The population of afferents also exhibited a range of initial burst amplitudes with respect to peak acceleration. Each color represents data from a different afferent.

3.4.2 Estimated intrafusal muscle force during stretch resembles history-dependent Ia afferent spiking

In contrast to our hypothesis that history-dependent Ia afferent spiking responses would resemble whole musculotendon force recordings based on feline studies (Blum, Lamotte D'Incamps, Zytnicki, and Ting 2017b), in rats, we found marked differences between spike rates and whole muscle force. Although a visible short-range force at stretch onset corresponded to the initial burst in the Ia response, the later, exponential rise in musculotendon force during constant velocity stretches was not typically reflected in Ia spiking responses. Further, when muscles were stretched with repeated ramp-release profiles, there was little apparent change in musculotendon force across identical sequential stretches, whereas dramatic changes in the Ia spiking response were observed (Figure 3-3A-B, E, left column). Yet, small differences in whole musculotendon force with respect to musculotendon length were observed in first stretch compared to subsequent responses (Figure 3-3B, right column).

However, muscle spindle spiking responses closely resembled estimated muscle fiber waveforms and their first time-derivatives, i.e. yank, across a variety of muscle stretch profiles (Fig 3-3C-D). Muscle fiber forces, estimated by subtracting noncontractile forces from whole musculotendon forces, exhibited both short-range force and force yield that matched muscle spindle initial bursts and dynamic response in ramp stretches (Fig 3-3C-

D). Further, estimated muscle fiber forces exhibited history-dependence during repeated ramp-release stretches similar to those observed in muscle spindle responses, but not recorded musculotendon length-related or force-related variables.

3.4.3 Pseudolinear combinations of estimated muscle fiber force and yank predicted Ia spiking waveforms across stretch conditions

The muscle fiber force-related model was able to predict the transient dynamics of Ia afferent spike rates including the initial burst, dynamic response, and rate adaptation across stretch velocities (Figure 3-4). In each example plotted here, muscle fiber force and yank were able to account for >90% of variance in the firing rates for ramp-hold trials, which was representative of the best fits across the 11 afferents analyzed here. The force-related model typically accounted for >80% variance in each afferent ramp-hold-release dataset.

During ramp-hold-release stretches, muscle fiber force components typically accounted for a large amount of variance in the instantaneous firing rates, contributing to the dynamic response of the predicted firing profile during positive velocity stretch and to the rate adaptation during isometric plateau (Figure 3-4A,C – dark blue component). Yank components typically predicted the initial burst of spikes at stretch onset and sometimes

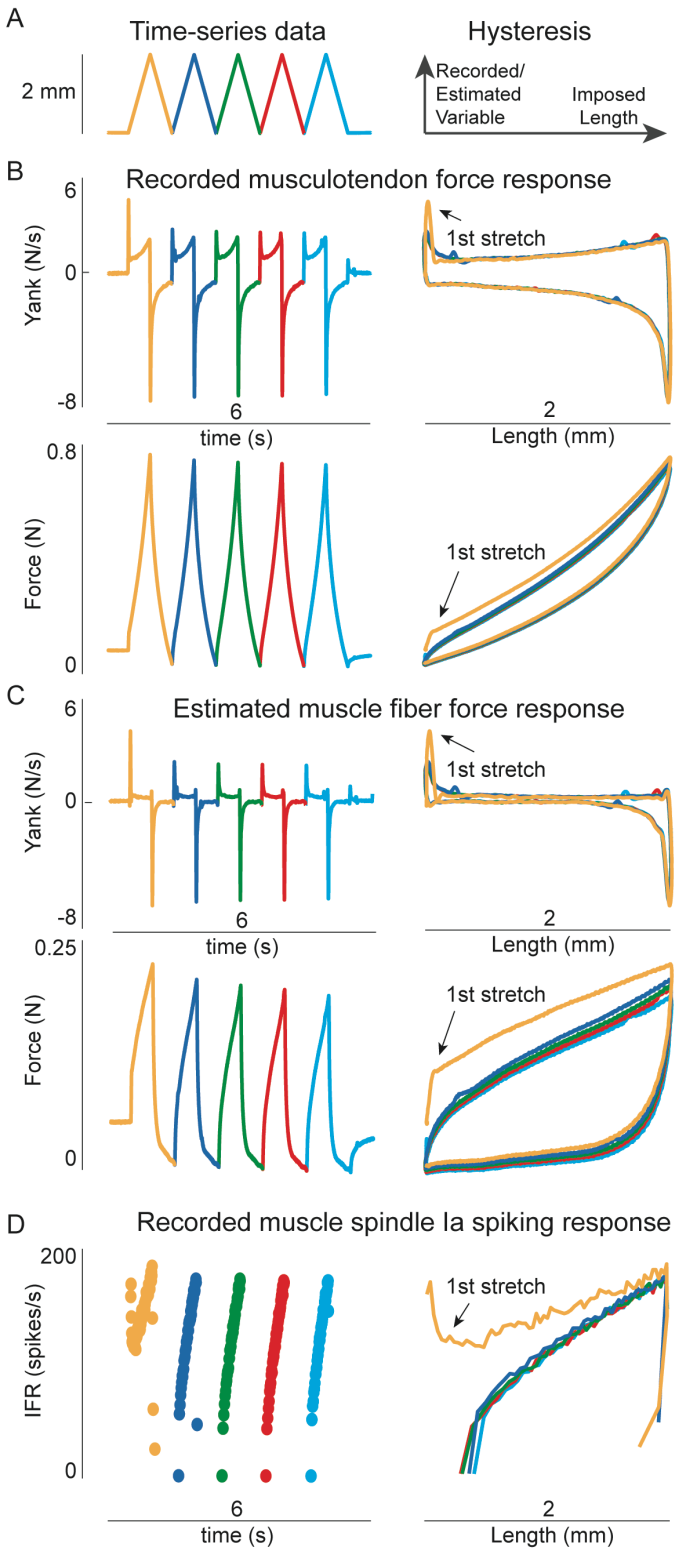

Figure 3-3 – Measured and estimated history-dependent variables of the muscles and Ia afferents. The left column contains data plotted against time in the horizontal axis. The right column contains the same data plotted against imposed length during perturbation (hysteresis plots). **(A)** An example repeated ramp-release perturbation is shown on the left.

Colors indicate different repeated perturbations for clarity in the hysteresis plots. Example axes for the hysteresis plots are shown on the right. **(B)** Recorded musculotendon force in response to the length perturbation in A is shown on the top, and calculated rate change in force, yank is shown on the bottom. Notice slight visible history-dependence between first response (yellow) and subsequent responses (blue, green, red, cyan). **(C)** Instantaneous firing rate from a Ia afferent in response to the perturbation is shown. Left and right columns show same data, but hysteresis plot was made into a continuous trace for clarity. Notice the distinct differences in firing rate between first response (yellow: initial burst and dynamic response) and subsequent responses (blue, green, red, cyan: nonexistent initial burst and reduced dynamic response). **(D)** Estimated muscle fiber force response to the length perturbation in A is shown on the top, and corresponding calculated muscle fiber yank is shown on the bottom. In the estimated muscle fiber force, notice the predominately larger dynamic response in the first compared to subsequent responses, and in the estimated muscle fiber yank, notice the larger peak at stretch onset in the first compared to subsequent responses.

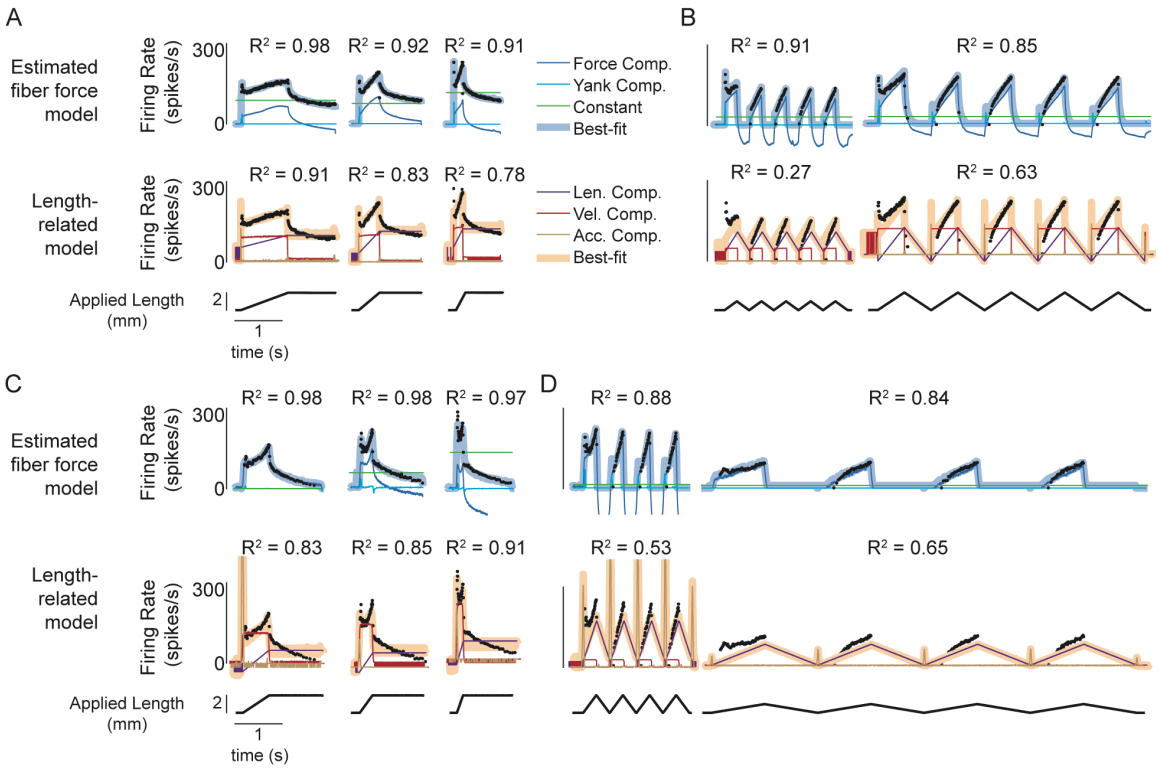

Figure 3-4 – Comparison of the ability of force- and length-related models to predict Ia afferent firing responses to stretch. **(A)** Model predictions for 3 2mm ramp-hold stretch trials at increasing velocity for a single afferent (black lines on bottom represent applied length, left to right: 2, 4, 9 mm/s). Cool colors represent estimated fiber force-related model prediction and components: thick gray-blue line – model prediction; blue – force component; cyan – yank component; green – constant component. Warm colors represent length-related model prediction and components for same afferent data: thick orange-yellow line – model prediction; purple – length component; red – velocity component; brown – acceleration component. Goodness of fit (R^2) displayed above corresponding fits

for each trial. **(B)** Model predictions for 2 ramp-release stretches applied at 4 mm/s (left: 1mm, right: 2mm). Data from same afferent as in A. **(C)** Model predictions for 3 3mm ramp-hold stretch trials at increasing velocity for a different afferent (left to right: 4, 8, 16 mm/s). **(D)** Model predictions for 2 ramp-release stretches applied (left: 2mm, 8mm/s; right: 1mm, 1mm/s). Data from same afferent as in C.

contributed to the dynamic response in the predicted firing profile (Figure 3-4A,C – cyan component; for this afferent, the yank component was found to have a threshold such that it primarily contributed to the initial burst).

The muscle fiber force-related model was also able to predict history-dependent changes in the Ia response in repeated ramp-release stretches. Similar to our study in feline (Blum, Lamotte D'Incamps, Zytnicki, and Ting 2017b), when the muscle was held at rest for at least 10 seconds, the muscle spindle response to the first stretch was characteristically different than the response to the subsequent stretches (Figure 3-4B,D). In contrast to our feline study, the best-fit muscle *fiber* (i.e., not whole-muscle) force-related model exhibited analogous changes in its prediction, predicting the initial burst at stretch onset and large dynamic response in the first stretch-release cycle followed by absent initial bursts and reduced dynamic responses in the subsequent cycles. The ability of the force-related model to predict history-dependent changes to Ia firing did not depend on perturbation amplitude.

The length-related model performance did not perform as well as the force-related model, despite re-optimization of parameters for each trial (Figure 3-4). This model tended to predict the magnitude of the initial burst and dynamic response with reasonable accuracy, though the transient details, i.e., the full time-course of the waveform, were typically not predicted. Consistent with our previous finding, the length-related model was incapable of predicting rate adaptation in the spiking response, because no model

component contained such a feature (Blum, Lamotte D'Incamps, Zytnicki, and Ting 2017b).

Further, the length-related model was not able to predict the history-dependent changes to Ia firing in repeated ramp-release perturbations. The identical nature of the length-related variables in each stretch-release cycle prohibited any history-dependent effects from being predicted. This tended to under-predict the dynamic response during the first stretch response and over-predict the dynamic response for the subsequent stretch trials (Figure 3-4 B, D). Further, initial bursts were either not predicted at all or were predicted for every stretch-release cycle; neither case occurred in any Ia afferent trial.

The differences in model performance (sum of squared errors calculated for each trial) were significant in all 11 afferents for ramp-hold-release trials included in this analysis (Figure 3-5A-B; asterisk: $p < 0.05$). In fact, for these trials (Figure 3-5A-B), the R^2 values for the force-related model (blue dots) were almost always larger than those of the corresponding length-related model values (red circles).

The muscle fiber force-related model also outperformed the length-related model repeated ramp-release stretch trials ($n = 9$), (Figure 3-5C-D). As was the case for the ramp-hold trials, R^2 values for the force-related model (blue dots) in these trials were almost always larger than those of the corresponding length-related model values (red circles). The differences in model performance were significant in 8 out of 9 afferents included in this analysis (Figure 3-5C-D: asterisks; 8/9 afferents $p < 0.05$).

No general relationship between either stretch velocity or length and model performance (for either model) was evident across the afferent population.

3.4.4 Best fit force-related model performance consistent across trial characteristics, despite varied model parameters

There was a general decreasing relationship between k_F values and maximum perturbation length for all stretch trials included in the analysis. In afferent datasets containing more than 1 perturbation length value (Figure 3-6A, top row). There was not an obvious general relationship between k_F and perturbation velocity (Figure 3-6B, top row).

The noncontractile tissue parameters varied across trials, but without any systematic relationships to perturbation length or velocity. There were no clear trends

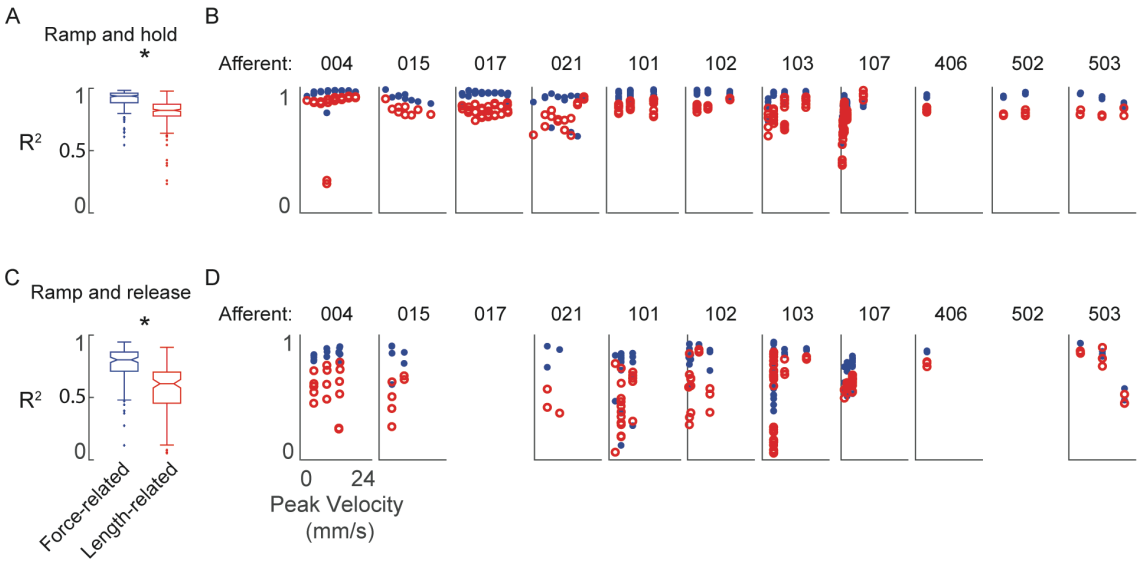

Figure 3-5 – Comparison of force- and length-related models to predict Ia afferent firing rates across all trials and afferents. **(A)** Box and whisker plots representing model goodness of fit (R^2) values for all ramp and hold trials for both estimated fiber force- (blue) and length-related (red) models. Midlines in boxes represent the median of the data. Notches represent the 95% confidence interval of the median. The tops and bottoms of the boxes correspond to the 75th and 25th percentiles of the data. Whiskers represent the edges of the distribution and individual data points are outliers. Asterisk above plot indicates a significant difference between the model performance measurements (one-way ANOVA performed on cumulative squared model errors; $p<0.05$). **(B)** Individual trial R^2 for all ramp and hold perturbations for each afferent plotted against stretch velocity. Blue dots represent the estimated muscle fiber force-related model and red circles represent that for the length-related model. These data cumulatively make up the box plots in A. **(C)** Box and whisker plots representing model goodness of fit (R^2) values for all repeated ramp-release trials for

both estimated fiber force- (blue) and length-related (red) models. Asterisk indicates significant difference between the model performance measurements (one-way ANOVA performed on cumulative squared model errors; $p<0.05$). **(D)** Individual trial R^2 for all repeated ramp-release perturbations for each afferent plotted against stretch velocity. These data cumulatively make up the box plots in C.

evident in any of the noncontractile tissue parameters (Figure 3-6A, rows 2-4), and thus, no clear covarying noncontractile tissue parameters with k_F. There also was no relationship between any of the noncontractile tissue parameters and perturbation velocity (Figure 3-6B, rows 2-4).

3.4.5 Changes to muscle spindle encoding caused by axonal stimulation predicted by reducing yank and constant component of pseudolinear model

Muscle spindle primary afferents exhibited marked changes to their response waveforms after application of a neural perturbation. In this experiment, all 6 Ia afferents responded with expected stereotypical features (initial burst, dynamic response, plateau firing) in response to ramp-hold perturbations (Figure 3-7A). As expected, each afferent's response exhibited a unique combination of initial burst, dynamic response, and plateau firing rate magnitudes. In trials where we applied a depolarizing current to the axon immediately preceding an identical mechanical perturbation, antidromic action potentials caused the same 6 Ia afferents to fire with characteristically different waveforms (ex: Figure 3-7B). In these trials, no afferent response contained an initial burst, and several afferent responses exhibited a reduced dynamic response and/or a reduction in plateau firing rate. In the third trial (identical conditions to the first control trial), each afferent responded with the expected stereotypical firing patterns we observed in the first trial (Figure 3-7C).

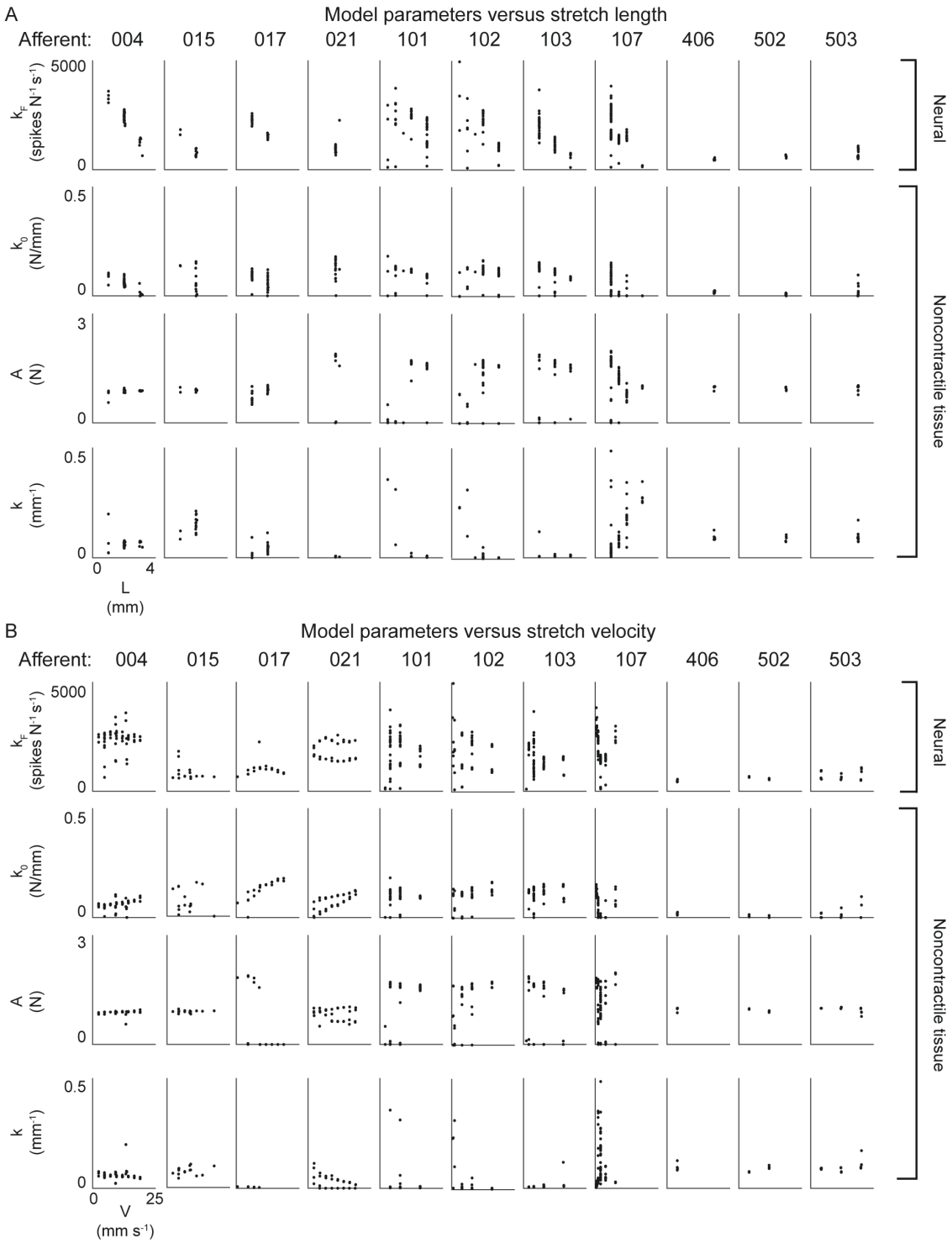

Figure 3-6 – Variability in four model parameters across perturbation characteristics for each afferent. **(A)** Variability in model parameters across imposed perturbation length. Top row – model sensitivity to estimated muscle fiber force. Notice the decreasing trend in the

data with respect to imposed length in afferents with more than one value of imposed length. Second row – noncontractile tissue model linear stiffness. Third row – noncontractile tissue model weight on exponential spring. Fourth row – noncontractile tissue model exponential stiffness parameter. **(B)** Same parameters as in A, plotted against stretch velocity.

The pseudolinear model containing estimated muscle fiber force and yank was able to account for all observed firing features for all 6 afferents in the pre- and post-stimulus control trials (mean $R^2 \pm$ St. Dev. = 0.85 ± 0.12 (pre-), 0.85 ± 0.07 (post-) with yank component; mean $R^2 \pm$ St. Dev. = 0.66 ± 0.12 (pre-), 0.62 ± 0.11 (post-) without yank component). The differences in model performance between fits with and without yank sensitivity were significant at the $\alpha = 0.05$ level (Figure 3-7D). In these trials, the model with yank sensitivity predicted initial bursts, dynamic response, and plateau firing with rate adaptation. In all 6 afferents, the yank component accounted for the initial burst at stretch onset, whereas in 4 afferents it accounted for some of the dynamic response (ex: 3-Figure 7A,C: cyan lines). The force component accounted for the rate adaptation feature and at least a portion of the dynamic response in all 6 afferents (Figure 3-7A,C: dark blue lines). There was no significant difference in the model sensitivity to force between fits with and without yank sensitivity (Figure 3-7F). There were no significant differences in the constant component between fits with and without yank (Figure 3-7G).

Significant reduction of the yank and constant components accounted for changes to the muscle spindle IFRs during stimulation trials (mean $R^2 \pm$ St. Dev. = 0.90 ± 0.12). There was no significant difference in model performance between these trials and the model fits with yank sensitivity in the control trials at the $\alpha = 0.05$ level (Figure 3-7D). In each of the 6 afferent responses, the contribution of the yank component to the best- fit prediction was made zero to account for the lack of initial bursts in all responses (Figure 3-7E). This

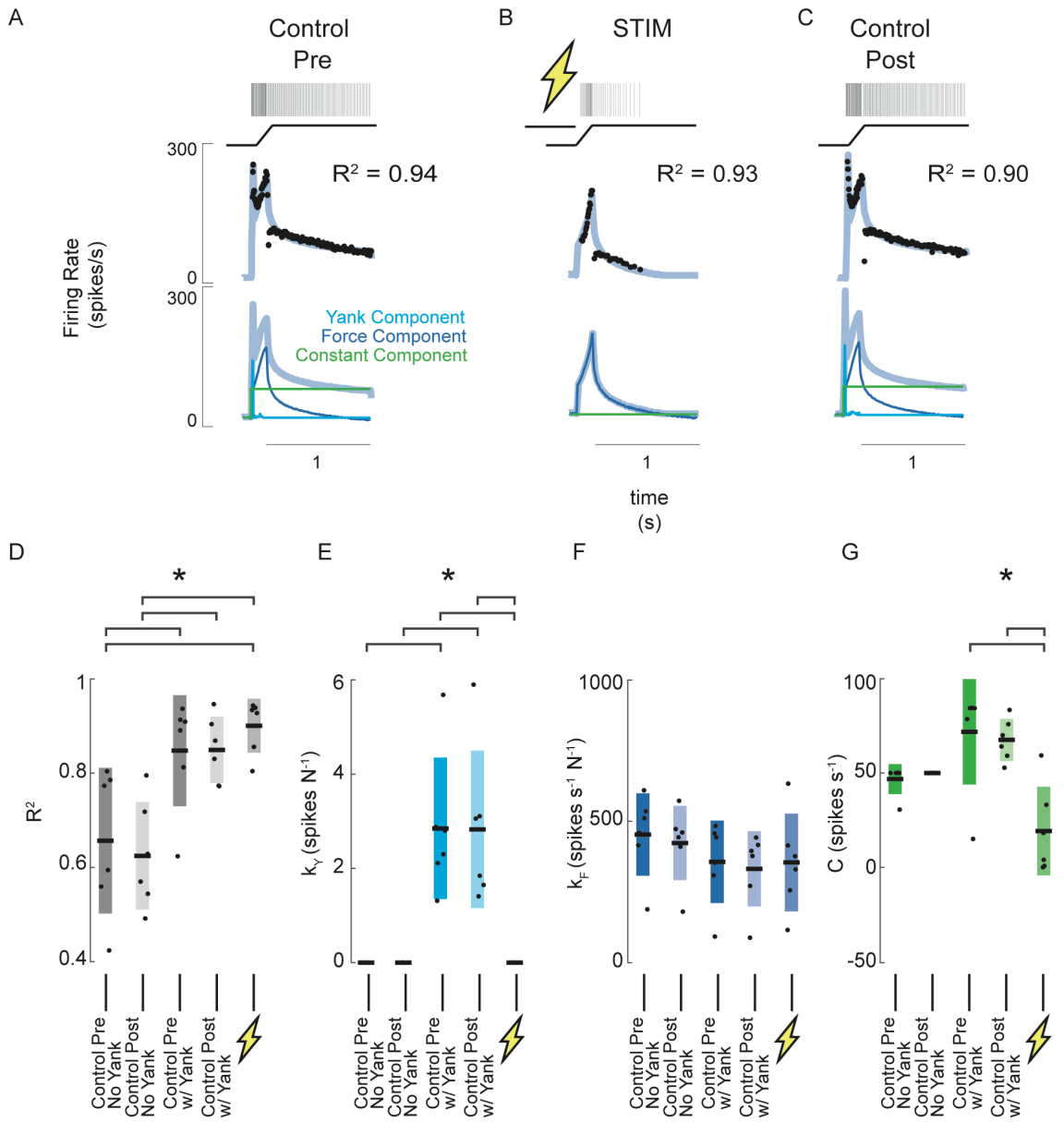

Figure 3-7 – Estimated muscle fiber force-related model predicts changes in muscle spindle encoding caused by axonal stimulation. **(A)** Example of pre-stimulus control trial consisting of a 3 mm ramp-hold stretch at 20 mm/s. Raster represents the times of recorded action potentials in response to the ramp-hold stimulus shown directly below it. Black dots represent the afferent IFR corresponding to the raster. The gray-blue line represents the model prediction using force, yank, and constant components. Below this are the same model prediction as above (grey-blue) and model prediction components (blue – force component; cyan – yank component; green – constant component). **(B)** Example of stimulus trial consisting of the same stretch applied as A, with a depolarizing current applied to the axon directly prior to stretch. The model fit in this trial represents the best-fit without the yank component. Notice the quality of fit does is roughly equal in this trial with that of the pre-stimulus trial in A, but no yank component was necessary. **(C)** Example of post-stimulus control trial. Same stretch and model components were used as in A. **(D)**

Goodness of fit (R^2) of force-related model for 6 afferents subjected to the same trials as shown in A-C. The first two columns show R^2 values of the model fits without yank components for the pre- and post-stimulus control trials, respectively, for all 6 afferents. The third and fourth columns from the left show R^2 values for the model fits with yank components for the pre- and post-stimulus control trials, respectively, for the same 6 afferents. The fifth column shows R^2 values for the model fits for the stimulus trials. This model did not use a yank component. **(E)** Model sensitivity to yank for the same model fits and afferents as D. **(F)** Model sensitivity to force for the same model fits and afferents as D and E. **(G)** Model constant component for the same model fits and afferents as D-F. Brackets above plots indicate significant differences between the means ($p < 0.05$).

also affected the best-fit predictions in which the yank component contributed to the dynamic response. The force components accounted for the majority of the variance in these afferent responses, after they were re-fit using optimization. There were no significant differences in the force sensitivity between any of the control groups and stimulation trials (Figure 3-7F). Interestingly, there was a significant reduction in the constant component of the model's best-fit prediction compared to those of the control trials with yank sensitivity (Figure 3-7G).

3.4.6 Changes to muscle spindle encoding caused by oxaliplatin chemotherapy predicted by reduced fiber force component of pseudolinear model

Our model was able to account for changes to the Ia afferent IFR waveforms caused by platinum-based chemotherapy. As demonstrated previously, muscle spindle Ia afferents in rats treated with oxaliplatin chemotherapy exhibit significant changes to their ability to sustain firing rates during an isometric hold after stretch (Bullinger, Nardelli, Wang, et al. 2011). We fit our pseudolinear muscle fiber force-related model with and without yank sensitivity to three example afferents from these previous experiments.

The model yank component accounted for the majority of variance explained in the recorded IFRs by the best-fit model reconstruction (Figure 3-8A). Because the plateau

firing was significantly reduced in these afferents, the initial burst accounted for a relatively larger amount of variance of the IFR waveform. In all three afferents, the model performance was significantly greater when yank was included in the fit (Figure 3-8). We could not directly compare the force component for the fits of this dataset with those of healthy afferents, however, we observed that the threshold for the force component was

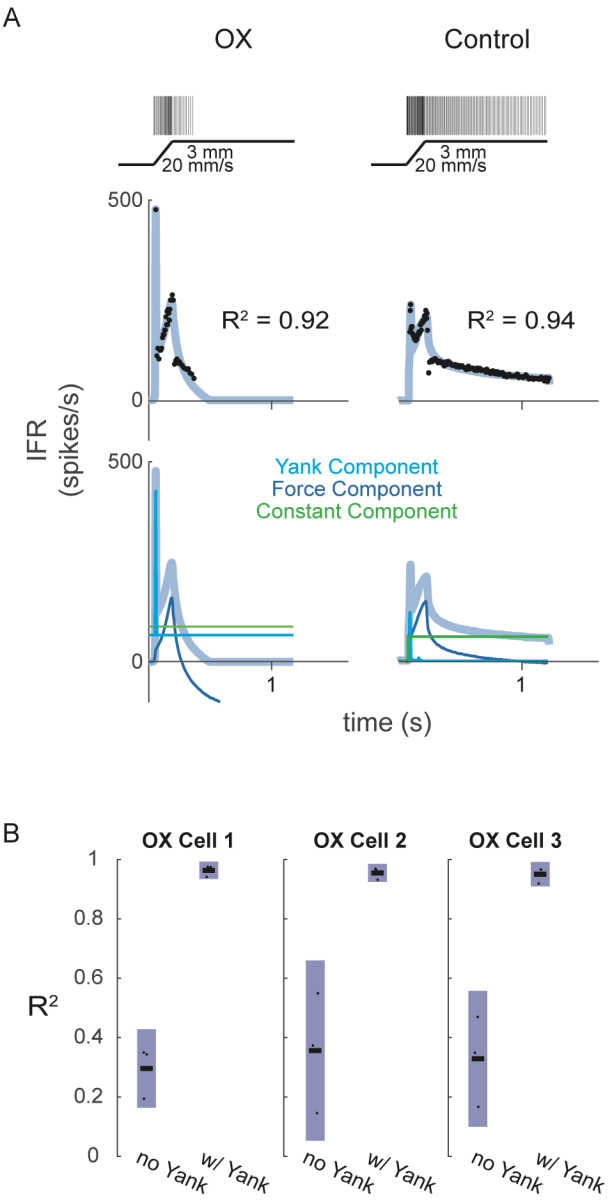

Figure 3-8 – Estimated muscle fiber force-related model predicts changes in muscle spindle encoding caused by oxaliplatin-induced channelopathy. **(A)** Example Ia afferent responses to stretch and corresponding model predictions. Left column shows a typical Ia

afferent response to a ramp-hold stretch applied to the triceps surae of a rat treated with oxaliplatin chemotherapy (Bullinger et al. 2011). Right column shows typical response of Ia afferent in response to same ramp-hold stretch. Rasters indicate times at which action potentials are recorded and are shown above imposed stretches. Below are the IFR and corresponding model fits shown above the same model fits with their respective components. **(B)** Variance of muscle spindle Ia afferent responses accounted for by force-related model with (right bar in each plot) and without (left bar in each plot) yank for 3 Ia afferents from 3 oxaliplatin-treated rats. Black horizontal bars represent the means, blue bars represent the standard deviations, and black dots represent the data points from each trial (3 trials per afferent).

selected such that the best-fit reconstruction predicted a cessation of plateau firing before the end of the plateau period (Figure 3-8A, left).

3.4.7 Range of afferent phenotypes predicted by estimated intrafusal force-related currents applied to a model neuron

We predicted muscle spindle spiking responses to stretch using estimated intrafusal force and yank components (plus a constant component) as a current input to a conductance-based model neuron (Figure 3-9A). We were able to match the firing waveform of the Ia afferent by hand-tuning the relative weights of the force, yank, and constant components before applying them to the model neuron as a stimulus current (Figure 3-9B). As expected, the yank component contributed to the initial burst and dynamic response, the force component contributed to the dynamic response and plateau firing, and the constant component contributed to raising the mean firing rate.

By varying the relative sensitivity of the neuron to each component, we were then to generate a family of firing characteristics resembling muscle spindle firing phenotypes observed in the literature. By changing the relative weights of the force and yank components, we revealed specific changes to the firing waveforms in response to the same stretch perturbation (Figure 3-9C). Generally speaking, different muscle spindle Ia

afferents tend to fire with different levels of initial burst, dynamic response, and plateau response. Changes to each of these features were revealed in this model by adjusting relative sensitivities to force and yank (Figure 3-9C).

A reduction in the model's yank sensitivity reduced the initial burst as well as the dynamic response in firing rate. As sensitivity to yank was decreased (Figure 3-9C – left

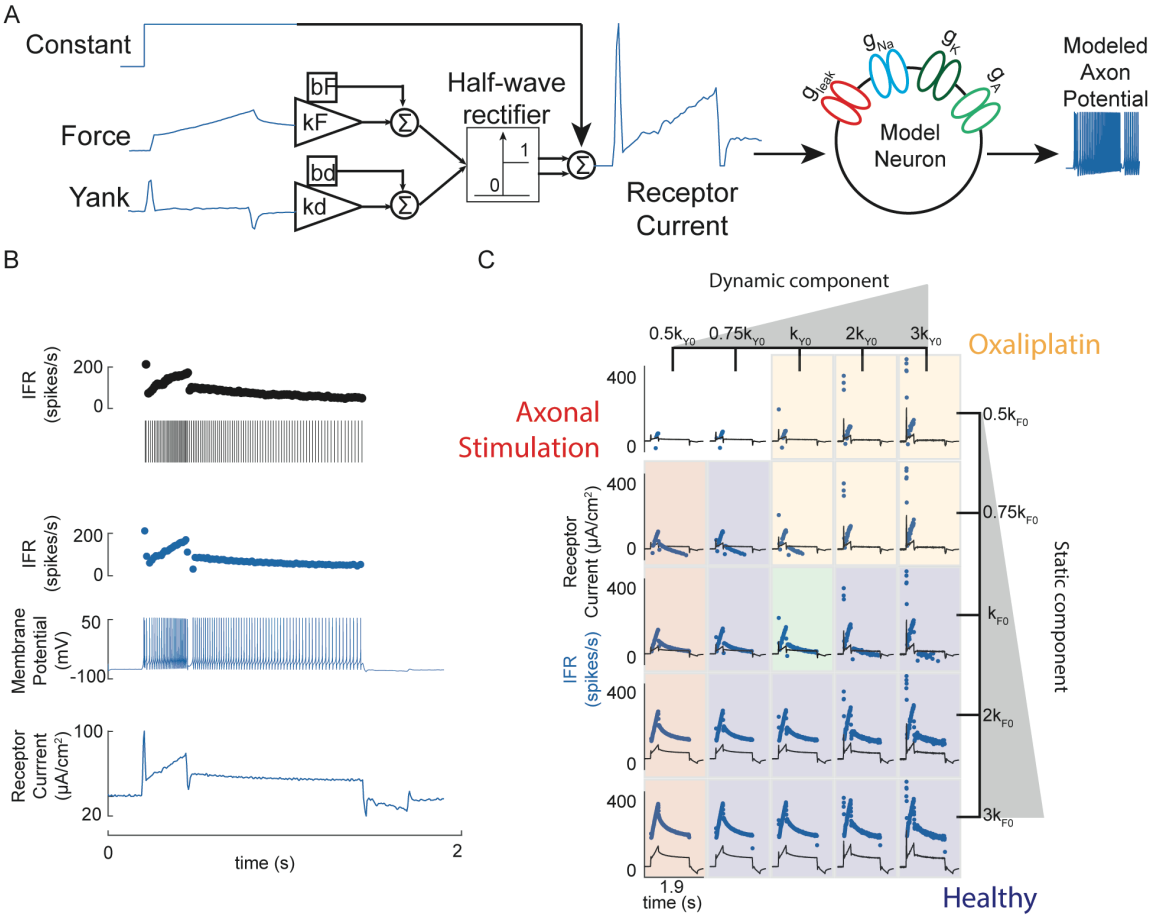

Figure 3-9 – Estimated fiber force-related model predicts range of muscle spindle afferent phenotypes when used as input to model neuron. **(A)** Schematic diagram of modelled mechanotransduction. Force and yank components are scaled, offset, half-wave rectified, and added to a constant to form the modelled receptor current. This current is used as an input to a model neuron, which transforms the currents into a membrane potential containing action potentials. **(B)** Example of simulation data. Black raster and dots represent spike times and IFR, respectively, of a Ia afferent in response to a 2 mm, 10 mm/s ramp-hold stretch. Blue dots and membrane potential represent the output of the model described in A. The bottom blue trace is the hand-tuned nominal receptor current used as

an input to the model neuron based on the three components of the force-related model. **(C)** Model neuron outputs with varying receptor current sensitivity to force (vertical axis) and yank (horizontal axis). Values of parameters are expressed in relation to the nominal values used in the simulation in B. Green box in the middle represents the nominal model parameters (same as the simulation in B). Blue shaded boxes represent responses "healthy" phenotypical muscle spindle Ia afferent responses containing an initial burst, dynamic response, and plateau response within the range observed experimentally. Red shaded boxes represent the phenotypical responses expected during the axonal stimulation procedure (e.g. Figure 3-7) caused by a reduction in the dynamic yank component. Yellow shaded areas represent the phenotypical responses expected after treatment with oxaliplatin chemotherapy (e.g. Figure 3-8) caused by a reduction in the static force component.

to right) the initial burst at stretch onset was reduced, and eventually nonexistent. This is analogous to the antidromic spike train's effect on the muscle spindle encoding as seen in Figure 3-7.

As sensitivity to force was decreased (Figure 3-9C – bottom to top), we observed an obvious reduction in plateau firing in the model. Second, a reduction in the force sensitivity reduces the amount of time the muscle spindle Ia afferent is able to maintain a plateau firing response. Once the force sensitivity was reduced enough, the plateau firing was eradicated completely. An analogous phenotype observed by Bullinger and colleagues (Bullinger, Nardelli, Wang, et al. 2011) is a typical Ia afferent response after the animal was treated with oxaliplatin, a platinum-based chemotherapy treatment (Figure 3-9C, Figure 3-8A). This phenotype is described by a healthy initial burst and dynamic response, but inability of the afferent to maintain steady firing during isometric hold. Additionally, when force sensitivity was decreased in the model (Figure 3-9C, bottom to top), there was a decrease in dynamic response, though the dynamic response was never completely removed from the model's firing response.

Finally, changes to the neural sensitivity to force and yank accounted for the range of dynamic behaviors of the healthy afferents presented in this paper (Figure 3-10A-B). By adjusting the nominal sensitivities the same relative amounts (0.1-5 times nominal values for force and yank) for 4 recorded stretch trials at different velocities (as in Figure 3-10C), we produced afferent spiking responses that accounted for a large area of both dynamic index (Figure 3-10D) and the initial burst amplitude (Figure 3-10E) variance in our recorded data.

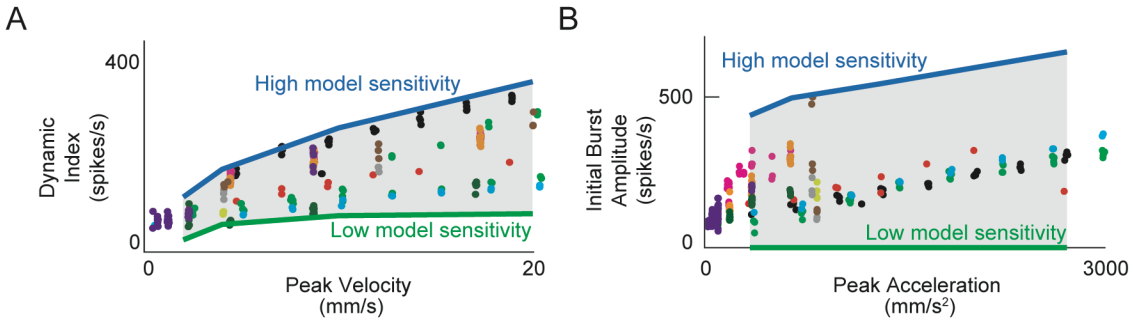

Figure 3-10 – Estimated muscle fiber force model predicts inter-afferent variability of healthy afferent firing properties across perturbation velocity and acceleration. **(A)** Same dynamic index data shown in Figure 3-2 (colored dots) with predicted range of dynamic indices from model (gray shaded area). Nominal simulations were performed with the same force and yank model sensitivities for 4 stretch trials (2, 4, 10, 20 mm/s) from the same animal. Model parameter sweeps were performed for force and yank sensitivities for each of the 4 trials from 0.1 to 5 times the nominal value for each parameter. Green line represents the minimum dynamic indices from each of the 4 parameter sweeps from trials for which there was a spiking response (usually corresponding to low force and yank sensitivities). Blue line represents maximum dynamic indices from each of the 4 parameter sweeps (usually corresponding to high force and yank sensitivities). Gray shaded area represents plausible space of simulated dynamic index. **(B)** Same initial burst data shown in Figure 3-2 (colored dots) with predicted range of initial bursts from same simulations as in A. Green line represents minimum initial burst values from each of the 4 parameter sweeps from trials for which there was a spiking response (this value was 0 for each of the 4 sweeps). Blue line represents maximum initial burst values from each of the 4 parameter sweeps (corresponding to high yank sensitivity). Gray shaded area represents plausible space of simulated initial burst amplitudes.

3.5 Discussion

We presented evidence that muscle spindle Ia afferents respond to the force and yank of their intrafusal fibers and that the spindle has partially-independent sensitivities to each of these variables (Lewis and Proske 1972b; Hunt and Ottoson 1975; Banks et al. 2009; Hasan 1983; Kruse and Poppele 1991; Banks et al. 1997). As a proxy for intrafusal muscle fiber force, we estimated whole muscle fiber force by analytically removing noncontractile tissue force from recorded musculotendon force (Hill 1953). By varying relative sensitivities of the resulting estimated muscle fiber force and yank, we were able to reconstruct a range of firing properties across different afferents, stretch conditions, and neural perturbations. We accounted for history-dependent changes in muscle spindle IFRs by using a single set of fiber force and yank model sensitivities. We showed that an electrical and a pharmacological (Bullinger, Nardelli, Wang, et al. 2011) mechanism of neural perturbation to muscle spindles independently affect the spindle's steady state and transient firing, which was accounted for in our model by differential sensitivity to force and yank, respectively. Finally, we showed that we could account for the apparently wide range of muscle spindle sensitivities in response to an identical stretch by varying the sensitivity of a model neuron to force- and yank- based depolarizing currents. This same combination of force and yank not only predicted variability in firing characteristics across normal muscle spindles, but also in those subject to electrical and pharmacological perturbations.

History dependent muscle fiber forces are masked by non-contractile tissues in passive rat muscle and likely reflect calcium-dependent muscle cross-bridge interactions (Campbell and Lakie 1998; Campbell and Moss 2000; Campbell and Moss 2002; Proske

and Morgan 1999). We found a significant component of history-dependent force within the recorded musculotendon force despite little initial visual evidence. While it is unlikely that we were able to perfectly dissociate force components using our idealized mechanical model structure of the muscle (Winters 1990), we are confident that our estimated muscle fiber force waveforms are closely related to the mean force waveform from the muscle fibers. Analogous history dependence in single permeabilized muscle fibers has been shown at varying activation levels but does not exist in unactivated fibers (Getz, Cooke, and Lehman 1998; Campbell and Lakie 1998; Campbell and Moss 2000; Campbell and Moss 2002). In these studies, the history-dependent properties were attributed to complex actin-myosin interactions manifesting as history-dependent muscle force in the presence of calcium. We interpret our analogous observation to mean that, even in a deeply anesthetized animal with no electrical activation of the muscle, there is a basal level of tonic activation from intracellular calcium ions in both intra- and extrafusal muscle fibers that contributes to history-dependent forces (Proske and Stuart 1985; Proske and Morgan 1999). Thus, electrically-quiescent muscles are not mechanically "passive," per se.

Transient muscle spindle spiking responses to stretches likely arise from mechanically-gated ionic currents related to the tension in the intrafusal fibers (Bewick and Banks 2015; Carrasco, Vincent, and Cope 2017; Bullinger, Nardelli, Wang, et al. 2011; Delmas and Coste 2013; Bewick 2015). Compared to other mechanoreceptors, muscle spindle primary sensory endings are unique in that they terminate on the central "sensory" region of intrafusal muscle fibers located in series with the striated muscle of the polar region of the same fibers (Ruffini 1898; Banks et al. 2009; Banks, Harker, and Stacey 1977; Banks, Barker, and Stacey 1979; Boyd 1976; Boyd 1962). When the muscle is moved, the

sensory region, assumed to behave as an ideal elastic (P. Matthews 1981; Hasan 1983), is stretched proportionally to the force response of the muscle fiber (Boyd 1976; Boyd et al. 1977). Thus, a debate as to whether the muscle spindle encodes the force or length of its sensory region is needless if the sensory region behaves as an ideal elastic. However, pressure- or force-gated ion channels in mammalian mechanoreceptors have been suggested and identified in a range of dorsal root ganglia cells, shedding light on the potential mechanism for force-related encoding in the muscle spindle endings (Carrasco, Vincent, and Cope 2017; Bullinger, Nardelli, Wang, et al. 2011; Delmas and Coste 2013; Bewick and Banks 2015; Bewick 2015; Simon et al. 2010). We implemented this knowledge to a forward model of muscle spindle spiking by applying a force- and yank-related depolarizing current to a spiking model neuron (P. B. Matthews and Stein 1969; Dayan and Abbott 2001), which accounted for all transient features of muscle spindle IFRs.

Differential sensitivities to force and yank in muscle spindle IFRs could be attributed to variations in mechanical structure between muscle spindles (Liu, Eriksson, Thornell, and Pedrosa-Domellöf 2002b; Liu et al. 2005; Thornell et al. 2015; Cooper and Gladden 1974; Gladden 1976). Classically defined as “dynamic” and “static” components, yank and force could be predominately encoded in the same afferent IFR by different endings of the spindle (Jami and Petit 1979; Banks et al. 1997; Kruse and Poppele 1991). Mammalian muscle spindle primary afferents have endings on several intrafusal muscle fibers, each with different mechanical properties and gamma innervation (Cooper and Gladden 1974; Gladden 1976; Ruffini 1898; Boyd 1976; Boyd 1962; Sherrington 1894). Furthermore, spindles can vary in their numbers of total sensory endings (Banks et al. 2009; Banks, Harker, and Stacey 1977; Banks, Barker, and Stacey 1979). The Ia afferent endings on the

dynamic bag1 intrafusal fiber may account for components of the IFRs we have identified as yank-related, whereas the bag2 fiber and chain intrafusal fibers may predominately encode force-related information (Kruse and Poppele 1991; Banks et al. 1997; Boyd et al. 1977). Therefore, differences in sensitivities to force and yank between muscle spindles may simply be a factor of the number of sensory endings a particular Ia afferent has on the different intrafusal fibers. In further support of this hypothesis, group II muscle spindle afferents, which have no endings on bag1 intrafusal fibers, exhibit IFRs that are much less dynamic than those of Ia afferents (P. B. Matthews and Stein 1969; P. B. Matthews 1963). An alternative hypothesis is that the spike generating mechanisms of the muscle spindle are responsible for differential sensitivities to force- and yank-related signals. In this hypothesis, intrafusal fiber force-related graded potentials are transduced to the heminodes of the muscle spindle afferent, where spikes are generated in both a proportional- and rate-sensitive manner.

The sensitivity parameters of our model to muscle fiber force and yank are implicitly related to the mechanical structure, mechanotransduction, and spike generation of the muscle spindle, and can thus quantify changes in one or more of these parts of the muscle spindles. In this paper, we reconstructed the IFRs of Ia afferents subjected to two neural perturbations.

Our model was not only able to quantify changes in the muscle spindle IFRs caused by stimulation but was also able to shed light on the mechanisms of differential encoding of force and yank by the spindle. The first neural perturbation we analyzed with our model was the effects of antidromic action potentials on the muscle spindle IFRs. Because antidromic action potentials preferentially eliminated the dynamic components of IFR in

response to stretch, our model reconstructed the IFR with high fidelity without any sensitivity to yank. In addition to supporting our hypothesis that yank and force-related components are encoded independently by the muscle spindle, this analysis supports the hypothesis that the dynamic and static components of the IFR arise from different branches of the muscle spindle sensory receptor (Banks et al. 1997). In normal muscle spindle encoding, graded membrane potentials are transformed into action potentials at heminodes of several branches and are summed together into a single spike train in the afferent fiber (Lin and Crago 2002; Banks et al. 1997; Boyd et al. 1977). In these experiments, we hypothesize that antidromic action potentials travel down the axon and follow the path of least resistance in the largest branch of the sensory receptor until it reaches the heminodes of that branch (Carrasco, Vincent, and Cope 2017). The largest branch of the muscle spindle receptor belongs to the bag1 ending, which has long been considered the source of dynamic muscle spindle IFRs.

Our model was also capable of reconstructing the impaired muscle spindle IFRs in rats treated with platinum-based chemotherapy (Bullinger, Nardelli, Wang, et al. 2011). As discussed in a previous paper, these spindles exhibit no marked changes to their dynamic sensitivities or axonal conduction of action potentials but do show an inability to sustain firing to a tonic stimulus. The model presented here predicts the changes to the firing rate by reducing the relative sensitivity to force. Interestingly, previous studies found no differences between muscle force in response to stretch in oxaliplatin-treated and healthy rats (Bullinger, Nardelli, Wang, et al. 2011); there is no evidence that spindles are receiving a different mechanical stimulus when similar stretches are applied to the musculotendon. Thus, our model's predicted changes to the static force component of firing implies a purely

neural deficit caused by oxaliplatin. Because our spike-generating mechanism was consistent throughout our simulations producing healthy and oxaliplatin-like phenotypical responses, our model predicts that oxaliplatin causes a change to the mechanotransductive process within the spindle receptor, which has not been hypothesized before. However, our model is incapable of testing another hypothesized location of effect of oxaliplatin: the persistent inward currents (PIC) of the spike-generating process in the heminode of the spindle. Further study should be conducted to pinpoint whether mechanotransduction or spike-generation of the muscle spindle primary afferent is primarily affected by oxaliplatin.

Because our model of muscle spindle encoding succinctly accounts for the range of dynamic and static sensitivities observed in muscle spindle IFRs, we believe it can be used as a tool to predict changes to sensorimotor control caused by other neurological diseases such as Parkinson's disease. One technical limitation of our model is that it relies on a recorded force variable from which we can estimate the history-dependent muscle fiber forces, whereas many sensorimotor control researchers are not equipped to measure muscle force. A forward mechanistic model of the intrafusal fibers could be used, but currently, no mechanistic models of muscle spindles are capable of history-dependence. Therefore, we emphasize the construction of such a forward model as a necessary next step.

CHAPTER 4. A THIXOTROPIC MODEL OF MUSCLE SPINDLE FUNCTION BASED ON CROSS-BRIDGE DYNAMICS

4.1 Introduction

Proprioception is the ability to perceive the location and state of our limbs in space that arises from sensory organs located within the musculotendons, joint capsules, and skin. Muscle spindles are generally considered to be the "primary" proprioceptive information source and are crucial for many sensorimotor tasks such as postural control (Horslen et al. 2013; Lockhart and Ting 2007; Welch and Ting 2009; Welch and Ting 2008), locomotion (Prochazka and Gorassini 1998b; Prochazka and Gorassini 1998a; Weber et al. 2007; Weber et al. 2006), targeted reaching (Scott and Loeb 1994), and others. Muscle spindles are unique proprioceptors in that they have their own intrafusal muscle fibers whose mechanics directly contribute to the mechanotransduction in the sensory endings of the spindle (Bewick and Banks 2015; Carrasco, Vincent, and Cope 2017; Blum, Lamotte D'Incamps, Zytnicki, and Ting 2017b). Altered muscle spindle function or central processing of muscle spindle information is implicated in a number of sensorimotor disorders such as muscular dystrophy (Swash and Fox 1976), stroke (Wilson, Gracies, et al. 1999; Wilson, Gandevia, et al. 1999; Kamper et al. 2003; Carey, Matyas, and Oke 1993; Ranatunga et al. 2010), Parkinson's disease (Conte et al. 2013; Konczak et al. 2009; Rickards and Cody 1997; Khudados, Cody, and O'Boyle 1999; Rothwell et al. 1983; Patel, Jankovic, and Hallett 2014), and spasticity (Dietz and Sinkjaer 2007; Hagbarth and Eklund 1968; Steg 1962; Sheean 2002), which manifests in many disorders. Yet, we lack tools to study how multi-scale physiological and pathological changes to muscle spindles may alter

sensorimotor control. Without a general model of muscle spindle function, researchers must rely on phenomenological descriptions of muscle spindle sensory function. It is therefore important for researchers to have a general mechanistic model of healthy muscle spindle function, which can be applied to different research questions examining muscle spindle function in different contexts.

We currently do not have a model of muscle spindle function that can account for both history-dependent and classical features of muscle spindle Ia afferents spiking responses to stretch. The lack of a general model of muscle spindle function is partially due to the fact that most models have been constructed for a particular context in which to study the sensory encoding of muscle spindles. For example, researchers have constructed phenomenological models of muscle spindle function in which the muscle spindle activity in steady state locomotion in a cat could be reconstructed reliably with a weighted combination of muscle length, velocity, and electromyographical (EMG) recordings (Prochazka and Gorassini 1998a; Weber et al. 2007). While this type of model has clear advantages for neural engineering applications, such as computationally tractability, they cannot be considered general because they require stereotyped movements (such as locomotion) and are not capable of reproducing any history-dependent features of muscle spindle encoding nor important transient activity such as the initial burst. Mechanistic models of muscle spindle function have had more general success reproducing muscle spindle responses to stretch. From reproducing experimentally identified nonlinear relationships with stretch variables (Houk, Rymer, and Crago 1981; Hasan 1983), initial bursts (Chen and Poppele 1978; Lin and Crago 2002; Hasan 1983), and effects of

anatomical structure and gamma activation (Mileusnic et al. 2006; Lin and Crago 2002; Hasan 1983).

Muscle spindles consist of several of their own muscle fibers encapsulated within the extrafusal (regular) fibers of a muscle. Within their capsule, sensory neurons of the muscle spindle wrap around specialized intrafusal muscle fibers, which are also innervated by efferent neurons, called gamma motor neurons. It is the tension of this intrafusal fiber that runs parallel to the regular extrafusal fibers that is detected by the muscle spindle and transmitted as action potentials to the central nervous system.

Thixotropic properties of intrafusal muscle contribute to both conscious and unconscious sensation of movements arising from muscle spindles but are often overlooked when considering proprioceptive inputs to the central nervous system. Thixotropy refers to the dependence of muscle force on the movement- and activation-history (Proske and Gandevia 2012; Proske, Morgan, and Gregory 1993; Monjo and Forestier 2018; Wilson, Gracies, et al. 1999; Tsay et al. 2014; Proske, Tsay, and Allen 2014; Proske and Morgan 1999). Prior movement in a muscle will reduce the stiffness of a muscle in response to stretch (Campbell and Lakie 1998; Campbell and Moss 2000; Campbell and Moss 2002; Rack and Westbury 1974) until the cross bridges are given enough time to reform, resetting the thixotropic property (Proske, Tsay, and Allen 2014; Proske, Morgan, and Gregory 1993). Further, when a muscle is stretched until cross-bridges reach a steady state, and then shortened, the internal compressive forces are not supported by the muscle and it falls slack (Proske and Gandevia 2012).

As opposed to previous mechanistic models of muscle spindle function which focused on morphological features of the muscle spindle (Lin and Crago 2002; Mileusnic et al. 2006), here we constructed a model which focuses on the muscular mechanisms that we hypothesize govern the transient firing activity in the muscle spindle sensory afferents. While thixotropic force responses have never been tested in intrafusal muscle fibers, here we combined experimental and theoretical evidence of thixotropy in extrafusal muscle fibers with hypotheses about how thixotropic effects affect the proprioceptive sense in order to construct a mechanistic model of intrafusal muscle. Our objective was to construct a model that predicted the time-history dependence of muscle spindle Ia afferents observed *in vivo*. Further, we tested whether the same model was capable of classical Ia afferent firing responses to stretch including inter-afferent variability to the same stretch (P. B. Matthews 1963; Blum, Lamotte D'Incamps, Zytnicki, and Ting 2017b), dynamic index scaling with stretch velocity (P. B. Matthews 1963), initial burst amplitudes scaling with stretch acceleration (Lennerstrand and Thoden 1968; Schäfer 1967; Schäfer and Kijewski 1974; Blum, Lamotte D'Incamps, Zytnicki, and Ting 2017b), and modulation of dynamic and static portions of a response via gamma activation (Boyd et al. 1977; Boyd 1976; Boyd 1962; Bewick and Banks 2015; Kruse and Poppele 1991).

4.2 Methods

4.2.1 Intrafusal muscle model

To simulate the hypothesized history-dependent mechanisms of intrafusal muscle fibers, we used a computational model of cross-bridge cycling. We implemented a model in Matlab based on a simplified structure of the model developed by Campbell (Campbell

2014), which incorporates the coupled dynamics between myosin heads and actin binding sites (Figure 4-1). We used a single half sarcomere to model the force developed in each intrafusal fiber considered part of our muscle spindle model. The force in each half sarcomere was calculated as a sum of two components: an active component generated by the cycling activity of a population of myosin heads and a passive component generated by a simulated linear spring modelling the contributions of titin in the half sarcomere.

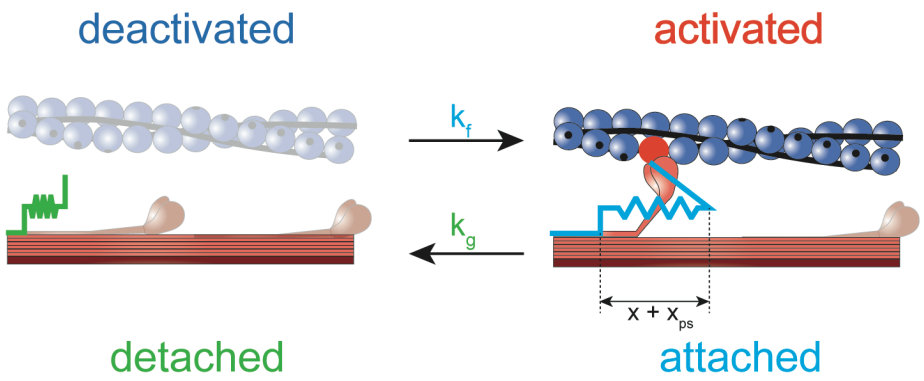

Figure 4-1 – Two-state dynamic system of myosin binding and unbinding. A population of detached cross bridges attaches at rate $k_f(x)$, and the population of attached cross bridges detaches at rate $k_g(x)$. When a cross bridge is formed at length x, an additional "powerstroke" length, x_{ps}, is applied to the cross bridge to generate a contractile force.

$$Total\ Force = \int_{-\infty}^{+\infty} \left(k_{cb}\ \rho f(x)\ \left(x + x_{ps}\right)\ dx\right) + k_{pas}(l_{hs} - l_0) \tag{13}$$

The model calculates the force of a half sarcomere at each time step by adding the forces generated from each myosin head attached to an actin binding site (active force) with the elastic force of titin (passive force). The total force equation used by the model is where the active force is calculated as the fraction of attached myosin heads, f, multiplied by the number density, ρ, unit stiffness of a single attached actin-myosin cross-bridge, k_{cb}, multiplied by the length of the cross-bridges, $x + x_{ps}$ (where x_{ps} represents the additional

displacement of an attached cross-bridge required to generate a "powerstroke" force when multiplied by k_{cb}), integrated across cross bridge lengths. The passive force is calculated as the length of the half sarcomere, l_{hs}, relative to a reference length, l_0, multiplied by a linear stiffness, k_{pas}.

4.2.1.1 Muscle activation

We simplified the coupled dynamics of Campbell (Campbell 2014) by controlling muscle activation directly, instead of ionic calcium concentration. At each time step of the simulation, the change activation level of the muscle is set by the modeller with the following relationship:

$$\frac{df_{act}(t)}{dt} = u(t), \tag{14}$$

where the change in the fraction of activated actin binding sites, $f_{act}(t)$, is determined by user input $u(t)$. The number of activated actin binding sites that was available for a cross bridge attachment was subject to overlap between the thin and thick filaments such that

$$f_{available}(t) = \min\left[f_{act}(t), f_{overlap}(t)\right] - f_{bound}(t), \tag{15}$$

where the fraction of available binding sites, $f_{available}$, is determined as the minimum between the fraction of myosin heads overlapped with the thin filament, $f_{overlap}$ (for details, see next section), and f_{act} minus the fraction of binding sites that already has a cross bridge attachment, f_{bound}.

4.2.1.2 Movements between thick and thin filaments

Movements between the thick and thin filaments affect the number of available binding sites. The number of available binding sites changes with interfilamentary movements by

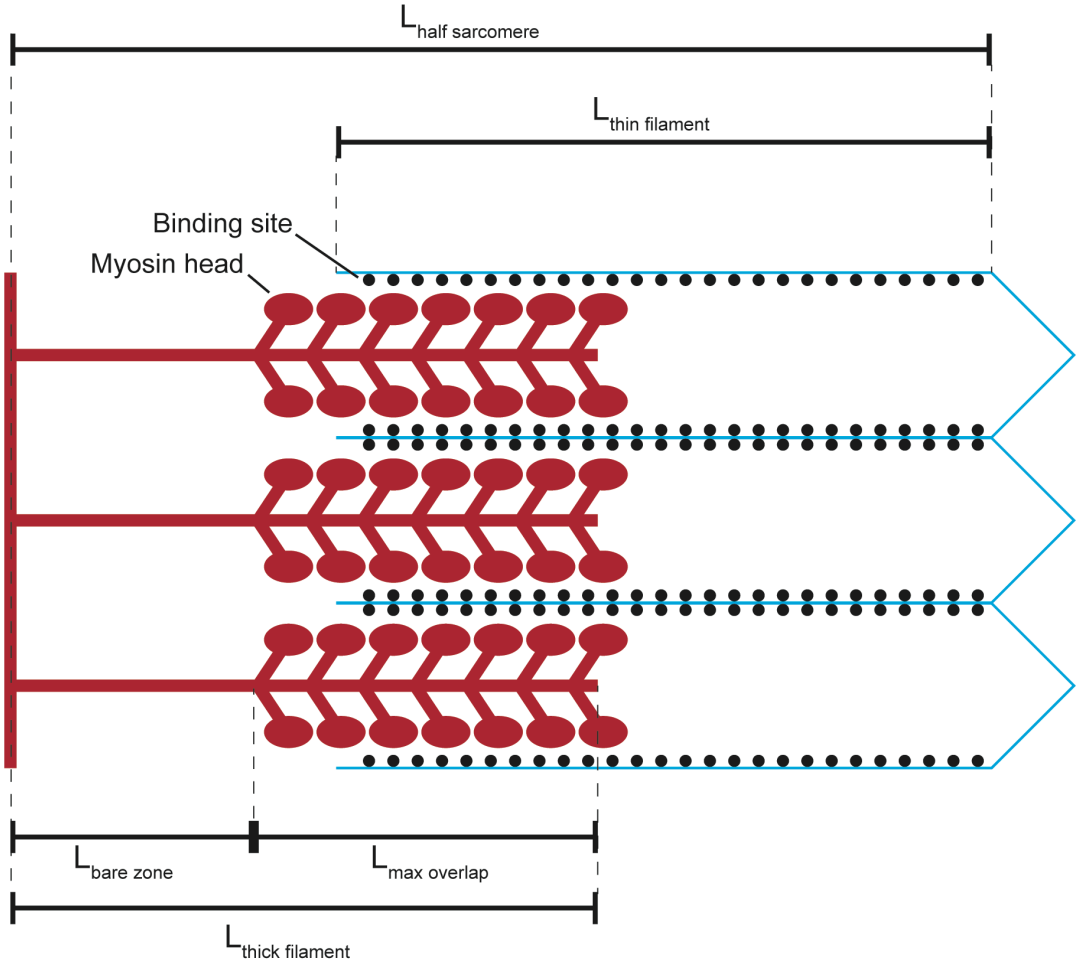

Figure 4-2 – Schematic of length variables accounted for in muscle model. The amount of overlap between the myosin heads of the thick filament (red) and actin binding sites of the thin filament (blue lines, black dots) is the relevant variable for the simulations. The fraction of overlap is simply the difference between the total length of the thick and thin filaments with the length of the half sarcomere, expressed as a fraction of the maximum potential overlap.

changing the proportion of overlap between the thick and thin filaments (Figure 4-2). The fraction of total myosin heads that overlap with the thin filament is calculated based as:

$$f_{overlap} = \frac{L_{thin\ filament} + L_{thick\ filament} - L_{half\ sarcomere}}{L_{\max overlap}} \quad (16)$$

where the numerator represents the amount of overlap between the filaments given the lengths of the thin filament, thick filament, and the half sarcomere ($L_{thin\ filament}$, $L_{thick\ filament}$, and $L_{half\ sarcomere}$ respectively), and the denominator represents the maximum possible amount of overlap between the filaments given the length of the thick filament and the "bare zone" of the thick filament that has no myosin heads, $L_{bare\ zone}$.

Interfilamentary movements also stretch or shorten the population of attached cross bridges. A change in half sarcomere length is scaled down by a factor, $c_{filament}$, to account for filament compliance and then used to shift the population of attached cross bridges. Linear interpolation is used to calculate the new cross bridge distributions.

4.2.1.3 Cross bridge population evolution

The myosin cycling dynamics were modelled using a two-state system in which each myosin head could either be attached as a cross bridge with length x, or detached. The numbers of myosin heads in each of these states were governed by the system of partial differential equations:

$$\frac{\delta A(x,t)}{\delta t} = k_f(x)D(t) - k_g(x)A(x,t), \quad (17)$$

$$\frac{\delta D(t)}{\delta t} = \int_{-\infty}^{+\infty} k_g(x)A(x,t)dx - \int_{-\infty}^{+\infty} k_f(x)D(t)dx, \tag{18}$$

where $A(x,t)$ is the number of attached myosin heads attached to actin binding sites at time t extended by length x and $D(t)$ is the number of myosin heads in the detached state. The rate equations $k_f(x)$ and $k_g(x)$ are the forward and reverse rates of myosin attachment, respectively, and are both functions of cross bridge length, x. The partial differential equations were simplified into a system of ODEs by solving the time-dependent equations simultaneously at each cross bridge length. The resulting system of ODEs was solved using a built-in Matlab ODE solver (*ode23*.m). Thick filament dynamics are coupled to the activation of the thin filament by the number of cross bridges participating in cycling:

$$n(t) = \int_{-\infty}^{+\infty} A(x,t)dx + D(t) \tag{19}$$

where the fraction of bound cross bridges is defined by the thick filament:

$$f_{bound}(t) = \int_{-\infty}^{+\infty} A(x,t)dx, \tag{20}$$

and the number of detached cross bridges is defined by the thin filament:

$$D(t) = f_{available}(t). \quad (21)$$

4.2.1.4 Length control mode

Length control mode is used by the model when the half sarcomere length is equal to the end-to-end length of the sarcomere (i.e., the half sarcomere is not slack). When in length control mode, the command length is applied directly to the half sarcomere, and the system of differential equations is solved as described earlier. The half sarcomere is updated in the following order: 1) The length of the half sarcomere and calcium concentration are each updated by the change in command length and change in command calcium concentration applied to the model, respectively, 2) the amount of filament overlap is updated, 3) thin filament dynamics are updated, 4) the population of myosin heads are allowed to evolve, and 5) the population of myosin heads is moved according to the change in length of the half sarcomere.

4.2.1.5 Slack mode

Slack mode is considerably more complicated than length control mode and contains several extra steps for solving the equations governing the model. At every time step, the model uses an iterative search (*fzero.m*) to find the length at which the force in the current-state half sarcomere would reach zero and compare it to the command length. If the command length is smaller than the "slack length" calculated, the model enters into slack mode; otherwise, the model stays in length control mode.

Once the model enters into slack mode, the model first evolves the cross bridge distribution in time based on the system of differential equations described earlier. The model then repeats the iterative search to find the slack length for the half sarcomere given the new cross bridge distribution and shifts it to the slack length for the half sarcomere. At the next time step, the model repeats the comparison between the command length and the slack length for the current state of the half sarcomere. If the command length is greater than the slack length, the model returns to length control mode; otherwise, the model stays in slack mode.

4.2.1.6 Model parameters

Model parameters were either chosen to match the default parameters from Campbell (2014) or hand-tuned so the model would exhibit desired features. All simulations used the same set of model parameters (Table 4-1).

Myosin attachment and detachment rates equations, $k_f(x)$ and $k_g(x)$, were selected such that the force response of the model would exhibit history-dependent features consistent with observations in both permeabilized muscle fibers and instantaneous firing rates of muscle spindle Ia afferents (Figure 4-3). Proske (Proske, Morgan, and Gregory 1992; Proske, Tsay, and Allen 2014; Proske and Gandevia 2012) hypothesized that history-dependent muscle spindle IFRs (and corresponding perceptual errors) are caused by a population of cross bridges within the intrafusal muscle that are unable to "keep up" with the rate of shortening during an imposed movement, causing the intrafusal muscle fibers to fall slack. To model this behavior, we selected rate equations that would produce

relatively slow cross bridge detachment during shortening, but would retain other desired characteristics, such as short-range stiffness (Figure 4-3).

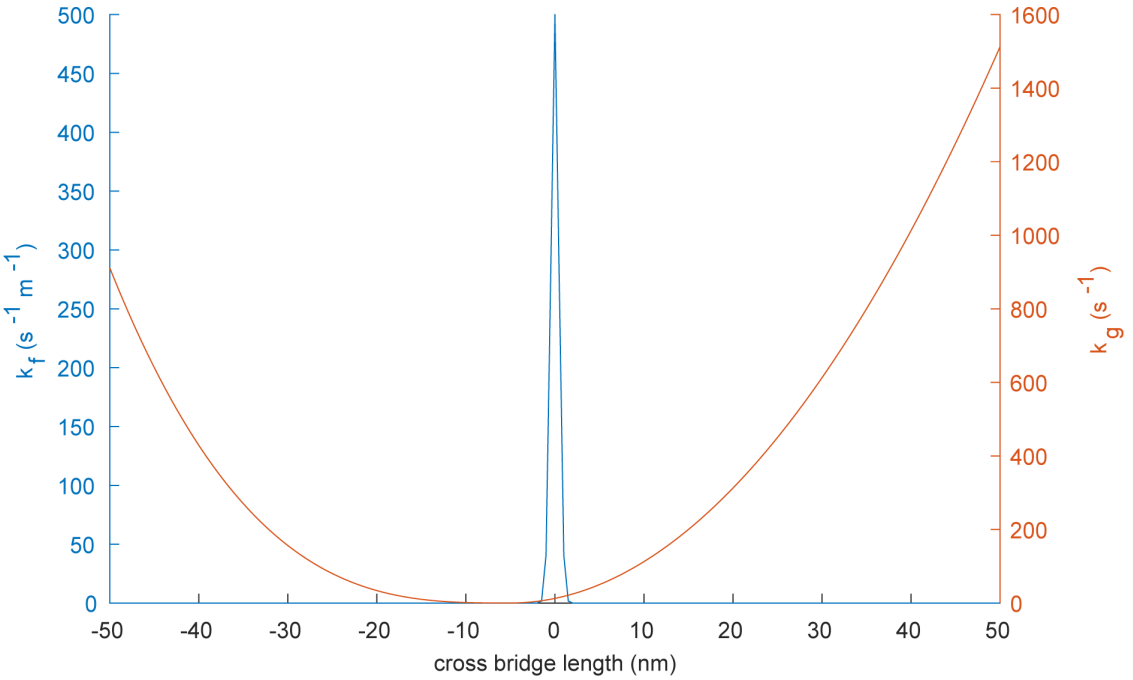

Figure 4-3 – Rate equations for myosin dynamics. The rate at which detached myosin heads will attach as a function of the length, $k_f(x)$ of attachment is a Gaussian function, centered around 0 nm (shown in blue). The rate at which attached cross bridges will detach as a function of their length $k_g(x)$ is an offset polynomial function (shown in orange).

Table 4-1 – Constant sarcomere model parameters

Parameter	Value	Units	Description
k_{cb}	1	mN m^{-1}	Unit cross bridge stiffness
x_{ps}	2.5	nm	Unit power stroke distance
$L_{thick\ filament}$	815	nm	Length of thick filament
$L_{thin\ filament}$	1120	nm	Length of thin filament
$L_{bare\ zone}$	80	nm	Length of bare zone
$c_{filament}$	0.5	-	Filament compliance factor
ρ_{cb}	6.9×10^{16}	m^{-2}	Cross bridge number density

l_0	1300	nm	Passive force reference length
k_{pas}	1500	N m^{-2} nm^{-1}	Passive force linear stiffness

4.2.2 Model of muscle spindle responses to stretch of intrafusal muscle

To model the transformation of intrafusal muscle fiber stress into a firing waveform, we used a pseudolinear combination of force and its first time-derivative, yank, based on previously published observations (Blum, Lamotte D'Incamps, Zytnicki, and Ting 2017b). Our model consists of two intrafusal muscle fiber models, a "static" fiber and a "dynamic" fiber based on observations that muscle spindle primary afferent responses to stretch consist of roughly two components (Jami and Petit 1979; Jami, Murthy, and Petit 1982; Boyd et al. 1977; Boyd 1976; Boyd 1962; Hasan 1983; Banks et al. 1997; Blum, Lamotte D'Incamps, Zytnicki, and Ting 2017b; Lewis and Proske 1972b), though any number could be used to match the number of fibers in a biological spindle. For these simulations, each muscle fiber model used identical parameters, but the contribution of each fiber to the neural firing rate varied. The equation describing the contribution of each fiber to the total firing rate is:

$$r(t) = r_{dynamic}(t) + r_{static}(t), \tag{22}$$

where the total firing rate of the afferent, $r(t)$, is a sum of the dynamic and static fiber components, or $r_{dynamic}(t)$ and $r_{static}(t)$, respectively. The static component was defined as:

$$r_{static}(t) = k_{Fs}\, F_s(t), \tag{23}$$

where k_{Fs} is a constant and $F_s(t)$ is the total force in the static fiber. The dynamic component was defined as:

$$r_{dynamic}(t) = \left\lfloor k_{Fd}\, F_d(t) + \; k_{\dot{F}d}\, \dot{F}_d(t) \right\rfloor, \tag{24}$$

where k_{Fd} and $k_{\dot{F}d}$ are constants, and $F_d(t)$ and $\dot{F}_d(t)$ are respectively the force and yank of the cycling cross bridges in the dynamic fiber. We chose to only include the cross bridge force of the dynamic fiber here, because this component is meant to represent the dynamic activity of the muscle that is encoded by the spindle.

The static and dynamic fibers are arranged in perfect mechanical parallel and were allowed to be activated independently. Thus, the actions of the dynamic and static fibers could be simulated simultaneously or sequentially.

4.2.3 Occlusion between dynamic and static components

To account for the evidence of so-called "occlusive interaction" between dynamic and static branches of the muscle spindle Ia afferent ending, we added the ability for the modeller to use a nonlinear summation of the static and dynamic components. Previous models have used complete occlusion (Lin and Crago 2002; Hulliger, Matthews, and Noth 1977) but we decided to use a partial occlusion based on more recent findings (Banks et al. 1997). With occlusion, the total firing rate of the model Ia afferent becomes:

$$r(t) = f_{occ} r_{dynamic}(t) + r_{static}(t), \qquad r_{dynamic} \geq r_{static} \tag{25}$$

$$r(t) = r_{dynamic}(t) + f_{occ} r_{static}(t), \qquad r_{static} > r_{dynamic} \tag{26}$$

where f_{occ} is an occlusion factor limiting the contribution of either component to the overall firing rate.

4.2.4 Simulations

We ran a small number of different simulation conditions to demonstrate the ability of our model to produce both classical and non-classical muscle spindle afferent firing characteristics.

4.2.4.1 Dynamic response simulations

To demonstrate the ability of our model to produce the classical fractional power relationship between the dynamic response of muscle spindle Ia firing rates and ramp velocity (P. B. Matthews 1963; Houk, Rymer, and Crago 1981; Hasan 1983), we applied a series of ramp-hold stretches to the model with each fiber's activation set to 0.3. The ramp stretches consisted of a pre-stretch isometric hold period, followed by a constant velocity stretch that varied linearly between trials from $0.079L_0$/s to $0.79L_0$/s, and another isometric hold period at its new length ($1.059L_0$). The duration of stretch was shortened proportionally to the stretch velocity to ensure the same total length was applied in each trial.

4.2.4.2 Time-history dependence simulations

To demonstrate the unique ability of our model to vary its own sensitivity to stretch based on the history of movement applied to the muscle (Haftel et al. 2004), we applied series of triangular ramp-release stretches with each fiber's activation set to 0.3. Each series consisted of three stretch-shorten cycles, with a $1.047L_0$ amplitude and stretch and shorten velocities of $0.079L_0$/s. The first two cycles were applied sequentially with no pause between them, whereas the third sequence was applied after a varied isometric hold period at L_0 ranging from 0 – 10 s.

4.2.4.3 Gamma activation simulations

To demonstrate the effects of muscle activation on the firing response of our model, we applied a range of activations to the static and dynamic fibers (Emonet-Dénand et al. 1977). We varied the activation levels of the static and dynamic fibers independently, between 0 – 1.0, before applying a $1.047L_0$ ramp-hold stretch at a constant velocity of $0.079L_0$/s. We tested the response of the muscle spindle firing rate model to these conditions with and without occlusion.

4.2.4.4 Amplitude-history dependence simulations

We tested one hypothesis of history dependence that has been confirmed in neither muscle fiber force nor muscle spindle firing data. Because we hypothesized history-dependent firing rates in muscle spindle afferents are caused by a history-dependent cross bridge cycling mechanism, we also hypothesize that the response of a muscle fiber or muscle spindle will also depend on the amplitude of movements applied prior to stretch.

To test this hypothesis, we applied a series of ramp-release stretches in a similar fashion to those applied for the time-history dependence simulations with each fiber's activation set to 0.3. However, instead of a third stretch-shorten cycle applied at different times after the first two cycles, here were applied a pre-stretch cycle at $0.079L_0$/s that varied in amplitude from 0 - $1.047L_0$.

4.3 Results

4.3.1 Response of intrafusal muscle model to imposed stretch and shortening

When we applied a series of successive $1.047L_0$ amplitude stretch-shorten cycles at $0.079L_0$/s constant stretch and shortening velocity, our model of intrafusal muscle responded with expected history-dependent features analogous to those observed in both muscle force and muscle spindle firing data (Figure 4-4). At stretch onset, there was a brief sharp rise in intrafusal force (Figure 4-4A, left), known as the short-range stiffness or short-range elastic component (Rack and Westbury 1974) (SREC). After the SREC, the force of the intrafusal fiber yielded to a new steady state force-length relationship, where the model remained until the first shortening period commenced.

When the muscle fiber was shortened, its length (Figure 4-4B, blue trace) initially followed the command length (Figure 4-4B, black trace), until the cross bridges could not keep up with the rate of shortening of the muscle. At this point, the command length and the length of the intrafusal fiber diverged: the command length continued to shorten at $0.079L_0$/s, whereas the fiber shortened at a much slower rate. Because the fiber was slack during this period, the command length reached its minimum value and started lengthening again before the muscle fiber length was able to converge with the command length.

Once the two lengths converged, the intrafusal muscle model began to generate a positive force in response to the remainder to the lengthening cycle. During this stretch period, there was no visible SREC or yield force. Once the muscle began to shorten again, a similar series of event occurred for the remainder of the stretch-shorten cycles. During the shortening period of the last cycle and into the final isometric hold at L_0, the intrafusal

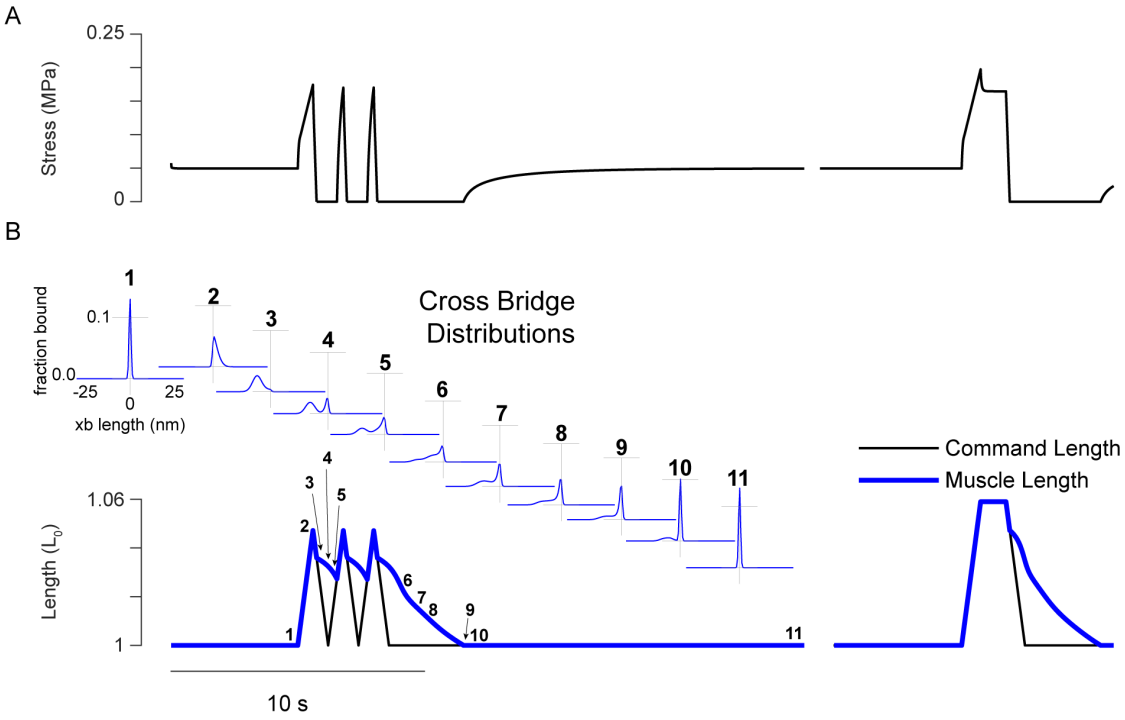

Figure 4-4 – Response of the intrafusal muscle model to different stretch sequences. **(A)** Force response of the muscle (activation = 0.3) to imposed stretches. **(B)** Imposed end-to-end length of muscle (black line) and actual muscle length (blue line), shown with corresponding cross bridge population distributions at various time points (small blue subplots). The model is initially in length control, and initiation of stretch sequence stretches moves the initial cross bridge population (1) into a new steady state distribution (2). Upon shortening, the model is unable to shorten as quickly as end-to-end command length, and the shortening cross bridges induce slack in the model (3). While the model is in isotonic mode, the model shortens against zero load (4) until the command length and the muscle length reconverge (5). This cycle is repeated for as many repeated stretch-shorten cycles as are applied. When the command length is returned to the initial length, the model shortens against zero load (6-8) until the model reaches its initial length, and force begins developing in the model again (9). As force develops (10), the population of cross bridges slowly becomes identical to its initial distribution (11).

muscle fiber was allowed to shorten against zero load until the muscle length reached L_0. Then, the model began to slowly regenerate force until it reached its initial value.

The response of the model to a $1.059L_0$ ramp-hold-release stretch (Figure 4-4B, right) at $0.079L_0$/s exhibited similar history-dependent and slackening features as the ramp-release sequences (Figure 4-4A, right). During the 1 second isometric hold period at following the stretch, the model exhibited stress relaxation until it reached an asymptotic plateau. Upon shortening, the muscle model exhibited a similar slackening and shortening phase, as described for the ramp-release sequence.

4.3.2 Response of the muscle spindle rate model to ramp-hold-release stretch

The muscle spindle model was capable of simulating a range of behaviors to the same stretch by varying the relative weights of the static fiber force, dynamic fiber force, and dynamic fiber yank contributions to the overall firing waveform. A spindle with relatively high dynamic fiber contributions ($k_{\dot{F}d}$ = 0.1; k_{Fd} = 1; k_{Fs} = 1) generated a firing waveform with a large dynamic response and initial burst, and a relatively low plateau response (Figure 4-5A). In contrast, a simulation with relatively low dynamic fiber contributions ($k_{\dot{F}d}$ = 0.05; k_{Fd} = 0.5; k_{Fs} = 1.5) generated a firing waveform with a small initial burst and dynamic response, and a relatively large plateau response.

4.3.3 Model dynamic response has fractional power relationship with stretch velocity

The intrafusal muscle fiber model exhibited force responses to increasing stretch velocity (Figure 4-6A) that were akin to the fractional power relationship observed classically in muscle spindle afferent responses to similar stretches (P. B. Matthews 1963).

Linearly increasing the stretch velocity of the ramp-hold stretches from 0.079L_0/s to 0.79L_0/s (Figure 4-6C) yielded diminishing increases in the peak force at the end of positive velocity stretch (Figure 4-6A), also known as the dynamic response.

As expected based on the response of the muscle model, the muscle spindle model ($k_{\dot{F}d}$ = 0.1; k_{Fd} = 1; k_{Fs} = 1) also exhibited a fractional power relationship with stretch velocity (Figure 4-6B). The model produced similar diminishing increases in firing response to the linear increases in stretch velocity as the intrafusal muscle model. Unexpectedly, the spindle model also produced an approximately linear increase in initial burst amplitude with stretch velocity (Figure 4-6B). Because our simulated stretch profiles

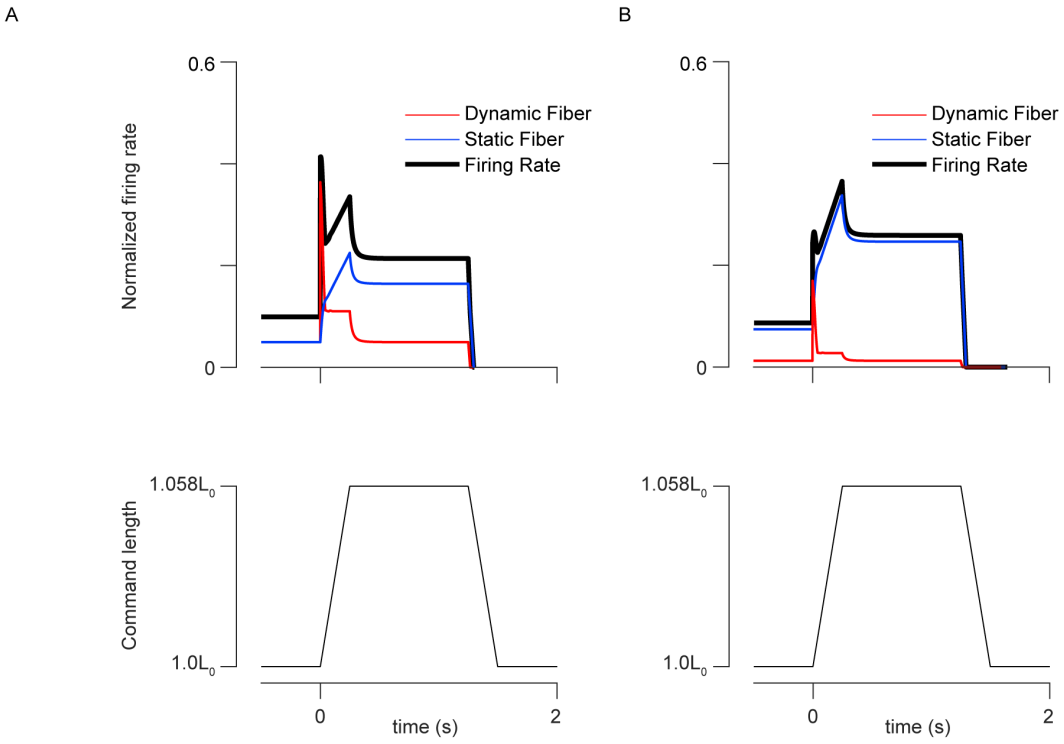

Figure 4-5 – Different predicted muscle spindle afferent response phenotypes predicted by changing the relative weights of contribution from the static and dynamic fibers. **(A)** Dynamic-weighted afferent response model ($\boldsymbol{k_{\dot{F}d}}$ = 0.1; $\boldsymbol{k_{Fd}}$ = 1; $\boldsymbol{k_{Fs}}$ = 1). This model exhibited a relatively high initial burst, dynamic response, and a lower level of tonic firing during plateau. **(B)** Static-weighted afferent response model ($\boldsymbol{k_{\dot{F}d}}$ = 0.05; $\boldsymbol{k_{Fd}}$ = 0.5; $\boldsymbol{k_{Fs}}$ =

1.5). This model exhibited a relatively small initial burst and dynamic response, and a higher level of tonic firing during plateau. Each response shown was simulated with same intrafusal muscle fiber models. All differences in simulated firing rate are due to differences in neural sensitivities.

reached peak velocity instantaneously, a linear increase in stretch velocity also requires a linear increase in stretch acceleration at the onset of stretch. Thus, the linear increase in predicted initial burst amplitude is consistent with previous studies showing a linear relationship between initial burst amplitude and stretch acceleration (Schäfer 1967; Schäfer and Kijewski 1974; Blum, Lamotte D'Incamps, Zytnicki, and Ting 2017b).

4.3.4 Reduction in dynamic response caused by prior movement scales inversely with inter-stretch time interval

When a series of three stretch-shorten cycles were applied to the model, the response to the first cycle was characteristically different from the second cycle (Figure 4-7, black traces). As described before, the first stretch response of the intrafusal muscle model exhibited an SREC and yield force whereas the second response was abbreviated and contained no SREC or yield force.

The muscle spindle model ($k_{\dot{F}d}$ = 0.1; k_{Fd} = 1; k_{Fs} = 1) exhibited analogous history-dependence: the first stretch response contained an initial burst at stretch onset followed by a steady increase in firing rate until the first applied shortening movement, whereas the second stretch response was much briefer and contained no initial burst. The peak predicted firing rate between the first and second stretch response were similar, but the waveform of the dynamic responses differed in that the first response had a shallower slope (after the initial burst) compared to the second response. This observation is consistent with data collected *in vivo* (Haftel et al. 2004).

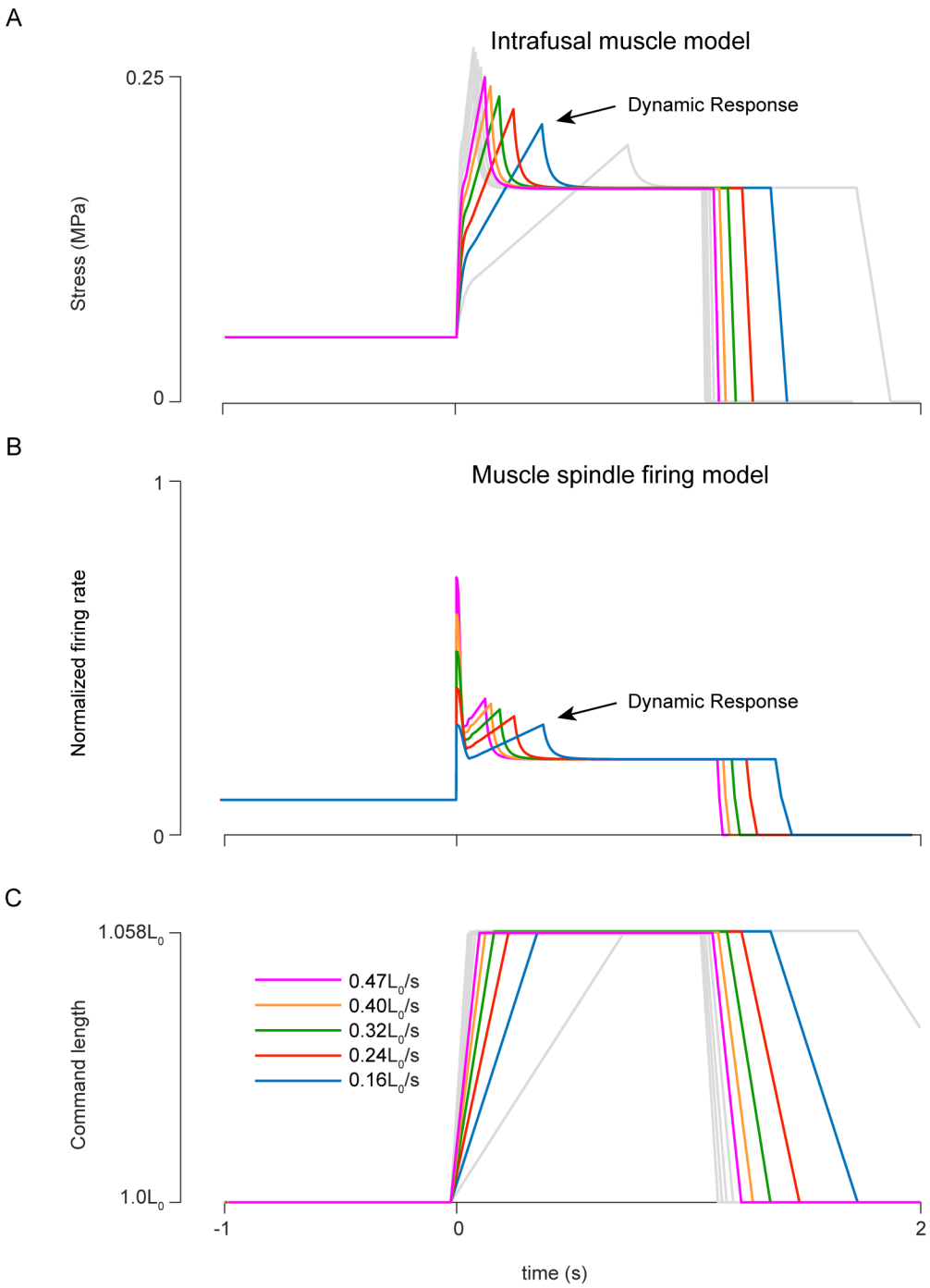

Figure 4-6 – Responses of model to increasing stretch velocity. Spindle model ($\boldsymbol{k_{\dot{F}d}}$ = 0.1; $\boldsymbol{k_{Fd}}$ = 1; $\boldsymbol{k_{Fs}}$ = 1) was stretched from 1.0L_0 to 1.058L_0 at rates linearly spanning the range 0.078L_0/s – 0.78L_0/s. Different colors represent subset of the data highlighted for clarity. **(A)** Response of intrafusal muscle model to increasing stretch velocity. The dynamic response of the muscle increases with stretch velocity in a sublinear fashion. **(B)** Response of muscle spindle firing rate to increasing stretch velocity. Responses to a subset of the velocity range are shown. The dynamic response of the muscle spindle firing rate is analogous to the sublinear relationship between muscle dynamic response and stretch

velocity in A. **(C)** Imposed length on the muscle spindle model for the range of different stretch velocities. The small differences in plateau length are due to rounding errors and do not exceed 0.5 nm above or below the target length.

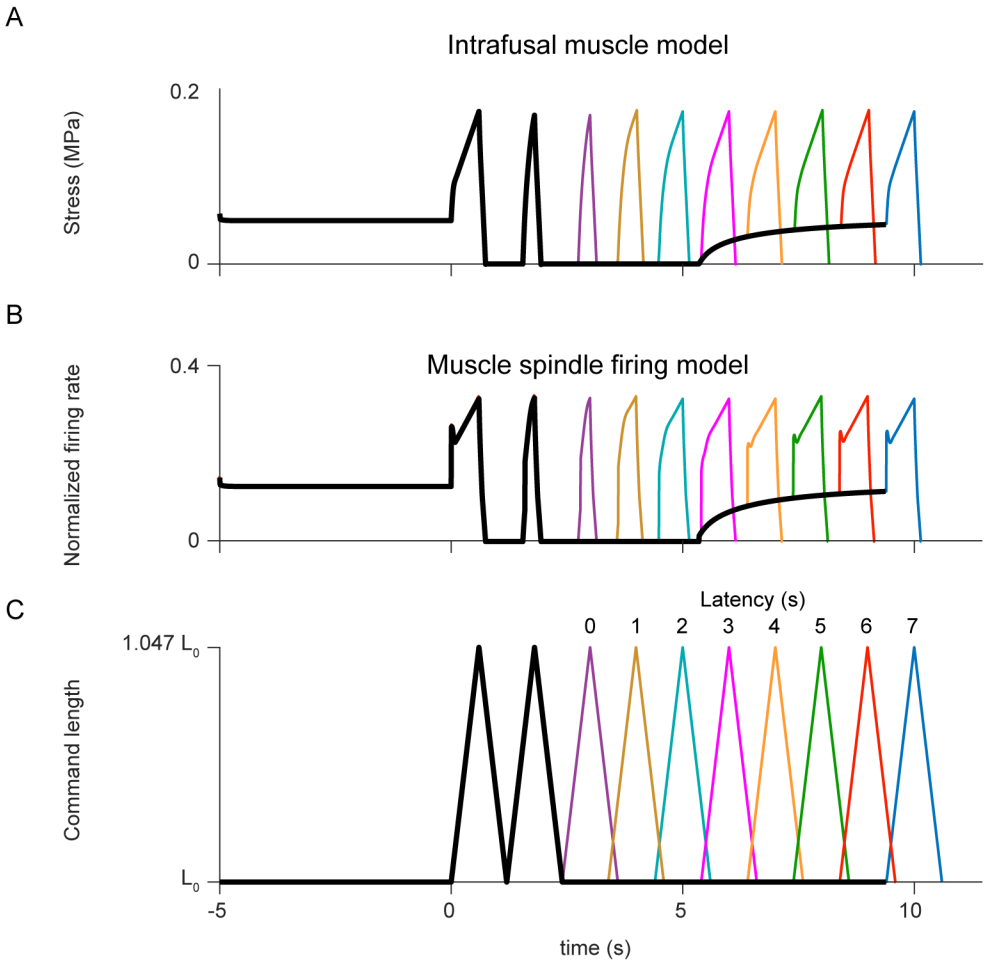

Figure 4-7 – Responses of model to increasing inter-stretch intervals. Spindle model ($\boldsymbol{k_{\dot{F}d}}$ = 0.1; $\boldsymbol{k_{Fd}}$ = 1; $\boldsymbol{k_{Fs}}$ = 1) was stretched with a sequence of three stretch-shorten cycles. Lengthening and shortening velocities were both 0.078L_0/s, and the maximum length reached during the stretch was 1.047L_0. Black traces represent first two cycles that were applied during each trial. Colored cycles represent the third cycle that was applied at different latencies after the first two trials. **(A)** Force response of intrafusal muscle model to stretch-shorten cycles at different latencies. **(B)** Rate response of muscle spindle afferent model to same latencies as A. **(C)** Stretch-shorten cycles on imposed muscle spindle model.

The model responses to the third stretch-shorten cycle, applied at latencies ranging from 0-8 seconds after the end of the second cycle, exhibited differences depending on when they were applied (Figure 4-7, colored traces). At zero seconds latency, the third

stretch response was identical to the second (Figure 4-7, purple trace). As time between cycles increased, the muscle spindle model response gradually recovered features similar to the first response. At 1-3 seconds latency, the dynamic response began to recover as the muscle model shortened between stretches, reducing slack in the model, allowing the force response to take a similar shape to that of the first cycle (Figure 4-7, gold, teal, magenta traces). At 4-6 seconds latency, the dynamic response continued to recover and the initial burst at stretch onset began to recover (Figure 4-7, yellow, green, red traces). The initial burst and dynamic response were both almost completely recovered by 7 seconds latency, at which time the model response to the third cycle closely resembled that of the first cycle (Figure 4-7, blue traces).

4.3.5 Reduction in dynamic response caused by prior movement scales with amplitude of pre-movement stretch

The model of intrafusal muscle exhibited decreases in its force response when two sequential stretch-shorten cycles were preceded with pre-stretches of varying amplitudes (Figure 4-8). As the amplitude of the pre-stretch was increased (Figure 4-8C, bottom to top), the SREC slope decreased, and the latency of its occurrence relative to the test stretch increased because the fiber became more slack during the first shortening phase as pre-stretch amplitude increased. (Figure 4-8A).

The muscle spindle model (($k_{\dot{F}d} = 0.1$; $k_{Fd} = 1$; $k_{Fs} = 1$) exhibited analogous history-dependence in its responses (Figure 4-8B). As pre-stretch amplitude increased from 0-$0.0055L_0$ (Figure 4-8B-C, purple, gold, teal, magenta traces), the initial burst at test stretch onset decreased until it was completely absent at a pre-stretch amplitude of

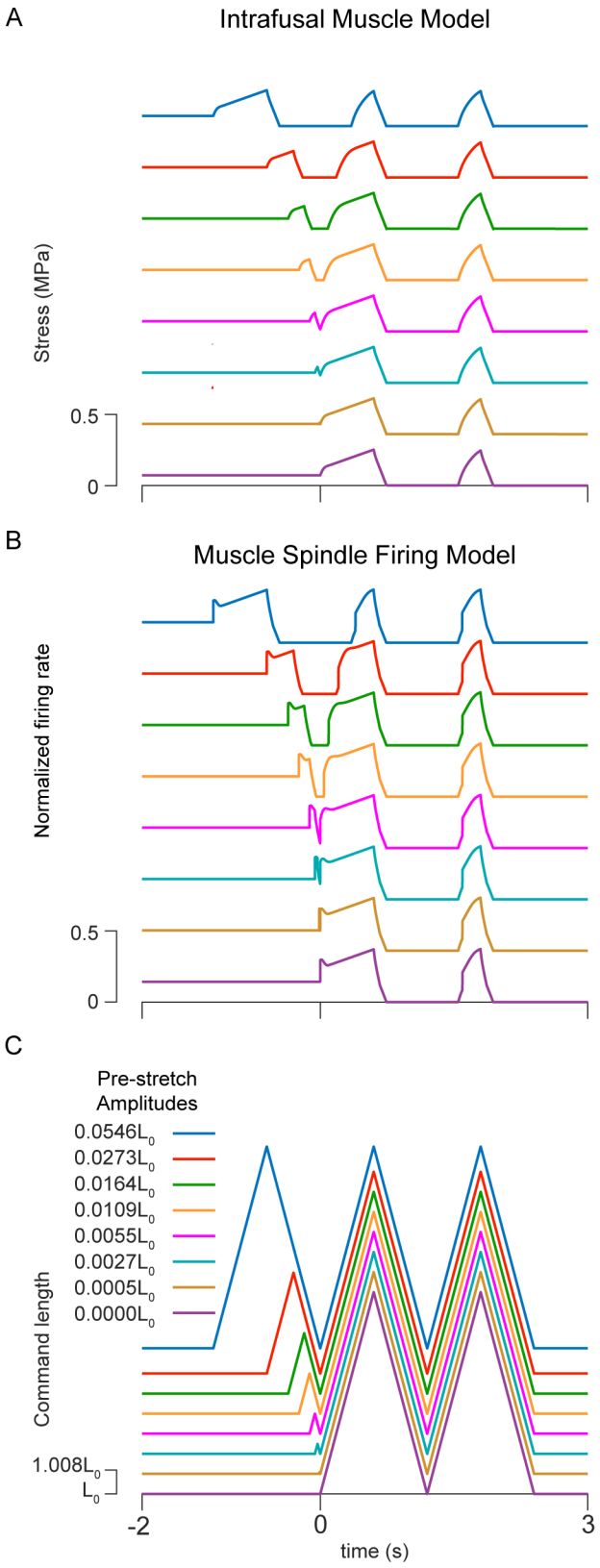

Figure 4-8 – Responses of model to increasing pre-stretch amplitude. Spindle model ($\boldsymbol{k_{\dot{F}d}}$ = 0.1; $\boldsymbol{k_{Fd}}$ = 1; $\boldsymbol{k_{Fs}}$ = 1) was stretched with a sequence of three stretch-shorten cycles. For

each trial, the first stretch-shorten sequence was varied in amplitude in the range $0L_0$ to $0.0546L_0$, but maintained at 0.079 L_0/s velocity. The second and third stretch-shorten cycles were applied immediately after the end of the first sequence, and were $1.0546L_0$ length and $0.079L_0$/s velocity stretches. **(A)** Intrafusal muscle model responses to changes in pre-stretch amplitude. All traces start at the same initial value; they are offset for clarity. Different colors correspond to different amplitudes of pre-stretch (decreasing top to bottom). **(B)** Model of muscle spindle firing rate responses to changes in pre-stretch amplitude. As in A, all traces start at the same initial value and are offset for clarity. Coloring convention identical to A. **(C)** Imposed length changes applied to the muscle spindle model. As in A and B, all traces start at the same value and are offset for clarity. Coloring convention is identical to A and B; values indicated to the left represent pre-stretch amplitudes.

$0.0109L_0$ (Figure 4-8B-C yellow traces). The dynamic response of the muscle spindle also decreased with pre-stretch amplitude from $0.0109\text{-}0.0546L_0$ (Figure 4-8B-C, yellow, green, red, blue traces).

4.3.6 Activation dependence of muscle spindle model response to stretch

Varying the activation of the intrafusal muscle model had several effects on the force waveform (Figure 4-9A). First, the baseline force increased proportionally with activation level. At stretch onset, the SREC increased in slope with activation level, implying a larger number of bound cross bridges were being stretched at the higher activation levels. Further, as activation increased, so did the relative dynamic force responses during positive velocity stretch. Plateau responses of the muscle model increased proportionally to the linear increase in activation level. As a result, the dynamic index of the muscle model increased with activation level.

Independent activation of the static and dynamic intrafusal muscle fibers caused an exaggeration of their respective contributions ($k_{\dot{F}d}$ = 0.15; k_{Fd} = 1; k_{Fs} = 1) to the muscle spindle firing rate (Figure 4-9 B-C). First, when static fiber activation was increased with

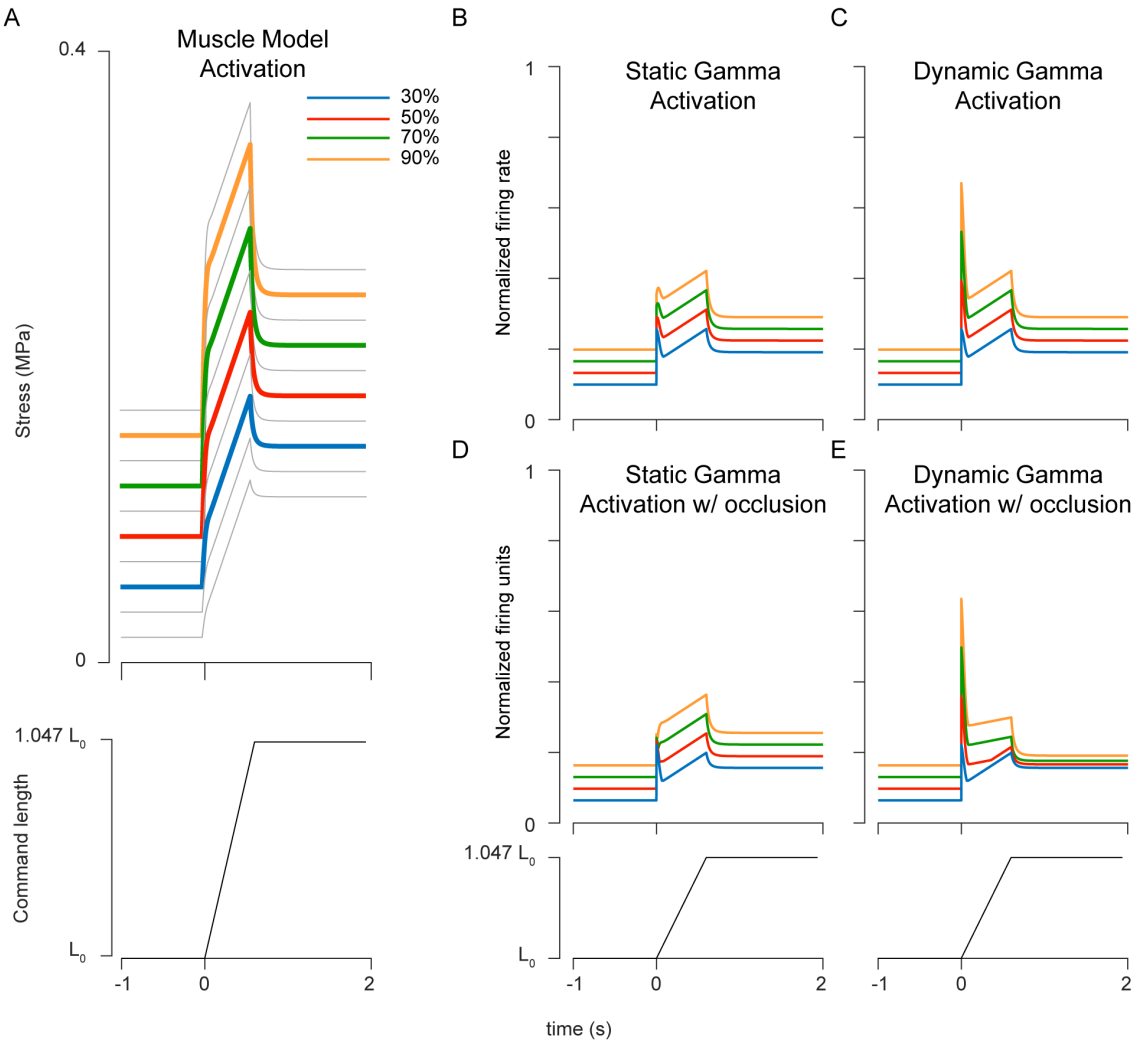

Figure 4-9 – Changes in model responses to stretch with changes in activation state of the intrafusal muscle fiber models. **(A)** Responses of a single intrafusal muscle fiber model at 10 activation levels (0.1-1.0 activation) to the same ramp-hold stretch (model stretched to $1.047L_0$ at 0.079 L_0/s velocity. Four responses corresponding to different activation levels are highlighted for clarity (blue = 0.3; red = 0.5; green = 0.7; yellow = 0.9 activation level). **(B)** Response of the muscle spindle firing rate model ($\boldsymbol{k_{\dot{F}d}}$ = 0.15; $\boldsymbol{k_{Fd}}$ = 1; $\boldsymbol{k_{Fs}}$ = 1) to the same stretch for four different levels of activation of the static intrafusal fiber model. **(C)** Response of the muscle spindle firing rate model ($\boldsymbol{k_{\dot{F}d}}$ = 0.15; $\boldsymbol{k_{Fd}}$ = 1; $\boldsymbol{k_{Fs}}$ = 1) to the same stretch for four different levels of activation of the dynamic intrafusal fiber model. **(D)** Same model, stretch, and activation parameters as in B, but model includes occlusion feature for competing static and dynamic contributions to the firing rate. **(E)** Same model, stretch, and activation parameters as in C, but model includes same occlusion feature as D.

constant dynamic fiber activation (30%), the effect on the firing rate was mostly to increase the average firing rate across all phases of the trial (Figure 4-9B). As static activation

increased to 90% (Figure 4-9, yellow trace), the prominence of the initial burst relative to the dynamic response decreased. There was also a slight increase in dynamic index with increase in static activation. These observations were within our expectations based on observations *in vivo* (Emonet-Dénand et al. 1977; Banks et al. 1997).

Dynamic fiber activation with constant static fiber activation (30%) created more exaggerated changes to the firing rate waveform (Figure 4-9C). We observed identical increases in baseline, dynamic plateau firing rates as in the static fiber activation. This was expected due to the identical structure of the dynamic and static fibers. In contrast to the static fiber activation, we observed marked increase in initial burst with increases in activation. These observations were not in agreement with observations from muscle spindles *in vivo*, where dynamic gamma activation has been shown to primarily increase the dynamic sensitivity of the spindle, with a lesser effect on the static portions of the firing rate (e.g., the plateau response).

Adding occlusion between dynamic and static contributions to the muscle spindle firing rate allowed for more independent control of dynamic and static features of the firing rate (Figure 4-9D-E). Increasing static fiber activation in the model with occlusion produced similar results as the model without occlusion (Figure 4-9D). Briefly, there were proportional increases in baseline and plateau firing rates, along with a slight increase in dynamic index. The biggest difference in the static activation trials with occlusion was that the initial burst decreased steadily with static activation, until it was completely eradicated at high activation levels.

Increasing dynamic fiber activation in the model with occlusion produced drastic differences in the dynamic index when compared to those from the model without occlusion. As dynamic activation increased, the initial burst amplitude and dynamic response increased (Figure 4-9D), as in the model without occlusion. However, the primary effect of occlusion in these simulations can be seen during the plateau response. Here, the increase in dynamic activation produced only a very small change in plateau firing rate. Therefore, the primary effect of occlusion in the model is to separate the effects of dynamic and static fiber activation on the dynamic and static portions of firing, respectively.

4.4 Discussion

This is the first model of muscle spindle function that can account for history-dependent and thixotropic effects. Muscle spindle thixotropy is implicated in a wide range of behaviors – from autogenic and brainstem-mediated standing balance (Honeycutt et al. 2012; Lockhart and Ting 2007; Welch and Ting 2008; Welch and Ting 2009; Safavynia and Ting 2013a; Safavynia and Ting 2013b) to conscious proprioceptive tasks (Proske, Morgan, and Gregory 1992; Proske and Gandevia 2009; Proske and Gandevia 2012; London et al. 2008; London and Miller 2013; Tsay et al. 2014; Proske, Tsay, and Allen 2014) – but has not been accounted for in a model of muscle spindle function until now. Instead of creating an explicit input-output relationship between muscle length and muscle spindle activity, we relied on the theoretical dynamical system of cycling cross bridges to model the force of the intrafusal muscle fibers in response to activation and stretch. We used a pseudolinear combination of force and yank of the intrafusal fibers (Blum, Lamotte D'Incamps, Zytnicki, and Ting 2017b) to transform the intrafusal force into muscle spindle firing rates that predicted a large array of classical and history-dependent responses.

Interestingly, by constructing a mechanistic model of muscle contraction, we were able to predict not only thixotropic muscle spindle responses to stretch for the first time in a model, but also classical features of muscle spindle responses as emergent properties of the model. The fractional power relationship between muscle spindle dynamic response and imposed stretch velocity is one of great relevance and has been observed in a number of conditions (P. B. Matthews 1963; P. B. C. Matthews 1972; P. Matthews 1981; Houk, Rymer, and Crago 1981; Prochazka and Gorassini 1998b; Prochazka and Gorassini 1998a; Haftel et al. 2004). Instead of an explicit fractional power relationship between the force output and the velocity input (Houk, Rymer, and Crago 1981; Hasan 1983; Prochazka and Gorassini 1998a; Chen and Poppele 1978) our model expresses such a relationship as an emergent property of the cross bridge cycling dynamics of the intrafusal fiber.

The short-range elastic component in our muscle model gave rise to the history-dependent initial burst in our model of muscle spindle firing. At stretch onset, a population of cross bridges centered around 0 length was stretched, causing a high-stiffness region of the force response. The slope of this region increased with stretch velocity, and by definition, the rate change of this slope (yank) increased with stretch acceleration. Because our model's initial burst was related to the yank of the dynamic fiber, our model exhibited a linear increase in initial burst amplitude with stretch acceleration. This feature of Ia afferent firing has been described before (Schäfer 1967; Schäfer and Kijewski 1974; Lennerstrand and Thoden 1968) as an acceleration code in the spindle. However, our model captures not only the sensitivity of the initial burst to changing acceleration, but also its history dependence, supporting the hypothesis that the initial burst is an "intrafusal manifestation" of the short-range property of muscle (Proske and Stuart 1985).

Additionally, our muscle spindle model accounted for the sharp decrease in sensitivity exhibited when the spindle is elongated beyond a certain "critical stretch" (P. Matthews and Stein 1969; Hasan and Houk 1975; Hasan 1983). In our simulations of intrafusal muscle, this shift in sensitivity manifested as the yield force during ramp stretch occurring directly after the SREC.

We used two identical intrafusal muscle model fibers to produce a range of firing waveforms by attributing the properties of the spindle response to two components (Blum, Lamotte D'Incamps, Zytnicki, and Ting 2017b; Emonet-Dénand et al. 1977). The majority of mammalian muscle spindle Ia afferents have endings on multiple intrafusal fibers, including bag1, bag2, and chain fibers, each of which contributes to the overall firing rate of the afferent (Banks et al. 1997). Instead of modeling many of these fibers in parallel, we chose to model a "static" and a "dynamic" fiber each of which could be activated independently. We felt that modeling the spindle response with components from two fibers would give us a similar degree of control over the spindle response as a biological muscle spindle because the intrafusal fibers are coupled by static and dynamic gamma motor neurons (Emonet-Dénand et al. 1977; Boyd et al. 1977; Boyd 1976; Boyd 1962; Banks et al. 2009; Banks, Harker, and Stacey 1977). In doing so, we accounted for the variance in spindle response phenotypes with a nonlinear summation of the weighted dynamic and static components (Hulliger, Matthews, and Noth 1977; Banks et al. 1997; Lin and Crago 2002). This strategy maintains a consistent level of computational efficiency, whereas an anatomically explicit model with as many as 5 or 6 endings on multiple intrafusal fibers would be burdensome (Banks et al. 2009).

Thixotropy is considered to be a property of passive muscle in which a non-cycling population of cross bridges form a stable bond, but our two-state model relied on slow cross-bridge cycling to generate force. Thixotropic effects in our model were thus dependent on a low activation level. Importantly, activation level in our model does not correspond directly with "muscle activation" as defined by many motor control researchers (recordable excitation, such as EMG), but instead reflects the number of available actin binding sites for cross bridge formation. Our definition of activation level results from the influx of free calcium ions from the sarcoplasmic reticulum resulting from action potentials of the muscle. Therefore, it is possible that a "passive muscle" (in the electrical sense) has a small basal level of intracellular calcium and cross bridge cycling (Proske, Morgan, and Gregory 1992; Proske and Morgan 1999; Blum, Lamotte D'Incamps, Zytnicki, and Ting 2017b).

Although our model robustly accounts for several classical and thixotropic features of muscle spindle firing, several improvements could be possible as more knowledge is gained about the nature of intrafusal contractile properties and the mechanosensitive properties of muscle spindle afferents. For example, single permeabilized muscle fiber experiments have been crucial for our understanding of skeletal muscle properties, but no such experiments have been done with intrafusal fibers. Such experiments would give a much clearer hypothesis about the properties we attempted to model. Instead, we relied on indirect evidence of intrafusal properties such as the slack hypothesis of psychophysical research (Proske and Gandevia 2012). We resisted overcomplicating the model presented in this paper with additional myosin states (Campbell 2014; Campbell and Moss 2000; Campbell and Moss 2002; Pate and Cooke 1989), multiple in-series half-sarcomeres

(Campbell 2009) or neural dynamics (P. B. Matthews and Stein 1969), but these features may be added as the need presents itself. A more computationally-tractable model of history-dependence may also be possible (McGowan, Neptune, and Herzog 2013) and development of such should be seriously considered if the relevant features of history-dependence can be captured in such a phenomenological description. Nevertheless, we believe that the model presented in this paper can serve as a useful tool for sensorimotor control research where muscle and muscle spindle thixotropic or other history-dependent effects may affect the outcomes.

CHAPTER 5. CONCLUSIONS

This body of work presents a combination of experimental, analytical, and theoretical approaches for modeling the history-dependent responses of muscle spindle Ia afferents to stretch. History-dependent, or thixotropic, effects of muscle spindle encoding are largely ignored by sensorimotor control researchers. Unfortunately, these effects are prevalent at multiple scales of biomedical research and failure to account for them could heavily bias our interpretation of data, leading to erroneous conclusions and hypotheses about neuromechanical systems in a compounding fashion. A primary reason for the lack of consideration for thixotropic effects of muscle spindle encoding in sensorimotor control research is because the prevailing hypotheses regarding thixotropy in muscle spindles have not been formalized into a tangible model.

The results from the experimental and analytical approaches in Chapter 2 provided a groundwork from which such a model of muscle spindle Ia thixotropic encoding could be built. From the analyses of the data in this Chapter, we were able to identify a potential set of thixotropic variables – muscle force and its first time-derivative, yank – that explain history-dependent Ia afferent spiking responses to a range of passive stretch conditions. Identification of these variables was a crucial step in the modeling process because it allowed us to formally test the standing hypotheses stating that history-dependence in muscle spindle encoding was due to an intrafusal cross bridge mechanism. As it turned out, recorded force and yank components combined in a summative manner were the best predictor of history-dependent muscle spindle firing rates in feline. Further, a single set of weights on the force and yank components in our model were able to predict a larger

amount of variance in each afferent dataset than length-related variables, implying a consistent neural sensitivity to force and yank.

We attempted to expand the model of thixotropic muscle spindle encoding in Chapter 3 by testing a similar summative model of force and yank components in a different mammal and tested whether it could explain changes in muscle spindle encoding caused by perturbations to the afferent. Because we used stretch perturbations that spanned the physiological range of locomotion for the rat triceps surae, our recorded force data was necessarily filtered by removing a force component we hypothesized to be due to the noncontractile portion of the force-length curve. After this filtering process, the resulting estimates of muscle fiber force and yank were able to account for a wide range of history-dependent muscle spindle Ia firing features. While we did not test the ability of a single set of weights on force and yank components to predict complete afferent datasets, as in Chapter 2, fitting the model to each individual trial yielded extremely high variance explained in the data. As such, we were confident in the ability of a single set of parameters in this model to predict data from any Ia afferent consistently for the same stretch parameters, which implies its utility in modeling changes caused by neural perturbations in Ia afferent encoding (Bullinger, Nardelli, Wang, et al. 2011). Indeed, the pseudolinear combinations of force and yank, estimated for each stretch perturbation individually, were able to not only account for changes in Ia firing rates caused by oxaliplatin chemotherapy but also those caused by antidromic stimulation of the muscle spindle afferent. Finally, we were able to use the pseudolinear combination of force and yank as an input to a model neuron to explain a wide range of dynamic muscle spindle firing features observed in the data we collected for this study.

In Chapter 4, we used bottom-up theoretical modeling of history-dependent cross bridge mechanisms to create a forward model of thixotropic muscle spindle encoding. We implemented hypotheses of muscle spindle thixotropy to create a population of "stable" cross bridges that were slow to detach when the muscle was shortened, creating slack in the fiber. We used two identical half-sarcomeres aligned in mechanical parallel to simulate a "static" and a "dynamic" fiber, each with independent activation, to mimic the components of muscle spindle Ia spike rates identified in Chapters 2 and 3. The static component of the total firing rate was related to the total force in the static intrafusal fiber, whereas the dynamic component was related to the force and yank caused by the cross-bridge cycling in the dynamic fiber. Varying the relative sensitivities of the firing rate to these components created a range of muscle spindle phenotypes when an identical stretch stimulus was applied to the model, analogous to the data collected in Chapters 2 and 3. This model was able to account for several thixotropic features of muscle spindle firing by design as well as several classical descriptions of the muscle spindle response as emergent properties of the intrafusal muscle model. Dynamic index of the model in response to increasing stretch velocity emerged as a sublinear function (e.g. fractional-power function) with respect to velocity (Houk, Rymer, and Crago 1981), which was actually a property of the intrafusal muscle fiber model's force response to stretch. The model was capable of time- and amplitude-history dependence in its stretch responses: features that have never been accomplished previously in a model of muscle spindle function. Finally, activation of the model's intrafusal fibers selectively increased the representation of static or dynamic features in the modelled firing rate.

5.1 Future experimental directions

The work presented here provides a large number of possibilities for future investigation.

Ideally, we would like to record the force of the intrafusal fibers directly in an isolated fiber preparation. In Chapters 2 and 3, we had to use passive force recorded during stretch from the whole triceps surae as a proxy for the force of the intrafusal fibers. While this was a suitable method for Chapter 2, it became apparent in Chapter 3 that additional processing of the muscle force was necessary for our model to work in the anesthetized rat. Instead of continuing to rely on recorded whole muscle forces to build a model of muscle spindle function, it would be enlightening to record similar force responses from isolated extrafusal – or even intrafusal – muscle fibers.

There are potential unexplored effects of muscle architecture on muscle spindle encoding in the triceps surae. Both Chapters 2 and 3 relied on random sampling of muscle afferents from the triceps surae muscle of the cat and rat. In reality, the triceps surae consists of three muscles – medial and lateral gastrocnemius and soleus – which each have their own unique architecture (e.g. origin, pinnation, etc.). It is currently unclear how the potential coding of stretch by muscle spindle afferents is affected by this. For example, the soleus consists of primarily slow muscle fibers in the rat, whereas the medial gastrocnemius of primarily fast muscle fibers. What effects, if any does this have on muscle spindles to similar stretches applied to the whole muscle?

An impactful next step to the research presented here would be to use muscle stretch perturbations that are more relevant to behavioral states in which muscle spindles are hypothesized to be most relevant. In this work, we necessarily used highly idealized and

controlled stretches of the isolated muscle to characterize and quantify the muscle spindle Ia afferent and muscle responses to stretch. One potential avenue of exploration in this regard could be to combine the experimental procedures of Honeycutt et al. (Honeycutt et al. 2012) and Haftel et al. (Haftel et al. 2004) to examine history-dependence in muscle spindles during horizontal plane perturbations to the intact limb. In Chapter 4, we not only reproduced time-history dependent muscle spindle firing, but also predicted an effect of pre-stretch amplitude on muscle spindle encoding. Combined with the tuning sensitivities demonstrated in the work of Honeycutt et al. and potential effects of muscle architecture on muscle spindle sensitivity discussed earlier, time- and amplitude history dependent interactions could create a complex system of information provided to the CNS from muscle spindle afferents that is more diverse than previously hypothesized.

Of course, the most relevant data for understanding the effects of thixotropic muscle spindle responses to stretch would be to record from muscle spindle afferents from awake, behaving animals. Electrodes have been successfully chronically implanted in both cat and rat DRGs (Weber et al. 2006; Weber et al. 2007; Kolarcik et al. 2012), but muscle spindle thixotropy has not been researched directly. Therefore, a potentially exciting category of experiments could be to measure the responses of muscle spindle afferents to horizontal plane perturbations to standing balance to awake animals with chronic DRG implants. These perturbations could be used to look at the direction-time-amplitude history dependence interactions on muscle spindle encoding to glean a better understanding of what information is available to the CNS for perturbation correction in an awake animal.

An exciting and quickly-growing technique in neuroscience that could be used to study the muscle spindle organ is optogenetics (Boyden et al. 2005). By genetically

inserting light-sensitive ion channels within specific neural subgroups, researchers have been able to directly control neural populations that were previously impossible to stimulate independently with electrical stimulation. An interesting use of optogenetics in muscle spindle research could be to independently control gamma motor neurons, which have unique genetic identifiers (Friese et al. 2009) during behavioral tasks, in order to gain a better understanding of the effects of gamma drive on sensorimotor control.

5.2 Future computational directions

Every new discovery in the biological muscle spindle provides another opportunity to update the computational representation of muscle spindle sensory encoding.

One important contribution in regard to developing a computational representation of muscle spindle history-dependence would be to make a model that is both computationally efficient and accurate in terms of history-dependent effects. Such a model does not currently exist; however, we believe one could be made. To our knowledge, history-dependent reduction in muscle stiffness and Ia firing rate are at maximums directly after a large perturbation to the muscle and are at minimums when the muscle has been at rest for several seconds. A potential method for creating a Hill-type model capable of these effects could be to measure a family of force-length and force-velocity curves from a mechanistic model (such as the one described in Chapter 4) at different stages of time- and amplitude-history dependence. The next step would be creating a lookup table of reduction factors that could be parsimoniously included in the Hill equation by specifying a point at which the force-length and force-velocity relationships could be interpolated to a value relevant to the current state-history of the muscle. While this would be less

computationally-efficient than a standard Hill-type model, we anticipate it would be several orders of magnitude more efficient than a model of cross bridge cycling and could be implemented into larger-scale musculoskeletal models of sensorimotor control.

If computation time is not important to a researcher, there are still several improvements that could be made to the thixotropic muscle spindle model presented in this work. The modular nature of the model presented here provides the ability to add more complex features to whichever portion of the model, such as the muscle or the receptor, as the researcher deems necessary. For example, we could add different myosin-actin interactions based on differences found in protein content between intrafusal muscle fibers (Liu et al. 2005; Liu, Eriksson, Thornell, and Pedrosa-Domellöf 2002b). We could also incorporate more complicated neural dynamics in order to have action potentials as the model output instead of a continuous firing rate equation.

We believe our model could lead to many new insights into the effects of impaired proprioception on behavior at multiple scales and inform new hypotheses about the mechanisms of disease. A key advantage in using a multiple-scale approach, as we have done here, is that our model can be used to the level of detail that is necessary for a specific impairment. For example, by incorporating our muscle spindle model in a large-scale musculoskeletal model of balance, a researcher could predict the effects of a channelopathy or neuromodulators by removing or altering ion channels from the model of mechanotransduction or spike-generation and observe the effects of the impairment on the model behavior. Another example of potential uses for our model is to predict the effects of altered history-dependent sensory encoding in spasticity – a symptom prevalent in children with cerebral palsy. Performance in clinical tests, such as the pendulum test, is

unexplained by current models but our model may provide insights into how spasticity may be affecting the modulation of the stretch reflex (Fowler, Nwigwe, and Ho 2000). These predictions can be used to inform new hypotheses that can be validated by experiments at multiple scales.

REFERENCES

Akay, Turgay, Warren G Tourtellotte, Silvia Arber, and Thomas M Jessell. 2014. "Degradation of Mouse Locomotor Pattern in the Absence of Proprioceptive Sensory Feedback.." *Proc Natl Acad Sci U S A* 111 (47). National Academy of Sciences: 16877–82. doi:10.1073/pnas.1419045111.

Banks, Robert W, D Barker, and M J Stacey. 1979. "Sensory Innervation of Cat Hind-Limb Muscle Spindles [Proceedings].." *Journal of Physiology* 293 (August): 40P–41P.

Banks, Robert W, D W Harker, and M J Stacey. 1977. "A Study of Mammalian Intrafusal Muscle Fibres Using a Combined Histochemical and Ultrastructural Technique.." *Journal of Anatomy* 123 (Pt 3). Wiley-Blackwell: 783–96. doi:10.1111/(ISSN)1469-7580.

Banks, Robert W, M Hulliger, H H Saed, and M J Stacey. 2009. "A Comparative Analysis of the Encapsulated End-Organs of Mammalian Skeletal Muscles and of Their Sensory Nerve Endings." *Journal of Anatomy* 214 (6): 859–87.

Banks, Robert W, M Hulliger, K A Scheepstra, and E Otten. 1997. "Pacemaker Activity in a Sensory Ending with Multiple Encoding Sites: the Cat Muscle Spindle Primary Ending.." *Journal of Physiology* 498 (Pt 1) (January): 177–99. doi:10.1111/(ISSN)1469-7793.

Bell, C. 1826. "On the Nervous Circle Which Connects the Voluntary Muscles with the Brain." *Philosophical Transactions of the Royal Society of London* 116 (0). The Royal Society: 163–73. doi:10.1098/rstl.1826.0016.

Bewick, Guy S. 2015. "Synaptic-Like Vesicles and Candidate Transduction Channels in Mechanosensory Terminals." *Journal of Anatomy* 227 (2): 194–213. doi:10.1111/joa.12337.

Bewick, Guy S, and Robert W Banks. 2015. "Mechanotransduction in the Muscle Spindle.." *Pflügers Archiv - European Journal of Physiology* 467 (1): 175–90. doi:10.1007/s00424-014-1536-9.

Blum, Kyle P, Boris Lamotte D'Incamps, Daniel Zytnicki, and Lena H Ting. 2017a. "Data From: Force Encoding in Muscle Spindles During Stretch of Passive Muscle." doi:10.5061/dryad.pd40m.

Blum, Kyle P, Boris Lamotte D'Incamps, Daniel Zytnicki, and Lena H Ting. 2017b. "Force Encoding in Muscle Spindles During Stretch of Passive Muscle." Edited by

Joseph Ayers. *PLoS Computational Biology* 13 (9): e1005767–24. doi:10.1371/journal.pcbi.1005767.

Boyd, I A. 1962. "The Structure and Innervation of the Nuclear Bag Muscle Fibre System and the Nuclear Chain Muscle Fibre System in Mammalian Muscle Spindles." *Philosophical Transactions of the Royal Society B: Biological Sciences* 245 (720). The Royal Society: 81–136. doi:10.1098/rstb.1962.0007.

Boyd, I A. 1976. "The Response of Fast and Slow Nuclear Bag Fibres and Nuclear Chain Fibres in Isolated Cat Muscle Spindles to Fusimotor Stimulation, and the Effect of Intrafusal Contraction on the Sensory Endings.." *Quarterly Journal of Experimental Physiology and Cognate Medical Sciences* 61 (3): 203–54.

Boyd, I A, M H Gladden, P N McWilliam, and J Ward. 1977. "Control of Dynamic and Static Nuclear Bag Fibres and Nuclearbag Fibres and Nuclear Chain Fibres by Gamma and Beta Axons in Isolated Cat Muscle Spindles." *Journal of Physiology*.

Boyden, Edward S, Feng Zhang, Ernst Bamberg, Georg Nagel, and Karl Deisseroth. 2005. "Millisecond-Timescale, Genetically Targeted Optical Control of Neural Activity." *Nature Publishing Group* 8 (9). Nature Publishing Group: 1263.

Bullinger, Katie L, Paul Nardelli, Martin J Pinter, Francisco J Alvarez, and Timothy C Cope. 2011. "Permanent Central Synaptic Disconnection of Proprioceptors After Nerve Injury and Regeneration. II. Loss of Functional Connectivity with Motoneurons." *Journal of Neurophysiology* 106 (5): 2471–85.

Bullinger, Katie L, Paul Nardelli, Qingbo Wang, Mark M Rich, and Timothy C Cope. 2011. "Oxaliplatin Neurotoxicity of Sensory Transduction in Rat Proprioceptors.." *Journal of Neurophysiology* 106 (2): 704–9. doi:10.1152/jn.00083.2011.

Burnham, Kenneth P, and David Anderson. 2003. "Model Selection and Multi-Model Inference."

Campbell, K S, and M Lakie. 1998. "A Cross-Bridge Mechanism Can Explain the Thixotropic Short-Range Elastic Component of Relaxed Frog Skeletal Muscle.." *Journal of Physiology* 510 (Pt 3) (August): 941–62. http://www.ncbi.nlm.nih.gov/pubmed/9660904.

Campbell, K S, and R L Moss. 2000. "A Thixotropic Effect in Contracting Rabbit Psoas Muscle: Prior Movement Reduces the Initial Tension Response to Stretch.." *Journal of Physiology* 525 Pt 2 (2): 531–48. doi:10.1111/j.1469-7793.2000.00531.x.

Campbell, Kenneth S. 2009. "Interactions Between Connected Half-Sarcomeres Produce Emergent Mechanical Behavior in a Mathematical Model of Muscle.." Edited by Roger Cooke. *PLoS Computational Biology* 5 (11). Public Library of Science: e1000560. doi:10.1371/journal.pcbi.1000560.

Campbell, Kenneth S. 2014. “Dynamic Coupling of Regulated Binding Sites and Cycling Myosin Heads in Striated Muscle..” *The Journal of General Physiology* 143 (3): 387–99. doi:10.1085/jgp.201311078.

Campbell, Kenneth S, and Richard L Moss. 2002. “History-Dependent Mechanical Properties of Permeabilized Rat Soleus Muscle Fibers..” *Biophysical Journal* 82 (2): 929–43. doi:10.1016/S0006-3495(02)75454-4.

Carey, Leeanne M, Thomas A Matyas, and Linda E Oke. 1993. “Sensory Loss in Stroke Patients: Effective Training of Tactile and Proprioceptive Discrimination.” *Archives of Physical Medicine and Rehabilitation* 74 (6): 602–11.

Carrasco, Dario I, Jacob A Vincent, and Timothy C Cope. 2017. “Distribution of TTX-Sensitive Voltage-Gated Sodium Channels in Primary Sensory Endings of Mammalian Muscle Spindles.” *Journal of Neurophysiology* 117 (4): 1690–1701. doi:10.1152/jn.00889.2016.

Chen, W J, and R E Poppele. 1978. “Small-Signal Analysis of Response of Mammalian Muscle Spindles with Fusimotor Stimulation and a Comparison with Large-Signal Responses.” *Journal of Neurophysiology* 41 (1). Am Physiological Soc: 15–27.

Chiel, Hillel J, Lena H Ting, Örjan Ekeberg, and Mitra J Z Hartmann. 2009. “The Brain in Its Body: Motor Control and Sensing in a Biomechanical Context..” *The Journal of Neuroscience : the Official Journal of the Society for Neuroscience* 29 (41): 12807–14. doi:10.1523/JNEUROSCI.3338-09.2009.

Coërs, C, and J Durand. 1956. “[New Morphological Data on Innervation of Neuromuscular Spindles]..” *Archives De Biologie* 67 (3-4): 685–715.

Connor, J A, and C F Stevens. 1971. “Prediction of Repetitive Firing Behaviour From Voltage Clamp Data on an Isolated Neurone Soma.” *The Journal of Physiology* 213 (1): 31.

Conte, Antonella, Nashaba Khan, Giovanni Defazio, John C Rothwell, and Alfredo Berardelli. 2013. “Pathophysiology of Somatosensory Abnormalities in Parkinson Disease..” *Nature Reviews. Neurology* 9 (12): 687–97. doi:10.1038/nrneurol.2013.224.

Cooper, S, and M H Gladden. 1974. “Elastic Fibres and Reticulin of Mammalian Muscle Spindles and Their Functional Significance..” *Quarterly Journal of Experimental Physiology and Cognate Medical Sciences* 59 (4): 367–85. http://eutils.ncbi.nlm.nih.gov/entrez/eutils/elink.fcgi?dbfrom=pubmed&id=4141107&retmode=ref&cmd=prlinks.

Cordo, Paul J, Carmen Flores-Vieira, Sabine M P Verschueren, J Timothy Inglis, and Victor Gurfinkel. 2002. “Position Sensitivity of Human Muscle Spindles: Single

Afferent and Population Representations..” *Journal of Neurophysiology* 87 (3): 1186–95. doi:10.1152/jn.00393.2001.

Cui, Lei, Eric J Perreault, Huub Maas, and Thomas G Sandercock. 2008. “Modeling Short-Range Stiffness of Feline Lower Hindlimb Muscles..” *Journal of Biomechanics* 41 (9): 1945–52. doi:10.1016/j.jbiomech.2008.03.024.

Day, James, Leah R Bent, Ingvars Birznieks, Vaughan G Macefield, and Andrew G Cresswell. 2017. “Muscle Spindles in Human Tibialis Anterior Encode Muscle Fascicle Length Changes..” *Journal of Neurophysiology* 117 (4): 1489–98. doi:10.1152/jn.00374.2016.

Dayan, Peter, and Laurence F Abbott. 2001. *Theoretical Neuroscience*. Vol. 806. Cambridge, MA: MIT Press.

De Groote, Friedl, Jessica L Allen, and Lena H Ting. 2017. “Contribution of Muscle Short-Range Stiffness to Initial Changes in Joint Kinetics and Kinematics During Perturbations to Standing Balance: a Simulation Study..” *Journal of Biomechanics* 55 (April): 71–77. doi:10.1016/j.jbiomech.2017.02.008.

Delmas, Patrick, and Bertrand Coste. 2013. “Mechano-Gated Ion Channels in Sensory Systems..” *Cell* 155 (2): 278–84. doi:10.1016/j.cell.2013.09.026.

Dietz, Volker, and Thomas Sinkjaer. 2007. “Spastic Movement Disorder: Impaired Reflex Function and Altered Muscle Mechanics.” *The Lancet Neurology* 6 (8): 725–33.

Dimitriou, Michael. 2014. “Human Muscle Spindle Sensitivity Reflects the Balance of Activity Between Antagonistic Muscles..” *The Journal of Neuroscience : the Official Journal of the Society for Neuroscience* 34 (41): 13644–55. doi:10.1523/JNEUROSCI.2611-14.2014.

Dimitriou, Michael. 2016. “Enhanced Muscle Afferent Signals During Motor Learning in Humans..” *Current Biology : CB* 26 (8): 1062–68. doi:10.1016/j.cub.2016.02.030.

Elek, J, A Prochazka, M Hulliger, and S Vincent. 1990. “In-Series Compliance of Gastrocnemius Muscle in Cat Step Cycle: Do Spindles Signal Origin-to-Insertion Length?.” *The Journal of Physiology* 429 (1): 237–58. doi:10.1113/jphysiol.1990.sp018254.

Emonet-Dénand, F, Y Laporte, P B Matthews, and J Petit. 1977. “On the Subdivision of Static and Dynamic Fusimotor Actions on the Primary Ending of the Cat Muscle Spindle..” *Journal of Physiology* 268 (3): 827–61. doi:10.1113/jphysiol.1977.sp011884/full.

Fowler, E G, A I Nwigwe, and T W Ho. 2000. “Sensitivity of the Pendulum Test for Assessing Spasticity in Persons with Cerebral Palsy..” *Developmental Medicine and Child Neurology* 42 (3): 182–89.

Friese, Andreas, Julia A Kaltschmidt, David R Ladle, Markus Sigrist, Thomas M Jessell, and Silvia Arber. 2009. “Gamma and Alpha Motor Neurons Distinguished by Expression of Transcription Factor Err3.” *Proceedings of the National Academy of Sciences* 106 (32). National Acad Sciences: 13588–93.

Fulton, J F, and J Pi-Suñer. 1927 “A Note Concerning the Probable Function of Various Afferent End-Organs in Skeletal Muscle.” *Journal of Physiology*.

Getz, E B, R Cooke, and S L Lehman. 1998. “Phase Transition in Force During Ramp Stretches of Skeletal Muscle..” *Biophysical Journal* 75 (6): 2971–83. doi:10.1016/S0006-3495(98)77738-0.

Gladden, M H. 1976. “Structural Features Relative to the Function of Intrafusal Muscle Fibres in the Cat..” *Progress in Brain Research* 44. Elsevier: 51–59. doi:10.1016/S0079-6123(08)60722-0.

Haftel, Valerie K, Edyta K Bichler, T Richard Nichols, Martin J Pinter, and Timothy C Cope. 2004. “Movement Reduces the Dynamic Response of Muscle Spindle Afferents and Motoneuron Synaptic Potentials in Rat..” *Journal of Neurophysiology* 91 (5): 2164–71. doi:10.1152/jn.01147.2003.

Hagbarth, Karl-Erik, and GORAN Eklund. 1968. “The Effects of Muscle Vibration in Spasticity, Rigidity, and Cerebellar Disorders..” *Journal of Neurology, Neurosurgery, and Psychiatry* 31 (3). BMJ Publishing Group: 207.

Hasan, Z. 1983. “A Model of Spindle Afferent Response to Muscle Stretch.” *Journal of Neurophysiology* 49 (4). American Physiological Society Bethesda, MD: 989–1006. doi:10.1152/jn.1983.49.4.989.

Hasan, Z, and J C Houk. 1975. “Transition in Sensitivity of Spindle Receptors That Occurs When Muscle Is Stretched More Than a Fraction of a Millimeter..” *Journal of Neurophysiology* 38 (3): 673–89. doi:10.1152/jn.1975.38.3.673.

Hill, A V. 1953. “The Mechanics of Active Muscle..” *Proceedings of the Royal Society of London. Series B, Biological Sciences* 141 (902): 104–17.

Honeycutt, Claire F, Paul Nardelli, Timothy C Cope, and T Richard Nichols. 2012. “Muscle Spindle Responses to Horizontal Support Surface Perturbation in the Anesthetized Cat: Insights Into the Role of Autogenic Feedback in Whole Body Postural Control.” *Journal of Neurophysiology* 108 (5): 1253–61.

Horslen, Brian C, Chantelle D Murnaghan, J Timothy Inglis, Romeo Chua, and Mark G Carpenter. 2013. "Effects of Postural Threat on Spinal Stretch Reflexes: Evidence for Increased Muscle Spindle Sensitivity?" 110 (4): 899–906.

Houk, J C, W Z Rymer, and P E Crago. 1981. "Dependence of Dynamic Response of Spindle Receptors on Muscle Length and Velocity.." *Journal of Neurophysiology* 46 (1): 143–66. doi:10.1152/jn.1981.46.1.143.

Hulliger, M. 1984. "The Mammalian Muscle Spindle and Its Central Control.." *Reviews of Physiology, Biochemistry and Pharmacology* 101: 1–110.

Hulliger, M, PBC Matthews, and J Noth. 1977. "Static and Dynamic Fusimotor Action on the Response of Ia Fibres to Low Frequency Sinusoidal Stretching of Widely Ranging Amplitude." *The Journal of Physiology* 267 (3). Wiley Online Library: 811–38.

Hunt, C C, and D Ottoson. 1975. "Impulse Activity and Receptor Potential of Primary and Secondary Endings of Isolated Mammalian Muscle Spindles" 252 (1): 259–81.

Hunt, C C, and R S Wilkinson. 1980. "An Analysis of Receptor Potential and Tension of Isolated Cat Muscle Spindles in Response to Sinusoidal Stretch.." *Journal of Physiology* 302 (May). Wiley-Blackwell: 241–62. doi:10.1111/(ISSN)1469-7793.

Huyghues-Despointes, Clotilde MJI, Timothy C Cope, and T Richard Nichols. 2003. "Intrinsic Properties and Reflex Compensation in Reinnervated Triceps Surae Muscles of the Cat: Effect of Movement History" 90 (3): 1547–55.

Hwang, Eun Jung, Maurice A Smith, and Reza Shadmehr. 2005. "Adaptation and Generalization in Acceleration-Dependent Force Fields." *Experimental Brain Research* 169 (4): 496–506. doi:10.1007/s00221-005-0163-2.

Insperger, Tamás, John Milton, and Gábor Stépán. 2013. "Acceleration Feedback Improves Balancing Against Reflex Delay" 10 (79): 20120763.

Jami, L, and J Petit. 1979. "Dynamic and Static Responses of Primary and Secondary Spindle Endings of the Cat Peroneus Tertius Muscle [Proceedings].." *Journal of Physiology* 296 (November): 109P.

Jami, L, J Petit, U Proske, and D Zytnicki. 1985. "Responses of Tendon Organs to Unfused Contractions of Single Motor Units.." *Journal of Neurophysiology* 53 (1): 32–42. doi:10.1152/jn.1985.53.1.32.

Jami, Léna. 1992. "Golgi Tendon Organs in Mammalian Skeletal Muscle: Functional Properties and Central Actions" 72 (3): 623–66.

Jami, LIRNA, K S Murthy, and J Petit. 1982. “A Quantitative Study of Skeletofusimotor Innervation in the Cat Peroneus Tertius Muscle..” *The Journal of Physiology* 325 (1). Wiley Online Library: 125–44.

Kakuda, N, T Miwa, and M Nagaoka. 1998. “Coupling Between Single Muscle Spindle Afferent and EMG in Human Wrist Extensor Muscles: Physiological Evidence of Skeletofusimotor (Beta) Innervation..” *Electroencephalography and Clinical Neurophysiology* 109 (4): 360–63.

Kakuda, Naoyuki, and Masanori Nagaoka. 1998. “Dynamic Response of Human Muscle Spindle Afferents to Stretch During Voluntary Contraction” 513 (2): 621–28.

Kamper, D G, R L Harvey, S Suresh, and W Z Rymer. 2003. “Relative Contributions of Neural Mechanisms Versus Muscle Mechanics in Promoting Finger Extension Deficits Following Stroke.” *Muscle & Nerve* 28 (3). Wiley Online Library: 309–18.

Khudados, Etedal, Frederick WJ Cody, and Donald J O’Boyle. 1999. “Proprioceptive Regulation of Voluntary Ankle Movements, Demonstrated Using Muscle Vibration, Is Impaired by Parkinson’s Disease.” *Journal of Neurology, Neurosurgery & Psychiatry* 67 (4). BMJ Publishing Group Ltd: 504–10.

Kolarcik, Christi L, Dennis Bourbeau, Erdrin Azemi, Erika Rost, Ling Zhang, Carl F Lagenaur, Douglas J Weber, and X Tracy Cui. 2012. “In Vivo Effects of L1 Coating on Inflammation and Neuronal Health at the Electrode–Tissue Interface in Rat Spinal Cord and Dorsal Root Ganglion.” *Acta Biomaterialia* 8 (10). Elsevier: 3561–75.

Konczak, Jürgen, Daniel M Corcos, Fay Horak, Howard Poizner, Mark Shapiro, Paul Tuite, Jens Volkmann, and Matthias Maschke. 2009. “Proprioception and Motor Control in Parkinson's Disease.” *Journal of Motor Behavior* 41 (6): 543–52.

Kruse, M N, and R E Poppele. 1991. “Components of the Dynamic Response of Mammalian Muscle Spindles That Originate in the Sensory Terminals..” *Experimental Brain Research* 86 (2): 359–66.

Lee, RjG, and W G Tatton. 1975. “Motor Responses to Sudden Limb Displacements in Primates with Specific CNS Lesions and in Human Patients with Motor System Disorders” 2 (03): 285–93.

Lennerstrand, G, and U Thoden. 1968. “Dynamic Analysis of Muscle Spindle Endings in the Cat Using Length Changes of Different Length-Time Relations..” *Acta Physiologica Scandinavica* 73 (1). Blackwell Publishing Ltd: 234–50. doi:10.1111/j.1748-1716.1968.tb04100.x.

Lewis, D M, and U Proske. 1972a. “The Effect of Muscle Length and Rate of Fusimotor Stimulation on the Frequency of Discharge in Primary Endings From Muscle Spindles in the Cat” 222 (3): 511.

Lewis, D M, and U Proske. 1972b. “The Effect of Muscle Length and Rate of Fusimotor Stimulation on the Frequency of Discharge in Primary Endings From Muscle Spindles in the Cat..” *Journal of Physiology* 222 (3): 511–35.

Lin, Chou-Ching K, and Patrick E Crago. 2002. “Structural Model of the Muscle Spindle..” *Annals of Biomedical Engineering* 30 (1): 68–83.

Liu, Jing-Xia, Per-Olof Eriksson, Lars-Eric Thornell, and Fatima Pedrosa-Domellöf. 2002a. “Myosin Heavy Chain Composition of Muscle Spindles in Human Biceps Brachii” 50 (2): 171–83.

Liu, Jing-Xia, Per-Olof Eriksson, Lars-Eric Thornell, and Fatima Pedrosa-Domellöf. 2002b. “Myosin Heavy Chain Composition of Muscle Spindles in Human Biceps Brachii..” *Journal of Histochemistry & Cytochemistry* 50 (2): 171–83. doi:10.1177/002215540205000205.

Liu, Jing-Xia, Per-Olof Eriksson, Lars-Eric Thornell, and Fatima Pedrosa-Domellöf. 2005. “Fiber Content and Myosin Heavy Chain Composition of Muscle Spindles in Aged Human Biceps Brachii..” *Journal of Histochemistry & Cytochemistry* 53 (4): 445–54. doi:10.1369/jhc.4A6257.2005.

Lockhart, Daniel B, and Lena H Ting. 2007. “Optimal Sensorimotor Transformations for Balance” 10 (10): 1329–36.

London, B M, L R Jordan, C R Jackson, and L E Miller. 2008. “Electrical Stimulation of the Proprioceptive Cortex (Area 3a) Used to Instruct a Behaving Monkey.” *IEEE Transactions on Neural Systems and Rehabilitation Engineering* 16 (1): 32–36. doi:10.1109/TNSRE.2007.907544.

London, Brian M, and Lee E Miller. 2013. “Responses of Somatosensory Area 2 Neurons to Actively and Passively Generated Limb Movements.” *Journal of Neurophysiology* 109 (6): 1505–13. doi:10.1152/jn.00372.2012.

Loram, Ian D, Constantinos N Maganaris, and Martin Lakie. 2004. “Paradoxical Muscle Movement in Human Standing” 556 (3): 683–89.

Luu, Billy L, Brian L Day, Jonathan D Cole, and Richard C Fitzpatrick. 2011. “The Fusimotor and Reafferent Origin of the Sense of Force and Weight.” *The Journal of Physiology* 589 (13): 3135–47.

Macpherson, Jane M, and Fay B Horak. 2013. “Posture.” In *Principles of Neural Science*, edited by Eric R Kandel, James H Schwartz, Thomas M Jessell, Steven A Siegelbaum, and A J Hudspeth, 5 ed. McGraw-Hill Education / Medical.

Matthews, Bryan H C. 1931. “The Response of a Muscle Spindle During Active Contraction of a Muscle.” *The Journal of Physiology* 72 (2): 153–74. doi:10.1152/japplphysiol.00908.2016.

Matthews, Bryan H C. 1933. “Nerve Endings in Mammalian Muscle.” *The Journal of Physiology* 78 (1): 1–53. doi:10.1113/jphysiol.1933.sp002984.

Matthews, P B. 1959. “The Dependence of Tension Upon Extension in the Stretch Reflex of the Soleus Muscle of the Decerebrate Cat..” *Journal of Physiology* 147 (3). Wiley-Blackwell: 521–46. doi:10.1111/(ISSN)1469-7793.

Matthews, P B. 1963. “The Response of De-Efferented Muscle Spindle Receptors to Stretching at Different Velocities..” *Journal of Physiology* 168 (3). Wiley-Blackwell: 660–78. https://www-ncbi-nlm-nih-gov.proxy.library.emory.edu/pmc/articles/PMC1359446/.

Matthews, P B C. 1964. “Muscle Spindles and Their Motor Control” 44 (2): 219–88. doi:10.1152/physrev.1964.44.2.219.

Matthews, P B, and R B Stein. 1969. “The Regularity of Primary and Secondary Muscle Spindle Afferent Discharges..” *Journal of Physiology* 202 (1). Wiley-Blackwell: 59–82. doi:10.1111/(ISSN)1469-7793.

Matthews, PBC. 1981. “Muscle Spindles: Their Messages and Their Fusimotor Supply.” *European Journal of Neurology*.

Matthews, PBC, and R B Stein. 1969. “The Sensitivity of Muscle Spindle Afferents to Small Sinusoidal Changes of Length” 200 (3): 723.

Matthews, Peter B C. 1972. “Mammalian Muscle Receptors and Their Central Actions.” *American Journal of Physical Medicine & Rehabilitation* 53, no. 3 (1974): 143-144

McGowan, C P, R R Neptune, and W Herzog. 2013. “A Phenomenological Muscle Model to Assess History Dependent Effects in Human Movement.” *Journal of Biomechanics* 46 (1): 151–57. doi:10.1016/j.jbiomech.2012.10.034.

Mileusnic, Milana P, Ian E Brown, Ning Lan, and Gerald E Loeb. 2006. “Mathematical Models of Proprioceptors. I. Control and Transduction in the Muscle Spindle” 96 (4): 1772–88.

Monjo, Florian, and Nicolas Forestier. 2018. “Muscle Spindle Thixotropy Affects Force Perception Through Afferent-Induced Facilitation of the Motor Pathways as Revealed by the Kohnstamm Effect..” *Experimental Brain Research*, February. Springer Berlin Heidelberg, 1–12. doi:10.1007/s00221-018-5207-5.

Nichols, T Richard, and Timothy C Cope. 2004. “Cross-Bridge Mechanisms Underlying the History-Dependent Properties of Muscle Spindles and Stretch Reflexes” 82 (8-9): 569–76. doi:10.1139/y04-074.

Pate, E, and R Cooke. 1989. “A Model of Crossbridge Action: the Effects of ATP, ADP and Pi..” *Journal of Muscle Research and Cell Motility* 10 (3): 181–96.

Patel, Neepa, Joseph Jankovic, and Mark Hallett. 2014. “Sensory Aspects of Movement Disorders..” *The Lancet Neurology* 13 (1): 100–112. doi:10.1016/S1474-4422(13)70213-8.

Prochazka, A, and M Gorassini. 1998a. “Models of Ensemble Firing of Muscle Spindle Afferents Recorded During Normal Locomotion in Cats..” *The Journal of Physiology* 507 (Pt 1) (February): 277–91. doi:10.1111/j.1469-7793.2001.0099b.x/full.

Prochazka, Arthur, and Monica Gorassini. 1998b. “Ensemble Firing of Muscle Afferents Recorded During Normal Locomotion in Cats” 507 (1): 293–304.

Proske, U, and D L Morgan. 1987. “Tendon Stiffness: Methods of Measurement and Significance for the Control of Movement. a Review” 20 (1): 75–82.

Proske, U, and D L Morgan. 1999. “Do Cross-Bridges Contribute to the Tension During Stretch of Passive Muscle?.” *Journal of Muscle Research and Cell Motility* 20 (5-6): 433–42.

Proske, U, and G J Stuart. 1985. “The Initial Burst of Impulses in Responses of Toad Muscle Spindles During Stretch..” *Journal of Physiology* 368 (November). Wiley-Blackwell: 1–17. doi:10.1111/(ISSN)1469-7793.

Proske, U, D L Morgan, and J E Gregory. 1992. “Muscle History Dependence of Responses to Stretch of Primary and Secondary Endings of Cat Soleus Muscle Spindles..” *Journal of Physiology* 445 (January): 81–95.

Proske, Uwe, and Simon C Gandevia. 2009. “The Kinaesthetic Senses” 587 (17): 4139–46.

Proske, Uwe, and Simon C Gandevia. 2012. “The Proprioceptive Senses: Their Roles in Signaling Body Shape, Body Position and Movement, and Muscle Force” 92 (4): 1651–97.

Proske, Uwe, Anthony Tsay, and Trevor J Allen. 2014. “Muscle Thixotropy as a Tool in the Study of Proprioception..” *Experimental Brain Research* 232 (11): 3397–3412. doi:10.1007/s00221-014-4088-5.

Proske, Uwe, David L Morgan, and J Edmund Gregory. 1993. “Thixotropy in Skeletal Muscle and in Muscle Spindles: a Review.” *Progress in Neurobiology* 41 (6): 705–21.

Rack, P M, and D R Westbury. 1984. “Elastic Properties of the Cat Soleus Tendon and Their Functional Importance..” *Journal of Physiology* 347 (February). Wiley-Blackwell: 479–95. doi:10.1111/(ISSN)1469-7793.

Rack, Peter MH, and D R Westbury. 1974. “The Short Range Stiffness of Active Mammalian Muscle and Its Effect on Mechanical Properties” 240 (2): 331.

Ranatunga, K W, H Roots, G J Pinniger, and G W Offer. 2010. “Crossbridge and Non-Crossbridge Contributions to Force in Shortening and Lengthening Muscle..” *Advances in Experimental Medicine and Biology* 682 (Chapter 12). New York, NY: Springer New York: 207–21. doi:10.1007/978-1-4419-6366-6_12.

Richmond, F J R, and V C Abrahams. 1979. “Physiological Properties of Muscle Spindles in Dorsal Neck Muscles of the Cat” 42 (20): 604–16.

Rickards, Christopher, and F W Cody. 1997. “Proprioceptive Control of Wrist Movements in Parkinson's Disease. Reduced Muscle Vibration-Induced Errors..” *Brain : a Journal of Neurology* 120 (6): 977–90.

Rigosa, J, D J Weber, A Prochazka, R B Stein, and S Micera. 2011. “Neuro-Fuzzy Decoding of Sensory Information From Ensembles of Simultaneously Recorded Dorsal Root Ganglion Neurons for Functional Electrical Stimulation Applications.” *Journal of Neural Engineering* 8 (4): 046019–14. doi:10.1088/1741-2560/8/4/046019.

Rothwell, J C, J A Obeso, M M Traub, and C D Marsden. 1983. “The Behaviour of the Long-Latency Stretch Reflex in Patients with Parkinson's Disease.” *Journal of Neurology, Neurosurgery & Psychiatry* 46 (1). BMJ Publishing Group Ltd: 35–44.

Rothwell, J C, M M Traub, B L Day, J A Obeso, P K Thomas, and C D Marsden. 1982. “Manual Motor Performance in a Deafferented Man..” *Brain : a Journal of Neurology* 105 (Pt 3) (September): 515–42.

Ruffini, A. 1898. “On the Minute Anatomy of the Neuromuscular Spindles of the Cat, and on Their Physiological Significance..” *Journal of Physiology* 23 (3). Wiley-Blackwell: 190–93.

Safavynia, Seyed A, and Lena H Ting. 2013a. “Long-Latency Muscle Activity Reflects Continuous, Delayed Sensorimotor Feedback of Task-Level and Not Joint-Level Error” 110 (6): 1278–90.

Safavynia, Seyed A, and Lena H Ting. 2013b. “Sensorimotor Feedback Based on Task-Relevant Error Robustly Predicts Temporal Recruitment and Multidirectional Tuning of Muscle Synergies” 109 (1): 31–45.

Schäfer, S S, and S Kijewski. 1974. “The Dependency of the Acceleration Response of Primary Muscle Spindle Endings on the Mechanical Properties of the Muscle..” *Pflügers Archiv - European Journal of Physiology* 350 (2): 101–22.

Schäfer, Sonja S. 1967. “The Acceleration Response of a Primary Muscle-Spindle Ending to Ramp Stretch of the Extrafusal Muscle” 23 (12): 1026–27.

Scott, S H, and G E Loeb. 1994. “The Computation of Position Sense From Spindles in Mono-and Multiarticular Muscles” 14 (12): 7529–40.

Sheean, G. 2002. “The Pathophysiology of Spasticity” 9 (s1): 3–9.

Shemmell, Jonathan, Matthew A Krutky, and Eric J Perreault. 2010. “Stretch Sensitive Reflexes as an Adaptive Mechanism for Maintaining Limb Stability” 121 (10): 1680–89.

Sherrington, C S. 1894. “On the Anatomical Constitution of Nerves of Skeletal Muscles; with Remarks on Recurrent Fibres in the Ventral Spinal Nerve-Root..” *Journal of Physiology* 17 (3-4). Wiley-Blackwell: 210.2–.258. doi:10.1111/(ISSN)1469-7793.

Simon, Anna, Fiona Shenton, Irene Hunter, Robert W Banks, and Guy S Bewick. 2010. “Amiloride-Sensitive Channels Are a Major Contributor to Mechanotransduction in Mammalian Muscle Spindles.” *The Journal of Physiology* 588 (1): 171–85.

Stapley, Paul J, Lena H Ting, Manuel Hulliger, and Jane M Macpherson. 2002. “Automatic Postural Responses Are Delayed by Pyridoxine-Induced Somatosensory Loss” 22 (14): 5803–7.

Steg, G. 1962. “The Function of Muscle Spindles in Spasticity and Rigidity.” *Acta Neurologica Scandinavica* 38 (s3). Wiley Online Library: 53–59.

Stein, R B, D J Weber, Y Aoyagi, A Prochazka, J B M Wagenaar, S Shoham, and R A Normann. 2004. “Coding of Position by Simultaneously Recorded Sensory Neurones in the Cat Dorsal Root Ganglion.” *The Journal of Physiology* 560 (3): 883–96. doi:10.1113/jphysiol.2004.068668.

Swash, Michael, and Kathleen P Fox. 1976. “The Pathology of the Muscle Spindle in Duchenne Muscular Dystrophy.” *Journal of the Neurological Sciences* 29 (1). Elsevier: 17–32.

Thornell, Lars-Eric, Lena Carlsson, Per-Olof Eriksson, Jing-Xia Liu, Catharina Österlund, Per Stål, and Fatima Pedrosa-Domellöf. 2015. "Fibre Typing of Intrafusal Fibres" 227 (2): 136–56. doi:10.1111/joa.12338.

Ting, Lena H, Stacie A Chvatal, Seyed A Safavynia, and J Lucas McKay. 2012. "Review and Perspective: Neuromechanical Considerations for Predicting Muscle Activation Patterns for Movement" 28 (10): 1003–14.

Tsay, A, G Savage, Trevor J Allen, and U Proske. 2014. "Limb Position Sense, Proprioceptive Drift and Muscle Thixotropy at the Human Elbow Joint" 592 (12): 2679–94. doi:10.1113/jphysiol.2013.269365.

Vallbo, AB. 1974. "Human Muscle Spindle Discharge During Isometric Voluntary Contractions. Amplitude Relations Between Spindle Frequency and Torque" 90 (2): 319–36.

Vincent, Jacob A, Hanna M Gabriel, Adam S Deardorff, Paul Nardelli, Robert E W Fyffe, Thomas Burkholder, and Timothy C Cope. 2017. "Muscle Proprioceptors in Adult Rat: Mechanosensory Signaling and Synapse Distribution in Spinal Cord." *Journal of Neurophysiology* 118 (5): 2687–2701. doi:10.1152/jn.00497.2017.

Weber, D J, R B Stein, D G Everaert, and A Prochazka. 2006. "Decoding Sensory Feedback From Firing Rates of Afferent Ensembles Recorded in Cat Dorsal Root Ganglia in Normal Locomotion." *IEEE Transactions on Neural Systems and Rehabilitation Engineering* 14 (2): 240–43. doi:10.1109/TNSRE.2006.875575.

Weber, D J, R B Stein, D G Everaert, and A Prochazka. 2007. "Limb-State Feedback From Ensembles of Simultaneously Recorded Dorsal Root Ganglion Neurons." *Journal of Neural Engineering* 4 (3): S168–80. doi:10.1088/1741-2560/4/3/S04.

Welch, T D, and Lena H Ting. 2009. "A Feedback Model Explains the Differential Scaling of Human Postural Responses to Perturbation Acceleration and Velocity." *Journal of Neurophysiology* 101 (6): 3294–3309. doi:10.1152/jn.90775.2008.

Welch, Torrence D J, and Lena H Ting. 2008. "A Feedback Model Reproduces Muscle Activity During Human Postural Responses to Support-Surface Translations.." *Journal of Neurophysiology* 99 (2): 1032–38. doi:10.1152/jn.01110.2007.

Welch, Torrence D J, and Lena H Ting. 2014. "Mechanisms of Motor Adaptation in Reactive Balance Control.." Edited by Ramesh Balasubramaniam. *PLoS ONE* 9 (5). Public Library of Science: e96440. doi:10.1371/journal.pone.0096440.

Wilson, L R, S C Gandevia, J T Inglis, J-M Gracies, and David Burke. 1999. "Muscle Spindle Activity in the Affected Upper Limb After a Unilateral Stroke." *Brain : a Journal of Neurology* 122 (11). Oxford University Press: 2079–88.

Wilson, Linda R, Jean-Michel Gracies, David Burke, and Simon C Gandevia. 1999. "Evidence for Fusimotor Drive in Stroke Patients Based on Muscle Spindle Thixotropy." *Neuroscience Letters* 264 (1-3). Elsevier: 109–12.

Winters, Jack M. 1990. "Hill-Based Muscle Models: a Systems Engineering Perspective." In *Multiple Muscle Systems*, edited by Jack M Winters and Savio L-Y Woo, 69–93. New York, NY: Springer. doi:10.1007/978-1-4613-9030-5.

Xiao, Rui, and X Z Shawn Xu. 2010. "Mechanosensitive Channels: in Touch with Piezo.." *Current Biology : CB* 20 (21): R936–38. doi:10.1016/j.cub.2010.09.053.